University of Strathclyde

Department of Naval Architecture, Ocean & Marine Engineering

Investigation of Trim Influence on Resistance, Seakeeping and Propulsive Performance

by

Emil Shivachev

A thesis presented in fulfilment of the requirements for the degree of

Doctor of Philosophy

Glasgow, UK

2021

Declaration

This thesis is the result of the Author's original research. It has been composed by the Author and has not been previously submitted for examination which has led to the award of a degree.

Signed: *Date:*

Acknowledgements

First of all, I would like to thank to my supervisor Professor Sandy Day for his supervision, valuable guidance and suggestions that he has provided throughout my PhD journey.

Furthermore, I would like to express my gratitude for my secondary supervisor, Professor Osman Turan. I owe him great thanks for all his support, advice, and encouragement along the way.

I would also like to express my appreciation to Dr. Mahdi Khorasanchi who was my supervisor in early stages of this study. He has been always a supportive mentor and made valuable contributions to this study.

I want to thank to my office mates in Livingstone Tower LT725 especially to Dr. Batuhan Aktas, Matthias Maasch, Anthony Romanowski and Dr. Naz Yilmaz for sharing their knowledge and friendship. I would also like to thank my colleagues in the department for creating a socially vibrant and friendly atmosphere.

My many thanks extend to all other friends that I met here in Glasgow who have supported me in so many ways and made my time more enjoyable.

I would like to thank to all my family members for their love. I am grateful to my sister Filiz Ozturk Filiz for all her endless support and love. I hope my wee nephew, Ege, enjoys the colourful images of ships in this thesis.

I would like to dedicate this thesis to my parents, my first teachers, Neriman ve Fikri Ozturk , who dedicated their life to teaching and taught me to love science. Without their support, this work would not exist.

Contents

List of Figures

List of Tables

Abstract

There has been a lot of interest in recent years in trim and ballast optimisation in which the ballast of a vessel is varied to reduce fuel consumption and green house gas emissions. Trim optimisation is one of the easiest and cheapest methods among many fuel-saving measures recommended by IMO as it does not require any hull shape modification or engine upgrade. Many existing ships are designed for a single operational condition with the aim of producing low resistance at their design speed and draft with an even keel. Given that a ship will often sail outside this condition over its operational life, the effect of trim on ships resistance and powering will be significant. However, limited research has been performed to investigate trim influence on ship performance. In many cases, the work has concentrated on minimisation of resistance; often focussing on calm-water resistance in model scale. The impact of trim on added resistance and propulsive performance of ships is less well understood.

In this context, the main aim of this PhD study is to gain an improved understanding of the impact of trim on the resistance, seakeeping and propulsive performance of vessels by using Experimental Fluid Dynamics (EFD) and Computational Fluid Dynamics (CFD) methods. This study covers model tests in towing tank, model scale and full scale CFD analyses for various operating points in calm water and waves.

This study consists of three main parts. In the first part, trim influence on the calm water resistance of the KRISO Container Ship (KCS) was investigated. A series of resistance tests for various trim angles and speeds were conducted at 1:75 scale at design draft. CFD computations were carried out for the same conditions and also for ballast draft with the hull both fixed and free to sink and trim. Trim influence on individual resistance components was

discussed. Full-scale numerical simulations are also carried out and differences between model scale and full-scale findings are discussed to investigate scale effects on optimum trim.

In the second part of this study, the effects of trim angles on added resistance and motion responses of KCS were evaluated experimentally and numerically in six different trim angles. Effects of trim angles on added resistance were analysed and results concerning the performance of the vessel at different trim angles were plotted. Experimental and numerical results for the heave and pitch motions and the added resistance were compared. Furthermore, the range of trim and wave conditions were identified for the application of the rapid linear potential flow method.

The study is then extended to include a model of the propeller to investigate the trim influence on the propulsive performance of the KCS. Self-propulsion simulations were performed using two different methods, namely, sliding mesh with 3-D propeller geometry and body force method based actuator disk approach. Effects of trim angles on propulsive characteristics were analysed and results concerning the performance of the vessel at different trim angles were plotted. The differences in optimum trim based on pure resistance simulations and self-propulsion simulations were investigated. As trim optimisation studies require the analysis of large number of different operating conditions, the applicability and accuracy of a quicker simplified actuator disk approach was tested.

This author believes that methods and findings presented in this study contribute towards better understanding of the trim influence on resistance and powering performance of ships. Additionally, these findings may be used to further develop accurate and efficient trim optimisation tools for minimizing fuel consumption and emissions accordingly.

Chapter 1 Introduction

Chapter 1 is dedicated to setting the scene for this thesis and providing an introduction. The chapter initially states the motivations to conduct research on trim influence on ships resistance and propulsive performance. Then aims of this research are revealed together with the necessary objectives that need to be accomplished in order to achieve the stated aim. Following this, a general layout of the thesis is provided.

1.1 General Perspectives

International maritime trade has been growing rapidly in recent years as a result of economic growth and industrial globalisation. Merchant shipping became a vital component of global trade as more than 80 per cent of trade is carried by sea. Container trade became the fastest growing segment with an annual average growth rate of around 8 per cent between 1980 and 2017 while dry bulk and tanker trade increased at an annual growth rate of 4.6 per cent and 1.4 per cent, respectively. (UNCTAD, 2017). In total, more than 10.7 billion tonnes of goods were transported in 2017 as shown in Figure 1-1.

The shipping industry is experiencing growing pressure under the influence of external conditions such as the sharp increase in fuel prices and over capacity of merchant shipping fleet within the last decade. Furthermore, growing awareness of the impact of maritime transport on the environment has led to more strict regulations imposed by the International Maritime Organisation (IMO). In 2011, IMO made amendments to MARPOL ANNEX IV and adopted new mandatory energy efficiency measures to reduce the greenhouse gas emissions from international shipping. These measures include Energy Efficiency Design Index (EEDI) for all new ships and Shipping Energy Management Plan (SEEMP) for all ships in operation (IMO, 2011). Recently, IMO adopted a new strategy stating its commitment to reduce the CO2 emissions of international shipping by 40% in 2030, aiming

towards 70% reduction in 2050 compared to 2008 levels which is the first long term plan to curb shipping emissions by IMO (IMO, 2019). Considering these factors, shipping companies find themselves obliged to improve their ships energy efficiency measures for increased efficiency – so as to continue to operate economically despite rising costs and to be able to cope with new environmental regulations.

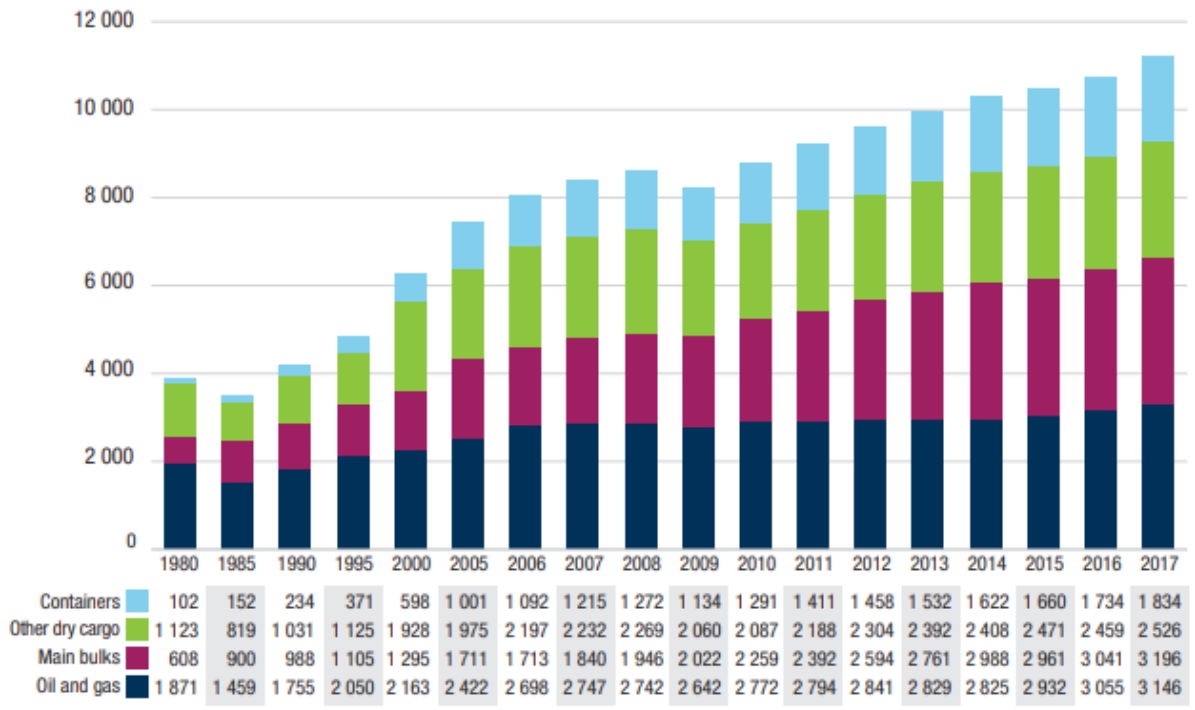

	1980	1985	1990	1995	2000	2005	2006	2007	2008	2009	2010	2011	2012	2013	2014	2015	2016	2017
Containers	102	152	234	371	598	1 001	1 092	1 215	1 272	1 134	1 291	1 411	1 458	1 532	1 622	1 660	1 734	1 834
Other dry cargo	1 123	819	1 031	1 125	1 928	1 975	2 197	2 232	2 269	2 060	2 087	2 188	2 304	2 392	2 408	2 471	2 459	2 526
Main bulks	608	900	988	1 105	1 295	1 711	1 713	1 840	1 946	2 022	2 259	2 392	2 594	2 761	2 988	2 961	3 041	3 196
Oil and gas	1 871	1 459	1 755	2 050	2 163	2 422	2 698	2 747	2 742	2 642	2 772	2 794	2 841	2 829	2 825	2 932	3 055	3 146

Figure 1-1 International maritime trade over selected years (Millions of tons loaded) (UNCTAD)

It is well known that fuel costs are one of the biggest operational costs and any reduction in fuel consumption can have a significant impact on operational expenses. Fluctuating fuel prices as shown in Figure 1-2 have been driving the ship owners and operators to be more efficient within the last decade. Fuel costs account for up to 50-60% of the total running costs of the vessel. (UNCTAD, 2010)Low operational costs are essential to be competitive in such conditions. Furthermore, fuel efficiency has become one of the key objectives in the shipping industry with the newly adopted mandatory measures to reduce emissions.

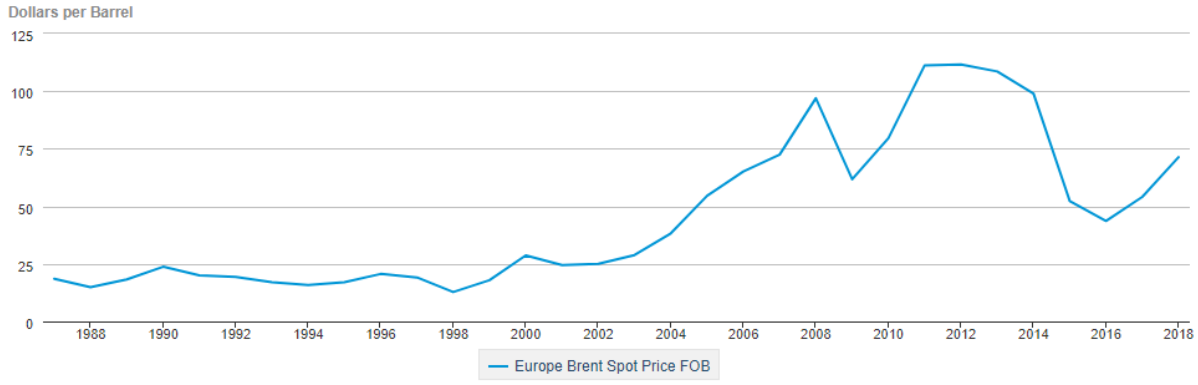

Figure 1-2 Historical Prices for Crude Oil (EIA)

These financial and environmental motives behind energy efficiency resulted in numerous investigations to find technical and operational measures which increase overall fuel efficiency and reduce emissions. The operational energy efficiency of a ship can be determined by its design, hull condition, machinery performance and operating conditions in terms of speed, draft and trim. Traditionally ship hulls are optimised for design speed and design draft based on the design contract condition. However, during a ships lifetime, it operates within a range of different speeds and drafts outside the design conditions. Industrial switch to slow steaming over the past years can be an example of how inefficient is to optimise ships at level trim for one speed and one draft. Given that a ship will often sail outside the design condition over its operational life and moreover some vessels such as LNG carriers return in ballast condition in one leg, the effect of trim on ships resistance will be significant. Trim optimisation can be regarded as one of the easiest and cheapest methods among many fuel-saving measures recommended by IMO as it does not require any hull shape modification or engine upgrade (IMO, 2016a).

Ships optimal position in the water considering the operating condition in terms of ballast, cargo and bunker relation has a significant impact on the resistance and thus fuel consumption. Effect of trim on the fuel consumption varies significantly for different hull shapes, size and vessel characteristics. Bertram, (2014) note that especially for ships with large transom sterns and bulbous bows, the power requirements for the best and worst trim may differ by more than 10%. For full-bodied hulls (tanker, bulker) the saving potential is smaller. Furthermore, optimum trim varies with different speed and draft values.

The traditional way to understand the effect of trim on hull performance is to carry out systematic model tests in a towing tank. However, model tests can be the most expensive approach for ships in operation as it requires building the physical model and conducting comprehensive tests. For new build ships, model tests will already be on the agenda and conducting a trim study at this stage would be the most cost-efficient approach.

CFD based trim optimisation tools are becoming popular in recent years to assess the effects of different trim conditions on ship performance as CFD capabilities are improving and being validated against model tests. CFD based trim optimisation tools may be more cost-effective as no additional hardware and measurement equipment such as sensors are required to monitor the operational parameters. A dense database consisting of previously calculated power requirements at different speed and draft values for different trim angles can be created and installed on any computer on board.

This work proposes to investigate the trim influence on resistance, added resistance and propulsive performance through the use of experimental and CFD methods to contribute to the understanding of energy efficient shipping operations.

1.2 Motivation

There has been a lot of interest in recent years in trim and ballast optimisation in which the ballast of a vessel is varied to reduce fuel consumption and emissions. Trim optimisation is one of the easiest and cheapest methods among many fuel-saving measures recommended by IMO as it does not require any hull shape modification or engine upgrade. However, as it will be discussed in Literature Review Chapter, limited research has been performed to investigate the effects of trim on ship resistance and power.

The impact of trim on added resistance in waves is perhaps less well understood, particularly with regard to non-linear effects, since many studies utilise standard linearised potential codes for computation of added resistance. To the best of the Author's knowledge, the majority of trim related studies have been performed at calm water and many of the added resistance studies have been conducted at level trim angles. Optimum trim attained at calm water may not have the same effect in a real sea environment as waves restrict overall ship

behaviour and lead to speed loss. Therefore, added resistance in waves at different trim angles should be investigated in ship operational optimization to increase energy efficiency. It may be beneficial to perform a comparison study between RANS CFD and potential flow calculations to identify ranges of ship speed, trim and wave conditions to which rapid linear potential flow calculations can be applied.

It is critical to predict the effective power of full-scale ships at different operating conditions in order to improve designs in the early stages. As full-scale CFD enables the prediction of actual ship performance in real operating conditions, it would be interesting to investigate the differences in optimum trim at model scale and full-scale vessels.

The impact of trim on the propulsive performance and the hull-propeller interaction in calm water is even less well-understood. In order to contribute to the improvement of vessels efficiency, it would be interesting to investigate the differences in optimum trim based on resistance tests/simulations and self-propulsion simulations. To the best of the author's knowledge, there is no study that investigates the differences in optimum trim between pure resistance simulations and self-propulsion simulations. Hence, this study aims to address this issue by conducting self-propulsion simulations at different trim angles. It also aims to investigate the applicability and accuracy of a quicker body force based virtual disk approach to estimate propulsive performance at different trim angles.

1.3 Aims and Objectives

The main aim of this PhD study is to gain an improved understanding of the impact of trim on the resistance, seakeeping and propulsive performance of vessels. This study will cover model tests, model scale and full-scale CFD computations for various operating points in calm water and waves.

The objectives of this study are as follows:

- To review the literature on trim optimisation of ships and to define the gaps in the literature.

- To develop skills and knowledge in CFD techniques by examining calm-water resistance

- To validate model scale predictions against tank tests

- To examine the impact of trim on calm-water resistance both model scale and full-scale

- To investigate the influence of trim on added resistance of a ship advancing in waves

- To correlate added resistance predictions based on potential flow methods with results obtained from CFD based predictions and model tests

- To indicate ranges of ship speed, trim and wave conditions to which rapid linear potential flow calculations suitable for adoption in preliminary ship design practice may be applicable.

- To investigate the trim influence on propulsive performance by extending the model to include a detailed model of the rotating propeller, using an approach such as a sliding mesh

- To investigate the applicability of simplified propulsion simulation approaches such as body force method based actuator disk for trim optimisation studies

1.4 Layout of the Thesis

In order to achieve above listed aim and objectives, this thesis is structured as follows:

- Chapter 2 (Literature Review): This chapter presents the critical review of the state of the art. It first outlines the fundamentals of trim and different trim optimisation tools which are available in the industry. Current trim optimisation methods are introduced to create a better understanding of existing methods. Following this, the historical development of the prediction methods for hull resistance, added wave resistance and propulsive performance is discussed. The chapter concludes by addressing overall findings from the literature survey including identified research gaps.

- Chapter 3 (Methodology) This chapter presents details of the experimental and numerical methods which have been used in this thesis for the investigation of trim influence on ships performance. The experimental approach is presented in detail and CFD methods that have been used are presented.

- Chapter 4 (Trim Influence on Calm Water Resistance) This chapter investigates trim influence on calm water resistance of the Kriso Container Ship (KCS) using computational fluid dynamics (CFD) in conjunction with towing tank tests. A series of resistance tests for various trim angles and speeds were conducted at 1:75 scale at design draft. CFD computations were carried out for the same conditions and also for ballast draft with the hull both fixed and free to sink and trim. After validating the applicability of the computational model, the same mesh, boundary conditions and solution techniques were used to obtain resistance values for different trim conditions at different Froude numbers. Trim influence on individual resistance components was discussed. Full-scale numerical simulations are also carried out and differences between model scale and full-scale findings are discussed in order to investigate scale effects on optimum trim. Finally, the conclusions are presented based on the overall findings obtained from this chapter.

- Chapter 5 (Trim Influence on Added Resistance) In this chapter, added resistance and motion responses of KCS were evaluated experimentally and numerically in six different trim angles. Firstly, experimental results were discussed for different trim angles at design speed in calm water and regular head waves. The ship motions and added resistance were measured for several wavelength conditions considering short and long wave ranges with wave steepness of 1/60. Next, computations of the towed model in head waves were performed using Unsteady Reynolds-Averaged Navier-Stokes (URANS) CFD and 3-D potential methods. Effects of trim angles on added resistance were analysed and results concerning the performance of the vessel at different trim angles were plotted. Experimental and numerical results for the heave and pitch motions and the added resistance were compared and URANS CFD simulation results showed good agreement with the experimental data for the ship in head waves. Also, the results were compared to those from potential theory and a range of trim and wave conditions were identified for the application of the rapid linear potential flow method.

- Chapter 6 (Trim Influence on Propulsive Performance) In this chapter, trim influence on the propulsive performance of KCS was investigated. Three modelling scenarios were investigated. First, we carried out calm water resistance simulations at six different trim angles to identify the optimum trim condition. Self-propulsion simulations were performed using two different methods, namely, sliding mesh with 3-D propeller geometry and body force method based actuator disk approach. The commercial CFD software package STAR-CCM+ was used for grid generation and for the numerical simulations of the resistance and self-propulsion tests. Level trim simulations were compared with available experimental data to validate the numerical model. Effects of trim angles on propulsive characteristics were analysed and results concerning the performance of the vessel at different trim angles were plotted. The differences in optimum trim based on pure resistance simulations and self-propulsion simulations were investigated. As trim optimisation studies require the analysis of a large number of different operating conditions, the applicability and accuracy of the quicker simplified actuator disk approach was tested.

- Chapter 7 (Conclusions and Future Research) This chapter presents a discussion of findings from the thesis and determines how well identified research aim and objectives are achieved. It closes with recommendations for related future research areas.

1.5 Summary

This chapter presented the general perspectives, the motivations behind this work, the aims and objectives, and the layout of this thesis.

Chapter 2 Literature Review

2.1 Introduction

Chapter 2 is dedicated to the critical review of the state of the art. Current trim optimisation methods are introduced to create a better understanding of existing methods. The chapter initially sets the scene with the fundamentals of trim and different trim optimisation tools which are available in the industry. Then physical components of hull resistance is presented. Following this, methods that are utilized for the prediction of resistance, added wave resistance and propulsive performance will be discussed. The chapter finally concludes with the overall findings from the literature survey including the associated research gaps.

2.2 Background

The trim of a floating ship is defined as the difference in forward draft T_F and aft draft T_A, and can be expressed as distance t in unit meter as shown in Equation (2.1) or as angle θ in unit degree Eq.(2.2).

$$t = T_F - T_A \tag{2.1}$$

$$\tan\theta = \frac{T_F - T_A}{L_{pp}} \tag{2.2}$$

Thus, trim is positive if the ship is trimmed by the bow and negative if the ship is trimmed by the aft. If there is no difference between forward draft and aft draft, this floating condition is defined as level trim or even keel. A schematic representation of the trim terms is given in Figure 2-1.

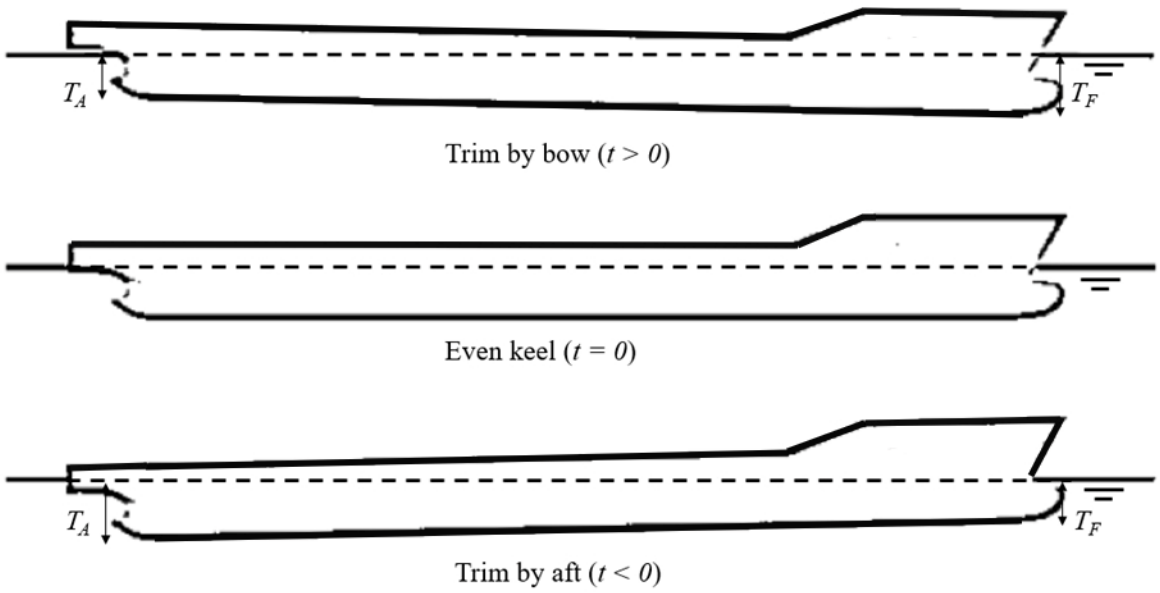

Figure 2-1 Description of trim conditions

As the ship trims around a transversal axis passing through the centre of flotation (LCF), this point is considered as fixed during the trim and draught of this point is the same as even keel condition.

Trim optimisation became widely popular within the marine industry in recent years. A market survey study conducted by HSH Nordbank (2013) with national and international shipping companies revealed that 71 per cent of the survey participants are using trim optimisation solutions for their ships. As it is already an attractive measure for ship owners, many different companies such as classification societies, ship operators and vessel monitoring system providers offer trim optimisation solutions. Some of the most significant trim optimisation tools that are available in the market and estimated savings are shown in the Table 2-1. According to these tools, vessels can expect to save 2-5% on average on fuel costs, with a corresponding reduction in greenhouse gas emissions when sailing under optimal trim conditions. Many of the available tools make use of CFD based databases while machine learning based trim optimisation systems are also popular within the industry.

Table 2-1 Some of the trim optimisation tools used in industry

Company	Product	Estimated Savings	Method	Maturity
DNV GL Group	Eco-Assistant	1% - 6%	CFD	Since 2009-10; over 200 vessels fitted.
GreenSteam	GreenSteam Data Collector and Optimiser	4% - 5%	Machine Learning	First tested in 2008; at least 17 installations to date
Force Technology	SeaTrim	3% - 15%	Model tests and CFD	First tested in 2007. Over 300 ships now using the product.
Eniram (Wartsila)	Dynamic Trimming Assistant	3-5%	Machine Learning	Installed on board many vessels since 2008 (Acquired by Wartsila in 2019)
Hapag-Lloyd	Trim Optimisation Software	1.5 – 2%	CFD	Installed trim optimisation software on 86 ships in 2016
ClassNK	ClassNK-NAPA GREEN	2.5 – 4%	CFD	Installed on-board many vessels since 2014
Herbert-ABS Software Solutions	Trim Optimisation Tool	n/a	Model tests	Loading software very well established (25 years), trim optimization tool since 2012.
Trelleborg	Trim Optimisation System	1 - 3%	Machine Learning	Developing Ship Performance Monitoring Systems for over 30 years
INTERSCHALT Maritime Systems AG	TROP trim optimisation module	2% - 3%	CFD	Trim TROP software element launched in 2012

SSPA has performed around 50 trim optimisation studies on a wide variety of ships, including LNG Carriers, tankers, bulkers, RO/ROs, PCTCs, containerships, and special purpose ships, such as reefer vessels (Abrahamsson, 2009). They have found that vessels with higher fuel consumptions and those that operate on long-haul well-defined trade routes such as: containerships, PCTCs, RO/ROs, and LNG Carriers can benefit the most from trim optimisation. It was stated that other type of ships can also benefit significantly by operating at a trim optimised condition. VLCCs and product carriers can achieve up to 10% to 15% in ballast and 5% to 8% in full load reduction in their powering requirements. They also stated the cost-effectiveness of the trim optimisation tools. It was noted that even if the ship does not achieve savings of high magnitude, an average power saving of around 1.25% (0.5% in full load and 2% in ballast condition) would be enough to cover the cost of a trim optimisation study in less than a year of utilisation. The payback time would be even shorter for a fleet of sister ships.

In recent years, machine learning techniques are also being used to identify the optimum trim condition. As the shipping industry is becoming more data-driven, machine learning based decision support systems have also been proven to result in considerable fuel savings for relatively low investment (Hansen and Freund 2010). These tools generally use real-time measurements from the sensors installed on ships in service and logged operational data to find the relation between trim and power and thus to calculate the optimal trim. However, this approach requires the installation of additional hardware and a lengthy data training period for the system to work efficiently. Bertram (2014) notes that these machine learning based systems may give good results but requires more training time and crew awareness.

2.3 Previous Research on Trim Optimisation

Following the popularity of trim optimisation as an attractive energy saving measure in the marine industry, an increasing number of researchers have studied the impact of trim on ship resistance. Hollenbach et al. (2007) investigated the importance of optimisation for off-design conditions to improve the overall performance of container ships. They have stated that small changes to trim on container ships may cause significant changes to power requirements as these vessels have large transom sterns and bulbous bows. Container ships have a high ballast water capacity to change the trim of the vessel therefore it may be easier to achieve savings

by adjusting the trim. Hansen and Freund (2010) stated that optimum trim changes for each vessel and operating parameters such as speed, draft and water depth. They have discussed the benefits of CFD based trim optimisation systems against other tools that use logged operational data to advise on optimum trim. It was shown that operating at optimum trim could save up to 9% instead of operating at level trim.

Larsen et al, (2011) carried out a broad trim optimization study, which involved investigation of resistance and propulsive origin factors by conducting model tests, high fidelity CFD and potential theory CFD. Detailed analysis of resistance coefficients, wake fraction, thrust deduction fraction, relative rotative and open water efficiencies were conducted. It was concluded that results from the model test were found in line with RANS CFD regarding the trim. However, potential theory CFD results didn't agree with two other methods and under predicted the change in performance when trimming. This may be explained by the use of simplified flow models in older CFD approaches. These methods such as potential flow, panel and Rankine singularity theory fail to predict breaking waves and have poor propeller modelling capabilities. Therefore, the results of these methods are less accurate compared to high fidelity flow models.

Kim et al. (2013) stated the increasing interest from shipowners regarding trim optimisation. They have presented an automated CFD analysis tool for trim optimisation. Numerical results were compared against experiments and found in good agreement at model scale. Bow trim conditions were found to be much more efficient especially in lower drafts due to differences in wave resistance.

Lv et al (2013) used a 3D panel method to investigate the wave-making resistance of Wigley hull operating at different trims and identified optimum trim angle for the lowest wave-making resistance. Benchmark Wigley hull was used to verify the method by comparing wave resistance and details of wave such as patterns and profiles. After that, numerical calculations are carried out for a container carrier at model scale and comparative model tests are conducted to assess the applicability of the method. It was found out that the proposed numerical method could be used for wave resistance prediction under certain trim and displacement conditions. Calculations proved that modified trim may reduce the wave resistance and results agreed with experiments.

Górski et al. (2013) also discussed the influence of trim on vessel performance. They focused on the understanding of the flow properties and their impact on ship resistance thus the fuel consumption and emissions. It was concluded that hull form is the most significant factor on effects of trim, especially for hulls with a bulbous bow or stern transom. They recommended the use of computational methods which can properly identify complex relationships and interactions of the flow around the hull in order to achieve savings on fuel consumption.

Reichel et al. (2014) have performed extensive series of experimental trim model tests for different ship types including tankers, container vessels, LNG carriers ro-ro vessels and the majority of them being container vessels. This study concluded that the change in trim mostly affected the wave-making resistance component of the total resistance. According to these tests, it is possible to achieve fuel savings of up to 15% at specific operating conditions compared to even keel. In overall fleet operations, it is possible to expect savings of around 2-3% through trim optimisation.

Iakovatos et al (2014) investigated the influence of trim on resistance of six different hull models through calm water experiments and pointed out the importance of experimental investigation of vessels' resistance performance to optimise vessels trim. Experiments were conducted for a semi-swath, a bulk carrier, a sailing yacht, a passenger vessel, a fishing vessel and a Ropax vessel. It was concluded that depending on the vessel type it is possible to achieve a reduction in total resistance by trimming the vessel properly. Trim by bow or by stern may have a positive or negative impact on the vessel's resistance depending on the vessel type and operating condition.

Sherbaz and Duan (2014) carried out a trim optimization study for KCS by employing CFD techniques at a model scale. The total resistance of KCS hull form is calculated at different Froude numbers to validate mesh, boundary conditions and solution techniques. After comparing these results with experimental values and finding good agreement, the same solution techniques were used to calculate resistance at different trim conditions. It was found that viscous resistance changes slightly with trim while wave-making resistance changes greatly similar to findings from other studies.

Park et al. (2015) carried out investigations on resistance performance for various trim conditions not only for the ship's original design speed but also for slow steaming conditions.

Further to the trim optimization, bulbous bow shape renovation was carried out for off design condition and both of CFD results, one is from an original bulbous bow shape, the other is from an optimised bulbous bow shape by the authors, are compared against each other to identify the reason for the improvement of resistance performance. They found that while wave-making resistance increased for all trim conditions, viscous resistance decreased in bow trim conditions.

Sun et al (2016) developed a trim optimization program through use of CFD for resistance calculations and tested it on a real container ship to prove the benefits of trim optimization. The numerical method is used to calculate the ship resistance at different trim conditions and to understand the reasons behind the resistance changes for trimmed conditions. The analysis of resistance components showed that the wave-making resistance component is the main source in the ship trim optimization for the container ship.

Maasch et al. (2017) investigated the extreme trim operation for an LNG carrier by conducting resistance and self-propulsion CFD simulations at ballast draft. Extreme trim concept focuses on operating at larger trim angles to reduce the ship's displacement and wetted surface area in order to achieve reductions in frictional resistance. They have achieved promising results with up to 28% reduction in delivered power.

2.4 Physical components of Hull resistance

In order to investigate the trim influence on ship resistance, one should understand ship resistance components and their behaviour. The resistance decomposition concept is well documented in the literature, e. g.(Larsson and Baba, 1996), (Molland, 2011). Therefore, this section can be limited to a short description of modern methods in resistance decomposition.

As the ship moves through water two features of flow can be observed; the wave pattern which is generated by the hull and turbulent flow along hull length and (as an extent of that) the wake which is formed behind the hull. Figure 2-2 shows the wave pattern and the formation of the wake.

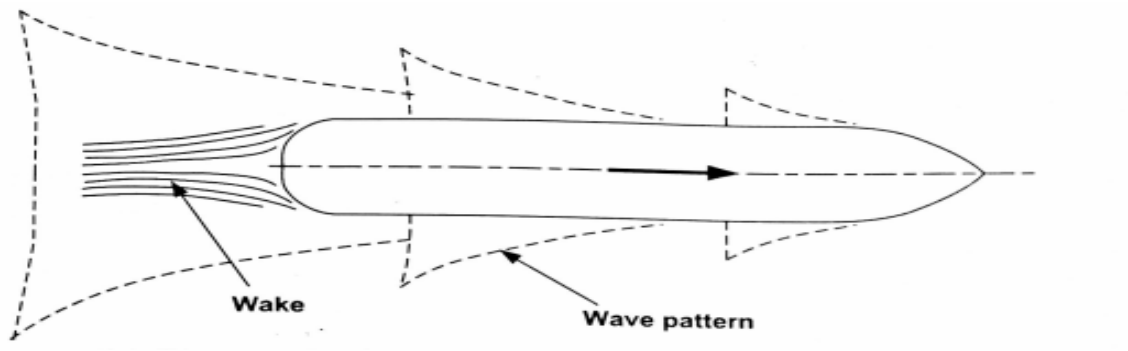

Figure 2-2 Wave pattern and formation of the wake behind the hull (Molland, 2011)

As a result, the waves and the wake absorb energy from the hull and hence create a resistance force on it. This resistance force is imparted to the hull as a distribution of pressure and shear forces on it. This phenomenon leads to a physical breakdown of resistance into the forces acting:

- Friction resistance (R_F)

The frictional resistance or total shear resistance is produced from the sum of fore and aft components of the tangential shear forces which act on the hull surface (Molland, 2011).

- Pressure resistance (R_P)

The total pressure resistance is the sum of the fore and aft components of the pressure force which act on each element of the hull surface. Due to the viscosity, the friction drag is developed, but the pressure drag depends partly on viscous effects and partly on hull wave-making (Molland, 2011).

- Total viscous resistance (R_v)

The ship's form creates a local flow field with velocities which is usually lower than the average velocity, although the average of the resulting shear stresses is higher. In addition, the vortices, the flow separation and the energy losses in the boundary layers prevent the increase of the stagnation pressure in the aft body. The viscous pressure resistance is higher on ships with full ship form than those with slender form (Bertram, 2012). The total viscous resistance is the sum of the skin friction resistance (R_F), the viscous pressure resistance (R_{PV}) and the wave breaking resistance (R_{WB})

- Wave making resistance (R_w)

The wave pattern can be analysed and measured into its components waves. The total wave resistance can be found by estimating the energy which is required to maintain each wave component (Molland, 2011). The wave resistance is made up of two parts, the basic hull wave-making resistance (R_{WM}) and the wave-breaking resistance (R_{WB}), which can be found by measuring the wave elevations from the ship.

Figure 2-3 shows how the total resistance (R_T) is affected by the different components of resistance and how each component interacts with the other.

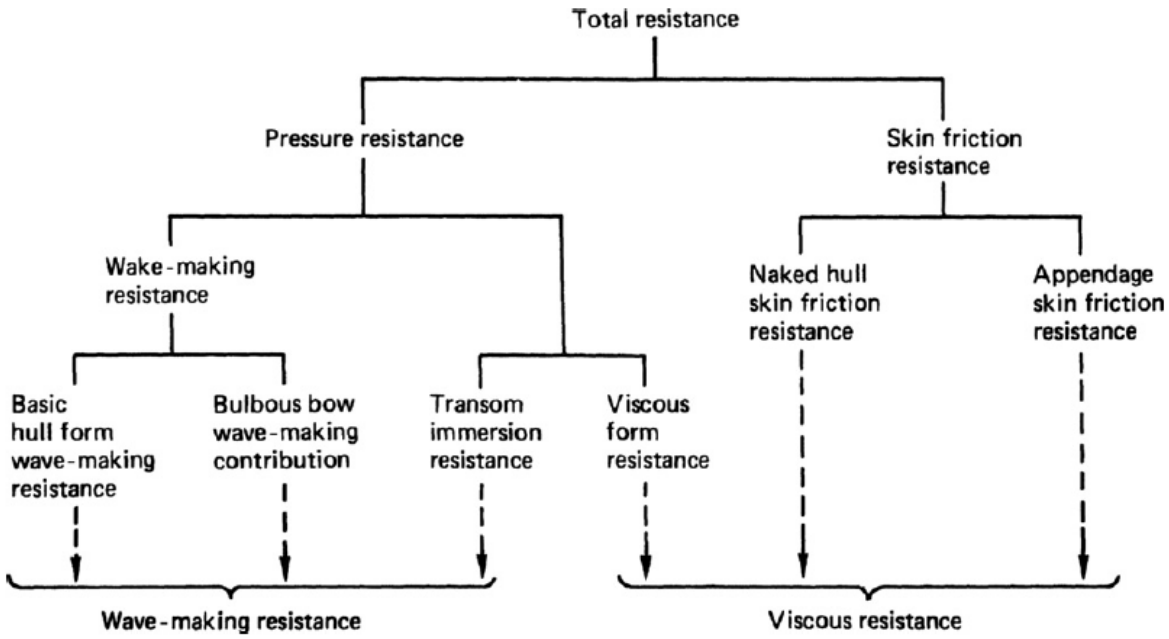

Figure 2-3 Components of ship Resistance (Carlton, 2012)

It can be seen that wave-making resistance consists of basic hull form wave-making resistance, bulbous bow wave-making resistance and transom immersion resistance. Bulbous bows and transom sterns are commonplace in the design of modern ships. Bulbous bows and transom sterns affect the resistance of the ship in several ways. As trimming the vessel would change the effective shape of the bulbous bow and may lead to transom immersion, it is possible to say that wave-making resistance would be the most affected resistance component by trim.

Furthermore, there are also some other additional resistance components that contribute to total ship resistance under service conditions, and they are known as secondary components. The prediction of the secondary components is important to estimate the maximum resistance

of a ship during its operation. The secondary components of resistance include the effects of appendages, roughness, shallow water and the added resistance due to wave and wind (R. Silva, 2013).

The appendage resistance is associated with the resistance due to the shaft, bilge keels and the rudder (R. Silva, 2013). In model tests, the appendages may be fitted to the models. In case where there are no appendages fitted on the hull, the resistance is called the bare hull resistance.

Shallow water operation causes an increase in friction resistance and also increases wave resistance. Model tests and numerical simulations can be used to investigate shallow water effects. (Bertram 2012).

The roughness of the hull, which might occur due to corrosion or due to the fouling condition, can increase the friction resistance considerably.

Wind resistance is associated with the above water hull and superstructure in motion of the ship through the air (Molland, 2011). It is especially important for ships with large lateral areas above the water level such as container ships and car ferries. In high-speed models, the air resistance can be significant and correction data should be used (Molland, 2011).

Another important component of resistance is the added seaway resistance which is characterized as an additional power to retain the required speed or as speed loss to maintain the engine's power constant (Bhattacharyya, 1978). The added resistance of a ship can be determined by experimental and computational methods and will be discussed in detail in section 2.5 of this literature review.

2.4.1 CFD applications for Prediction of Ship Resistance

Prediction of resistance is one of the oldest applications of CFD in ship hydrodynamics. The accuracy and capability of these methods have improved significantly with the developments in computer technology.

Table 2-2 below illustrates the historical development of numerical methods in ship resistance through main workshops and state of art capability at the time. It is possible to say that, for types of ships and operating conditions which have been analysed in these

workshops, the fidelity of CFD for resistance prediction has now reached and exceeded a level that is sufficient to be considered as a design tool. Surveying these workshop results reveals that resistance of the model-scale ships selected for test cases can be predicted, on average, within a few per cent from measurements made in towing tanks.

Table 2-2 Historical development of CFD capabilities for evaluating ship powering (Molland, 2017)

Location	Year	ITTC Proc. Resistance Committee[1]	Methods used	Test cases
Gothenburg	1980	16th (1981)	16 boundary layer-based methods (difference and integral) and 1 RANS	HSVA tankers
Gothenburg	1990	20th (1993)	All methods RANS except 1 LES and 1 boundary layer	HSVA tankers
Tokyo	1994	21st (1996)	Viscous and inviscid free-surface methods, and viscous at zero *Fr* (double hull)	Series 60 ($C_B = 0.6$) HSVA tanker
Gothenburg	2000	23rd (2002)	All RANS but with/without free-surface both commercial and in-house codes	KVLCC2, KCS, DTMB5415
Tokyo	2005	25th (2008)	RANS with self-propelled, at drift and in head seas	KVLCC2, KCS, DTMB5415
Gothenburg	2010	26th (2011) 27th (2014)	RANS with a variety of turbulence models, free surface, dynamic heave and trim, propeller, waves and some LES	KVLCC2, KCS, DTMB5415
Tokyo	2015[2]	28th (2017)	Two new hulls including Energy Saving Devices (JBC), Seakeeping, self propulsion and coursekeeping.	JBC, KCS, ONR Tumblehome

1994 Tokyo CFD workshop was organised to discuss viscous flow prediction with free surface and very good predictions of the wake contours of the surface ship were presented. As pointed by Zhang et al., by the time of the 2000 CFD workshop in Gothenburg, free surface RANS solvers had been remarkably improved and RANS methods have been widely used in many marine hydrodynamics applications. In 2005, self-propulsion prediction was included in the CFD workshop in Tokyo. In Tokyo 2015, a new benchmark ship Japan Bulk Carrier (JBC) was included for the first time to investigate the performance of Energy Saving Devices (ESD).

Recent results from the CFD workshops prove the ability and reliability of using CFD methods in ship hydrodynamics. (Larsson et al. (2014), Larsson et al. (2018)) Results from the CFD workshop in Gothenburg 2010 concluded that mean comparison error was below 2 per cent of the experimental values. The mean standard deviation was found 2.1% which proved a significant improvement from the 2005 result of 4.7%. RANS modelling approach is the most popular method for resistance simulations. surface capturing methods such as VOF and level-set for free surface. Two equation based, isotropic eddy viscosity turbulence models like k–ε and k-ω models are commonly used. Increasing use of high-performance computers in recent years allows creating larger grids from a few up to tens of million points to improve the spatial resolution of turbulent boundary layer and wake based on the area of interest.

In proceedings of 28th ITTC conference, CFD was deemed as a reliable tool to determine the resistance of ships however it was noted that a deviation of 3% to 8% may still be observed in comparison with model tests.

2.5 Added Wave Resistance

Added wave resistance is part of a ships total resistance that is caused by the encounter with the waves. It is defined as the difference between resistance in waves and resistance in calm water as illustrated in Figure 2-4.

Ship's performance in waves varies greatly from that in calm waters rough due to added wave resistance. (LLOYD, 1998) Added resistance can cause a 15-30% increase in the total resistance of the ship in a seaway (Perez Arribas, 2007). Therefore, prediction of added resistance is essential to evaluate the performance ships in service and many different approaches such as experimental, potential flow and CFD based methods have been developed in this respect.

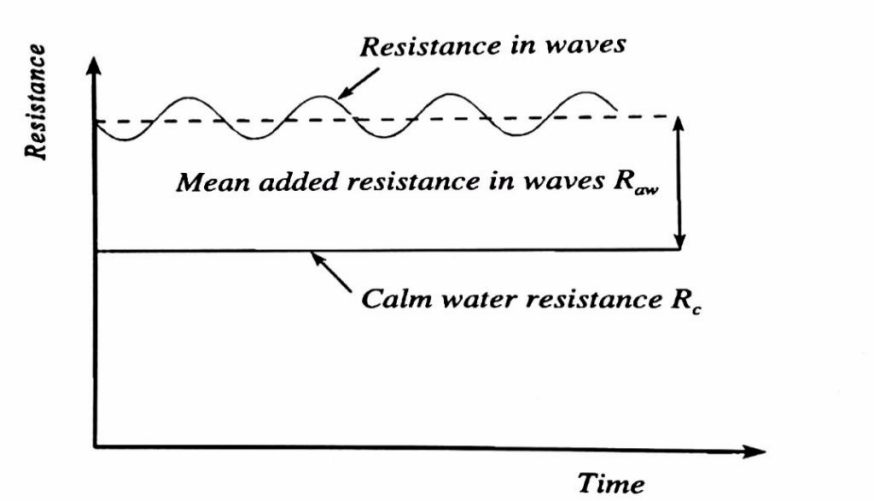

Figure 2-4: Added Resistance due to Waves (LLOYD, 1998)

2.5.1 Prediction of Added Wave Resistance

The prediction of the added resistance is vital to evaluate the ship performance in a seaway as there will always be waves on the sea. Therefore, it has been widely researched in the past years. Prediction of added resistance in waves is still a discussion topic within the marine research environment. Bertram (2016) discusses that there are no reasonably satisfactory methods available to predict the added power requirements in seaways at the present time. There are various methods that are being used. In general, model tests, numerical analysis, full-scale measurements and statistically derived design formulae are the main methods in this respect. Table 2-3 summarises these various experimental and numerical methods.

In model experiments, the model is tested in regular or irregular waves and the difference between the time-average of resistance in waves and still water at the same velocity is the added wave resistance (Bhattacharyya, 1978). Towing tank experiments are generally conducted for the head sea condition as the maximum added resistance is observed in head seas. Model tests can be expensive and time-consuming due to the waiting time between tests before the water is sufficiently calm enough for the next run. As it is necessary to build a physical model, towing tank experiments do not allow much flexibility for different design explorations in the early design stages. Also, scale effects and measuring uncertainties are present for motions with strong viscous effects. Despite these, experiments provide valuable information for the validation of numerical methods.

Table 2-3 Summary of prediction methods for added resistance due to waves (ITTC 7.5-02-07-02.8)

Type of Methods		Slender-body Theory	3D Panel Method		CFD	Experiments
			Frequency Domain	Time Domain		
Approach		2D Strip Method	Green Function		Euler Equation Based	Captive Test Regular or irregular wave
		Enhanced Unified Theory EUT	Rankine Panel Method		Navier-Stokes Equation Based	Free sailing Regular or irregular wave
Formulation	Far-field Method	Maruo's Formula	Momentum Conservation Method		*None*	*None*
	Near-field Method	*None*	Direct Pressure Integration Method		Direct Pressure / Shear Stress Integration	Total Force Measurements
	Short-wave Approximation	NMRI Formula	NMRI formula can replace diffraction components		*No need*	*No need*
Fidelity		Low	Good		Excellent	Excellent
Typical requirements: Hardware;Time		Personal Computer; Minutes	Computer Cluster or PC; Hours-days		Cluster; Days	Seakeeping basin; Days

Many researchers have investigated added resistance problem using linear and non-linear potential flow based methods over the years. Havelock (1940) became one of the first who expressed the analytical method for added wave resistance in regular waves (R_{AW}). This expression is a function of pitching and heaving and is written as follows:

$$R_{AW} = -\frac{k}{2}(F_a z_a \sin\varepsilon_{zF} + M_a \theta_\alpha \sin\varepsilon_{\theta M}) \tag{2.3}$$

where k is the wave number, Fa is the amplitude of the exciting force in heave, M_a is the amplitude of the exciting moment in pitch. z_a and θ_α are the amplitudes of the heave and pitch motions, ε_{zF} is phase lag between the exciting force and the heaving motion $\varepsilon_{\theta M}$ represents the phase between the exciting moment and the pitching motion.

Computational methods have evolved for seakeeping analysis since the 1950s. Many improvements have been developed on Havelock's analytical method in order to predict the added wave resistance. Strip methods are the oldest and most popular approach for seakeeping analyses. Strip methods are able to calculate heave and pitch motions reasonably

accurate for normal ships. There are two major techniques used to predict added resistance, namely the far-field method and the near-field method.

The far field method is based on momentum and energy conservation principles. It was first introduced by Maruo (1957) using the Kochin function which includes radiating and diffracting wave components. Joosen (1966) and Newman (1967) also applied this method to predict added resistance and wave drift of ships. Following this, Gerritsma and Beukelman (1972) introduced the radiated energy approach to predict added resistance in head seas which was widely used in strip theory codes due to its easy application. Salvesen (1978) confirmed the importance of accurate ship motion estimations to reliably predict added resistance in waves with the use of ship motions obtained from the strip theory method of Salvesen et al (1970).

In the near field approach, the added resistance is predicted by integration of the hydrodynamic pressure on the wetted body surface using Bernoulli's equation, and a Taylor expansion of the pressure about the mean position of the ship. It was first introduced by Boese (1970). Many researchers used the near-field method to investigate the added resistance Faltinsen et al (1980), Joncquez et al (2008), Kim and Kim (2011).

Findings from early analytical methods for the investigation of added wave resistance can be summarised as follows (Bhattacharyya, 1978):

- The added resistance in small waves is proportional to the square of the wave height
- Added resistance is a function of the pitch and heave motions and their phase relationship with the waves
- Added resistance is a non-viscous phenomenon and occurs due to the inertia and wave effects. Hence, according to the law of Froude, the added resistance of a full-scale model can be estimated by multiplying the added resistance of the model scale by the cube of scale factor.

On the other hand, as computational power increased significantly and access to these computational facilities became more widely available over the years, CFD techniques based on the solution of Reynolds Averaged Navier Stokes (RANS) have become a powerful tool to study ship motions and added resistance. Simonsen et al (2013) stated the importance of including effects of breaking waves, turbulence and viscosity in numerical methods, which

are ignored in the potential theory approach. RANS methods are capable of doing this as viscous effects can directly be incorporated into their equations. Many studies demonstrated the ability of CFD methods against experimental studies. Sato et al (1999) carried out one of the early studies to predict the motions of the Wigley hull by using CFD simulations. Orihara and Miyata (2003) investigated added resistance and motions of the S175 container ship with different bulbous bows using the RANS method. As the RANS method provided good results, more researchers used it to study different geometry and cases. Carrica et al (2007) studied the motions of a DTMB 5512 model in regular, small amplitude head waves. Castiglione et al. (2011) performed seakeeping analysis of a catamaran in waves with high wave amplitudes using the URANS approach. Simonsen et al. (2013) investigated the added resistance, ship motions and wake flow field of KCS in regular head waves by using Experimental Fluid Dynamics (EFD) and CFD methods. Tezdogan et al. (2015) focused on predicting ship motions and added resistance of full scale KCS at design and slow steaming speeds by performing URANS simulations using Star CCM+. An increase in effective power and fuel consumption due to added resistance was also calculated. Park et al (2016) investigated the added resistance of KVLCC2 tanker in head waves at different drafts by using EFD and potential theory methods. Kim et al. (2017) predicted the added resistance and ship motions of KVLCC2 at various speeds and wave steepnesses. Recently, Sigmund and el Moctar (2018) carried out an extensive study to investigate the added resistance and ship motions of four different ship types, which includes a cruise ship, a post-Panamax containership, a tanker, and Wigley hull, in short and long regular head waves and validated the results against experiments. Hizir et al. (2019) investigated the added resistance force components and non-linearity of added resistance and ship motions of KVLCC2 using CFD and 3-D potential flow methods.

To summarise, studies have shown that many different factors affect added resistance such as hull form, ship motions, speed, wave characteristics (height, length, steepness), wave encounter angle. Applicability of CFD and potential flow methods have been well investigated for ship added resistance prediction. However, the influence of trim on added resistance is less investigated and remains as a gap in the literature.

2.6 CFD applications for Prediction of Propulsive Performance

Accurate prediction of the self-propulsion performance of a ship is one of the main challenges in marine hydrodynamics. The traditional way to understand the propulsive performance of a ship is to conduct self-propulsion tests in a towing tank and extrapolate the results to full scale by following ITTC guidelines (ITTC, 2017). However, there are several difficulties and shortcomings regarding the towing tank tests. Self-propulsion experiments require rather larger facilities and experimental results from the model tests are subject to scale effects as the complete hydrodynamic similarity cannot be achieved between model and full-scale ship and flow properties are difficult to measure.

In recent years, Computational Fluid Dynamics (CFD) methods have been commonly used to predict the ship performance in line with rapid developments in computational resources and software programs. The use of CFD in self-propulsion prediction has gone through continuous improvement with the support of regularly held CFD workshops which included self-propelled cases (Larsson et al. (2014), Larsson et al. (2018)). KCS vessel has been used as a benchmark case in these workshops and also by many other researchers due to available open-access experimental data.

Many studies investigated calm water propulsion characteristics of KCS using simplified body force based methods without geometric modelling of the rotating propeller. (Krasilnikov (2013) Windén et al., (2014), Fu et al. (2015)) Using such methods can reduce the required computational effort significantly. Many researchers also investigated self-propulsion characteristics of KCS with actual rotating propeller geometry using sliding or over set grid methods at level trim condition (Lubke (2005), Carrica et al. (2010), Seo et al. (2010) Bugalski and Hoffmann (2011), Gaggero et al. (2015)). The results from such investigations mostly showed good agreement with experimental data. Following the experience gained from model scale predictions, an increasing number of studies focused on full-scale investigations in recent years. Bhushan et al. (2009) performed one of the early full-scale, self-propelled simulations for the fully appended Athena using rough-wall conditions. As they didn't have ship trials data, results were compared with the full-scale data extrapolated from model-scale measurements. Following this, Castro et al. (2011) performed full-scale self-propulsion computations of the KCS with the direct discretisation of the propeller using the dynamic overset approach. Results showed a good agreement with the

available data obtained in model scale following the ITTC testing procedures and differences in flow field between model and full scale were discussed. Visonneau et al. (2016) investigated the performance of energy-saving devices for another benchmark vessel, Japan Bulk Carrier, in the model and full scale.

Despite the above-mentioned studies focusing on prediction of self-propulsion characteristics of KCS at level trim, trim influence on propulsion performance has not been satisfactorily studied in the literature and remains as an important research gap. This study therefore aims to contribute to the literature in this field by investigating trim influence on the self-propulsion performance of KCS by utilising state of the art CFD methods.

2.7 Conclusion

This chapter has reviewed the literature on existing methods to understand the effect of trim on hull performance. Those various studies mentioned above provide a useful insight about the influence of trim on ship performance. However, it was shown that those studies still fall short of explaining the reasons behind changes in ship resistance at different trim operating conditions. The impact of trim on added resistance in waves and on propulsive performance is even less well understood.

As this study will mainly employ the use of CFD methods, CFD applications for the prediction of ship resistance, added resistance and self-propulsion performance have also been reviewed.

The following conclusions can be derived from the literature review study:

- Overall, it is possible to say that limited research has been performed to investigate the effects of trim on ship resistance. No specific CFD studies exist to compare the differences in optimum trim at model scale and full scale.
- It was found that the majority of trim related studies have been performed at calm water and many of the added resistance studies have been conducted at level trim angles. No specific study has been performed to investigate the trim influence on added resistance.

- Although there are many studies focusing on self-propulsion characteristics, the influence of trim on propulsion characteristics is rarely investigated. To the best of the author's knowledge, there is no study that investigated the trim influence on the self-propulsion performance of KCS.

Therefore, it is possible to say that the state of the art is missing detailed information that can be produced by means of an extensive experimental and numerical investigation to enable the prediction of trim influence on resistance, added resistance and propulsive performance.

Chapter 3 Methodology

3.1 Introduction

Chapter 3 is dedicated to the presentation of the experimental and numerical methods used within the framework of this thesis. The chapter initially provides information about the Kelvin Hydrodynamics Laboratory. Following this, model details, preparation for experiments, test methodology are outlined. After that, the computational fluid dynamics (CFD) method is presented with a brief introduction to the numerical modelling approach.

3.2 Experimental Fluid Dynamics (EFD)

In the previous chapter, it was stated that model testing in a towing tank is the traditional way to understand the effect of trim on hull performance. Model experiments provide many benefits for the prediction of resistance and especially the seakeeping performance of a ship. It is very difficult to predict the performance of a ship in various weather conditions without model tests experiments. The cost of conducting model experiments is relatively low considering the achieved valuable and useful data (LLOYD, 1998). Even though computational methods are rapidly becoming more useful as computers become more powerful and available, tank testing is still regarded as the most accurate way of providing reliable results for ultimate confidence. Experimental results are also the principal verification source for any numerical method result. The model is built before the ship and then many tests may take place in order to find the optimum hull design which will satisfy the operational requirements.

3.2.1 Kelvin Hydrodynamics Laboratory

Experiments were carried out in the Kelvin Hydrodynamics Laboratory of the University of Strathclyde. Kelvin Hydrodynamics Laboratory has the following specifications and features:

- Tank dimensions (LxWxD): 76m x 4.6m x 2.5m (Figure 3-1)
- Carriage: Driven along rails by a computer-controlled digital driven DC motor. The carriage has a velocity range of 0-5 m/s
- Wavemaker: Variable water depth computer-controlled four-flap absorbing wavemaker. Capable of generating regular and irregular waves of up to approximately 0.5m (Figure 3-2)
- Beach: At the opposite end to the wavemaker is a highly effective sloping beach to absorb the waves at the end of the tank and reduce reflection.
- Data acquisition and control system: PC based. (Up to 64 input and 20 output channels, sample rate up to 60Hz)

Kelvin Hydrodynamics Laboratory also consists of a workshop with a CNC router where models can be built. A trimming dock is located at the end of the tank in order to carry out the ballasting of the model and the inclining experiment. An overhead crane with scales enables to lift the model in and out of the model basin and ensure the mass of the model is correct.

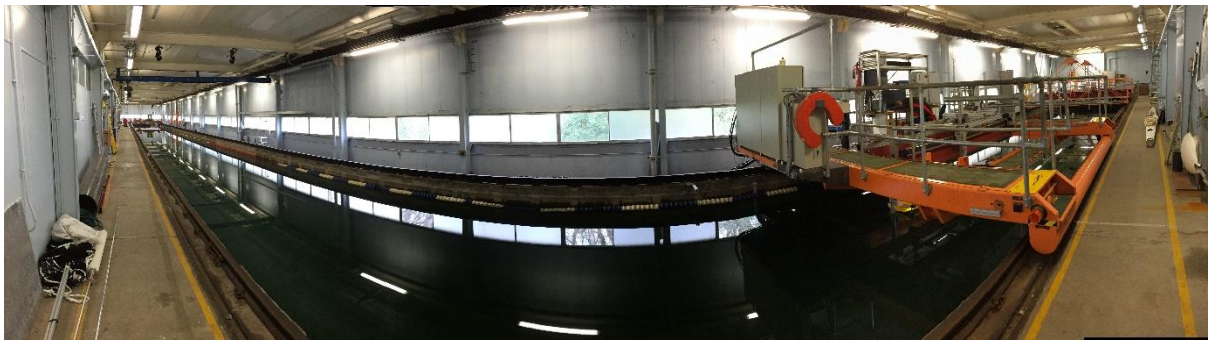

Figure 3-1 Kelvin Hydrodynamics Laboratory

Figure 3-2 Absorbing Wavemaker at Kelvin Hydrodynamics Laboratory

3.2.2 Description of the tested model

A model of the Kriso Container Ship (KCS) is used during the tests. KCS was designed by the Korea Research Institute of Ships and Ocean Engineering (KRISO) The KCS was originally developed to provide data for both flow physics analysis and CFD validation for a modern design container ship with a bulbous bow. Since conceived as a preliminary design in the 1980s, KCS is now widely used for investigation in numerical and experimental hydrodynamics as a benchmark ship model. Even though container ship designs change over the years, quantity of available data and open-source nature of the KCS container ship makes it a suitable selection for the scope of this study.

The model was constructed as geometrically similar to the full scale ship with a scale factor of 1/75. The model size was decided by considering the dimensions of the towing tank. Principal dimensions of the full scale and model scale ship are given in Table 3-1.

Table 3-1 Principal particulars of KCS in full-scale and model-scale

Dimensions	***Full scale***	***Model Scale***
Scale	1.00	75
LPP (m)	230.0	3.0667
BWL (m)	32.2	0.4293
D (m)	19.0	0.2533
T (m)	10.8	0.144
Displacement (m^3)	52030	0.1203
S w/o rudder	9530	1.675
CB	0.651	0.651
CM	0.985	0.985
Test condition		
T	10.8	0.144
Displacement (m^3)	52030	0.1203
S (m2) w/o rudder	9645	1.675
LCG	111.6	1.49

GM	0.60	0.097
Ixx/B	0.40	0.40
Izz/Lpp	0.25	0.25
Design speed		
U (m/s, full scale: kn)	24	1.426
Fr (based on Lpp)	0.26	0.26

Figure 3-3 KCS model

The model was of the bare hull surface (i.e. no appendages e.g. rudder, bilge keels). It was constructed of Glass Reinforced Plastic (GRP) and then a coating was applied. The inside of the model consisted of a hollow box lined with wood. This was to allow various mass

distribution inside the model to obtain different trim angles and for the location of the tow point. The model tow point is located at the LCG of the vessel and at a vertical point relative to the shaft line (Figure 3-4).

Studs are applied at the bow of the model in order to trip up the flow around the hull from laminar to turbulent flow as shown in Figure 3-4. This is done to ensure that turbulence is present over a realistic portion of the hull. The location of these studs was determined following International Towing Tank Conference (ITTC) set rules. (ITTC, 2002).

Fresh water was used in the experiments. The temperature of the water was monitored during the experiments in order to be able to evaluate the viscosity of the fluid according to the temperature.

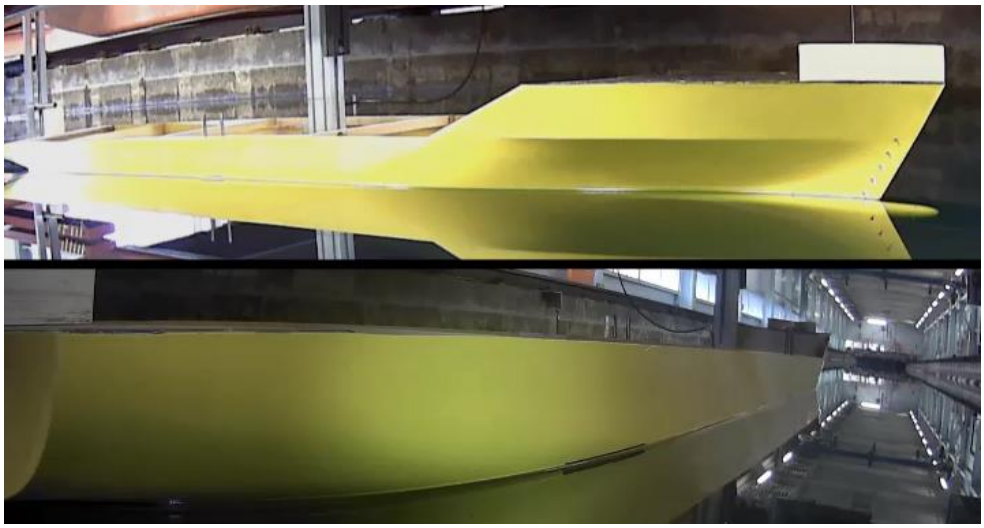

Figure 3-4 KCS Model attached to the carriage

3.2.3 Test Procedure

3.2.3.1 Ballasting the model

The model was weighted using the scales attached to the crane and weights were applied to achieve the total mass of the model to 120.3 kg as calculated. The total mass included all installed measurement devices and auxiliary components such as ultrasonic sensor, supporting structure, the tow point and the yaw guide that were attached to the model.

3.2.3.2 Inclining Test

After it was ensured that the model was ballasted correctly, the next step was to perform an inclining test to determine the vertical centre of gravity of the model. The position of the centre of gravity is vital as it determines the stability of the vessel. The inclining experiment is done by moving known masses over known distances across the beam of the model and measuring heeling angles (Figure 3-6 Swing test). From these values and use of geometry, the KG of the model is calculated.

Figure 3-5 Inclining test

The details of the inclining experiment can be listed as follows:

Two masses are placed on each side of the model on the top deck at the point of the LCG

The distance between the centres of the masses is measured. Half of which is the distance of each mass from the centre line of the model.

An inclinometer connected to a computer running the data recording program

After the accuracy of the acquired KG was deemed appropriate, the pitch radius of gyration (K_{yy}) could then be obtained. This determines how the vessel will pitch in waves. K_{yy} value is equal to 0.25 L_{BP} for most ships. This process involves swinging the model on a swing in the air and calculating its natural period through the mean period of a number of oscillations as shown in Figure 3-6 (Begovic, Day & Incecik 2011).

Figure 3-6 Swing test

3.2.3.3 Sensors

The following list contains the sensors that were installed to record the vessel motions and loadings during the towing test runs:

- One linear variable displacement transducer (LVDT) is located on the tow post and measures the vertical displacement of the model at this point i.e. the sinkage.

- The second LVDT is located at the bow of the model and records the vertical displacement of the bow i.e. bow motion.

• An ultrasonic sensor projects vertically downwards at a position forward of the bow. This measures the height of the water surface relative to the vessel.

• A load cell is located at the point by which the model is towed and therefore measures the force required to tow the vessel

• Another ultrasonic sensor is used and is attached to the towing carriage away from the model. This device measures the waves in the tank at an encounter velocity (i.e. carriage speed in head seas)

• There is a device that accurately measures the actual speed of the carriage within the drive system as the actual speed may slightly differ from the target speed.

• A laser distance measuring device on the carriage is used to measure the distance of the carriage from the wavemaker at the end of the tank.

• A wave probe is located in the tank close to the wavemaker and measures the amplitude of the generated waves.

The experimental setup is schematically shown in Figure 3-7.

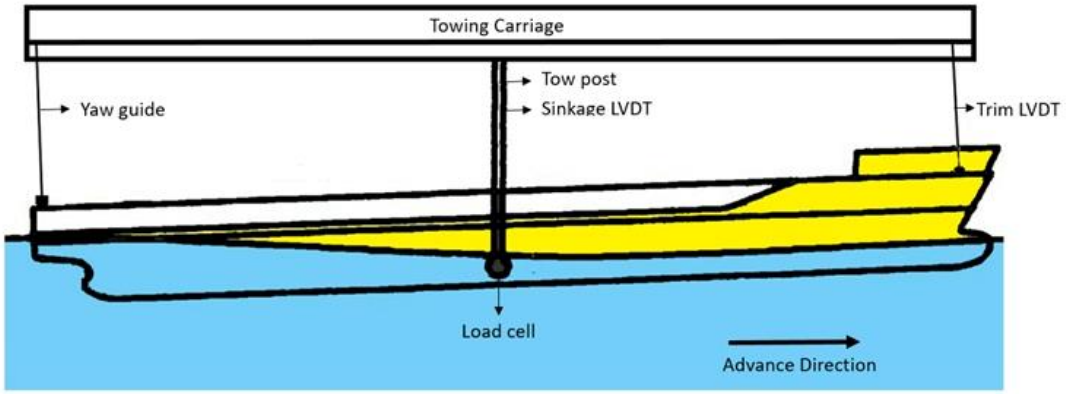

Figure 3-7 Experimental setup

3.2.3.3.1 Data Acquisition

A PC-based data acquisition running the “Spike” software and a CED 1401 A/D converter system was used to log all the measured data from the sensors listed above.

- Trim – Knowing the vertical displacement of the model at the tow point (sinkage) and the vertical displacement of the model at the bow (bow motion) and the distance between the LVDTs the trim angle of the model can be determined for each sampling point.
- Bow Sonic – Ultrasonic sensor at the bow
- WP Tank – Tank wave probe
- Carriage sonic – Ultrasonic sensor on carriage
- Bow motion – LVDT bow
- Sinkage – LVDT tow post
- Drag – Load cell
- Speed – Actual carriage speed measurement

A camera was also installed on the carriage in order to capture the motions at the bow and stern during the tests.

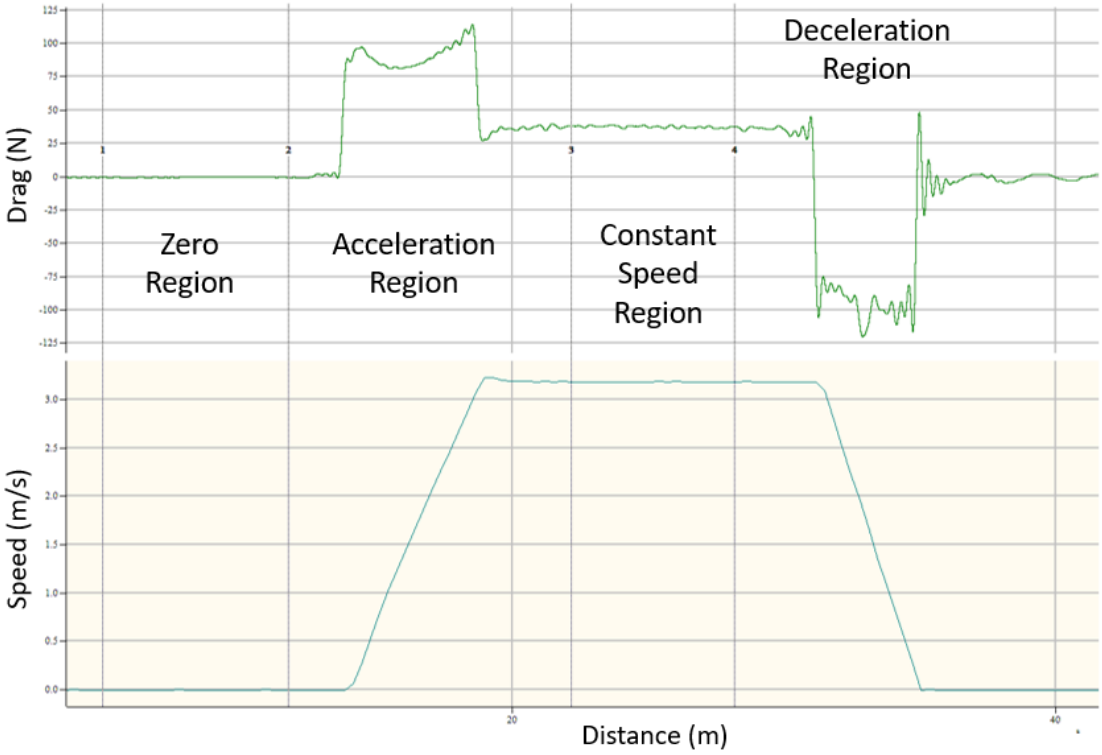

Figure 3-8 Data recording sample from tests

Figure 3-8 shows recorded data sample from a completed run of the carriage. Zero value of all measurements are taken before each run for a period of approximately 10 seconds while the model is stationary. After that, carriage starts to move and model is accelerated up to a desired speed and then speed is kept constant until the end of the tank where it is decelerated to a stop. Readings of the values are taken from constant speed region as shown in Figure 3-8.

3.2.4 Calibration of Equipment

It is essential to check the precision and calibration of measuring devices before performing towing tank tests. These devices are two LVDTs for measuring sinkage and bow motion, the load cell and the tank wave probe.

3.2.4.1 LVDT Calibration

The Linear Variable Differential Transformer (LVDT) is a device that converts a linear displacement into an electrical signal (voltage). This voltage is measured and multiplied by the factor to get a result for the vertical displacement. The LVDT for measuring the sinkage

and the bow motion were calibrated using a CNC machined block with known distances marked on it. Block is moved known distances and the voltage is measured at each displacement. Measured voltage values were recorded and plotted against displacement as shown in Figure 3-9 and Figure 3-10. A straight line is fitted through the points and the gradient of the line is calculated. The inverse of the gradient is the factor that is used to set the amplifier to give the accurate linear displacement measured by the LVDT.

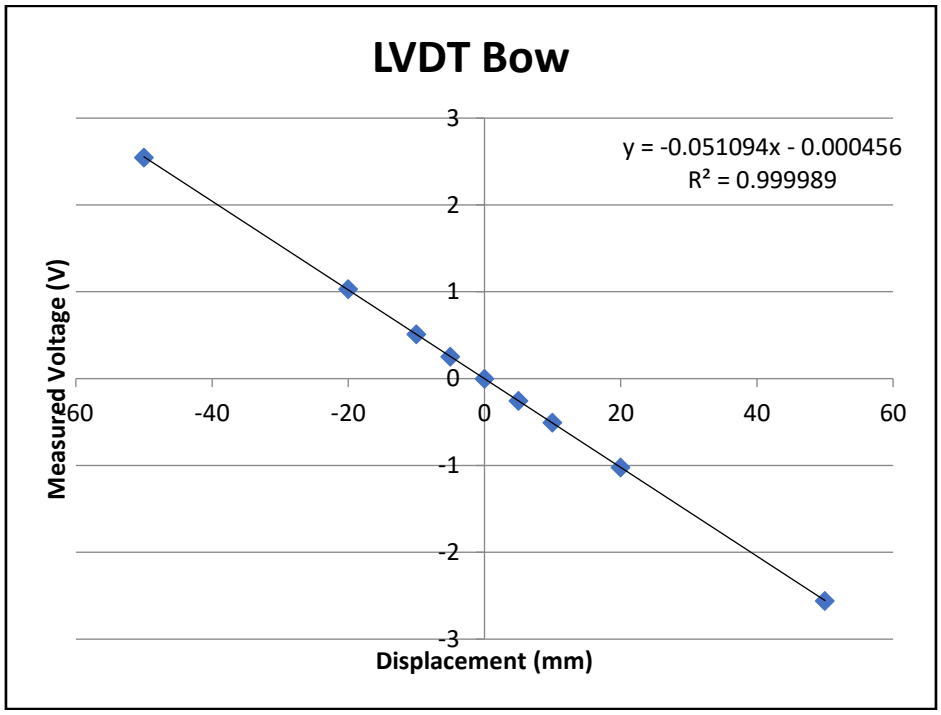

Figure 3-9 Bow LVDT calibration

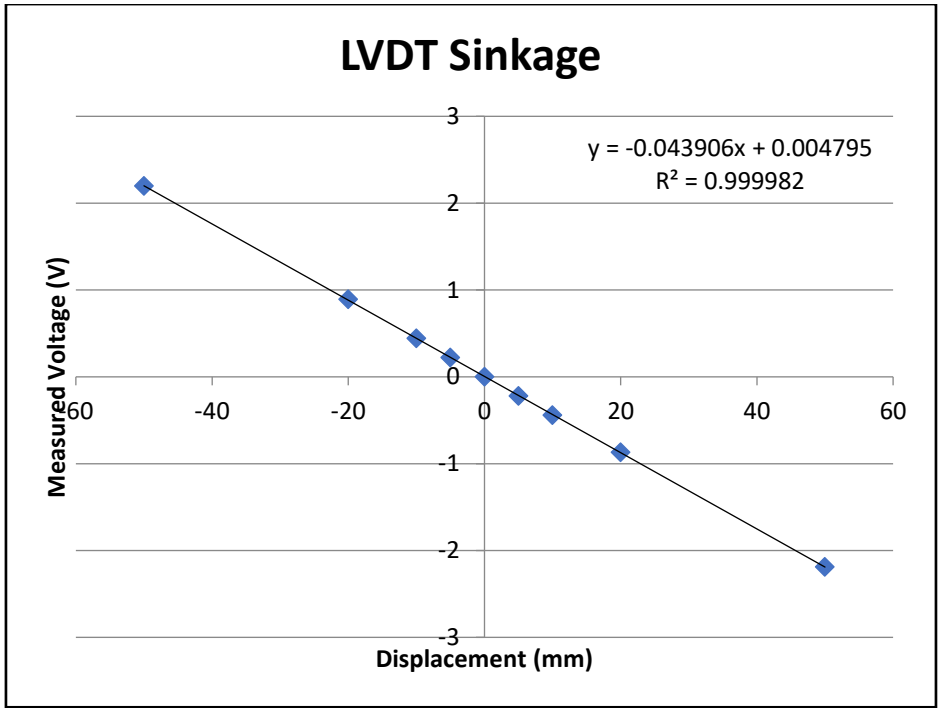

Figure 3-10 Sinkage LVDT calibration

3.2.4.2 Load cell calibration

A load cell can be defined as a transducer that converts a force into an electrical signal using a strain gauge arrangement within the device. The load cell is calibrated by securing it to a fixed point and suspending known weights from it and measuring the voltage so that a correlation and a zero value could be found. The weights were increased gradually to produce a proportional curve for the voltage induced against weight. Plotting the measured voltage against force a linear relationship is established. The graph from the load cell calibration is shown in Figure 3-11 and Figure 3-12.

Again a straight line is fitted through the points and the gradient of the line is calculated. The inverse of the gradient is the factor that is set in the amplifier in order to give a true reading for the load cell force.

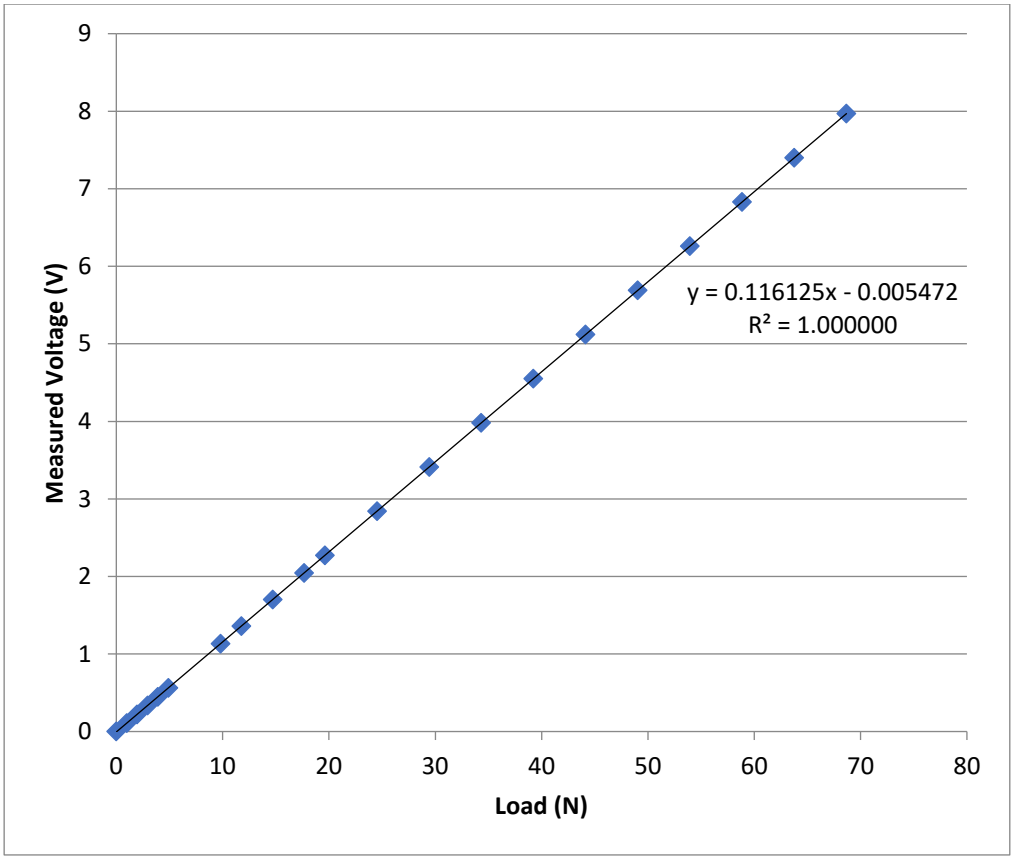

Figure 3-11 Load Cell calibration

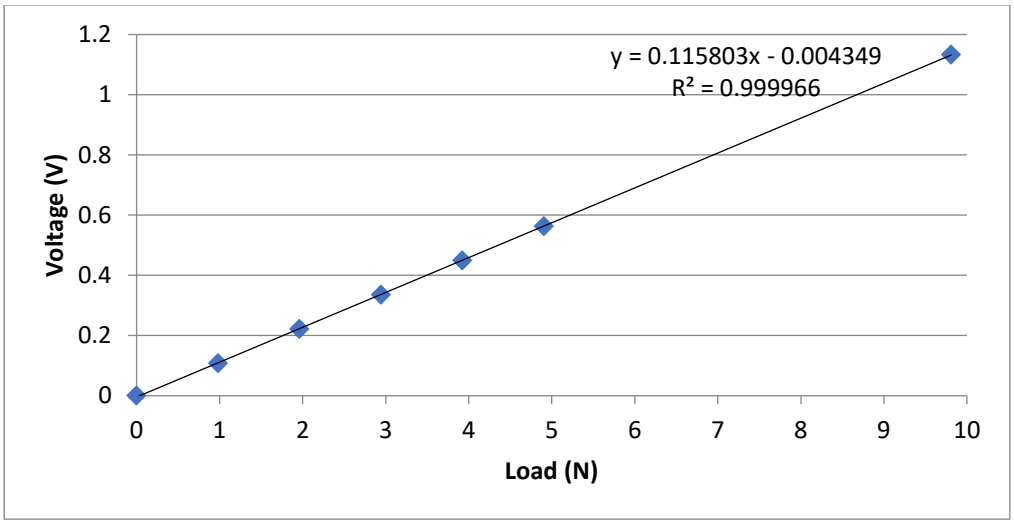

Figure 3-12 Load Cell calibration (range for load up to 10N)

3.2.4.3 Tank Wave Probe Calibration

A similar process to the two processes above is used to calibrate the tank wave probe. The tank wave probe acts as a transducer where the height of the wave surface generates an electrical signal. The voltage of the signal is measured and a value for the wave height is obtained. In order to calibrate the wave probe it is moved known distances and the measured voltage is recorded. Plotting these recorded points as measured voltage against distance moved generates the following linear relationship (Figure 3-13).

A straight line is fitted through the points and the gradient of the line is calculated. The inverse of the gradient is the factor which converts the input voltage to a wave height reading. For the wave probe the water level is approximately 82 times the measured voltage.

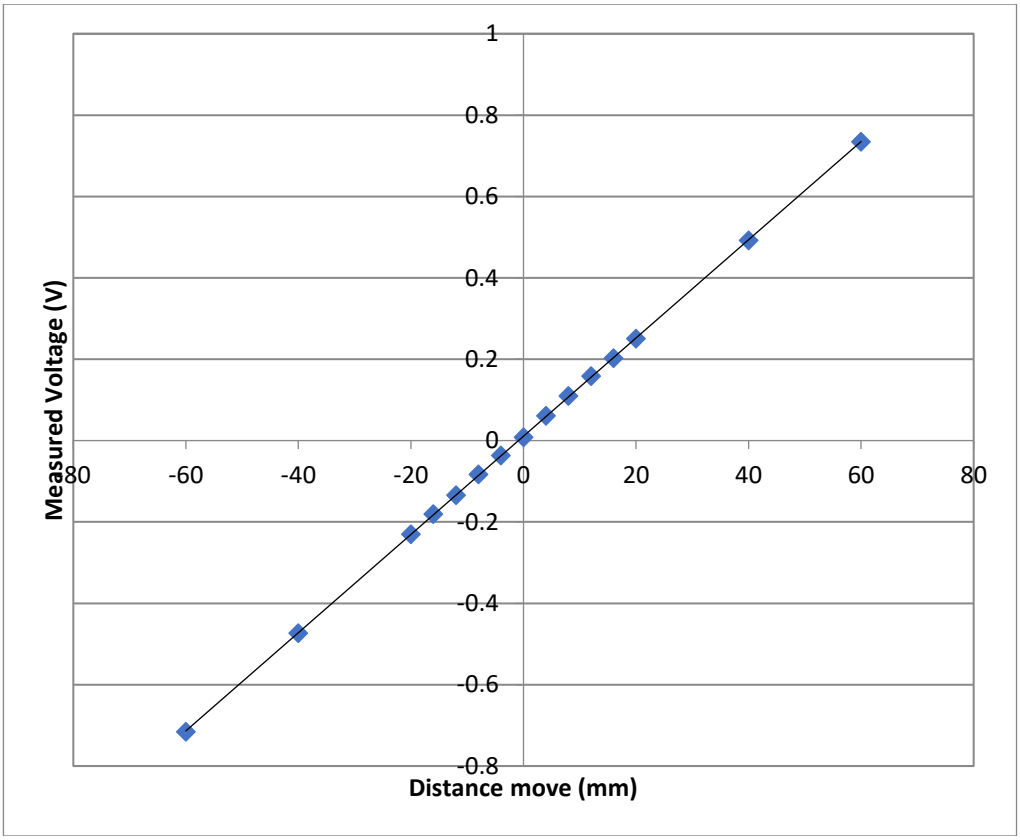

Figure 3-13 Wave probe calibration

3.2.5 Uncertainty Analysis

Uncertainty analysis of the experiments was carried out by repeating the resistance tests at the same conditions according to ITTC guides. (ITTC, 2014a) Tests were repeated 5 times at the velocity of Fr=0.26 which corresponds to the highest towing speed.

The standard uncertainty component of the mean from *N* repeat tests is estimated by

u'_A(mean)=StDev / √N

where StDev is the standard deviation. It should be noted that the standard uncertainty of any single tests can be estimated by StDev or

u'_A(single)= u'_A(mean) * √N

Table 3-2 Uncertainty of repeat measurements for total resistance, sinkage and trim with 95% confidence level

	R_T (N) at (15°C)				
Fr	Mean	*StDev*	u'_A(mean)	u'_A(single)	2.u'_A(single)
0.26	7.5073	0.49%	0.20%	0.49%	0.98%
	Sinkage				
Fr	Overall Uncertainty (mm)				%
0.26	0.302				4.8%
	Trim				
Fr	Overall Uncertainty (deg)				%
0.26	0.08				7.2%

It is shown from Table 3-2 above that resistance of this model is estimated at ±1.0% at 95% confidence level.

3.3 Computational Fluid Dynamics (CFD)

Computational Fluid Dynamics (CFD) methods become increasingly popular in recent years to investigate several marine hydrodynamics problems. CFD not only enables the use of the numerical towing tank approach, which refers to the investigation of the problem in model scale but also numerical sea trial approach as it is possible to investigate the problem in full scale.

Throughout this thesis, the commercial CFD software Star-CCM+ is used wherever an unsteady RANS approach has been applied. General processes of solving a CFD problem, which are Pre-processing, Solving and Post-processing, were followed. Figure 3-14 present a typical workflow process with STAR-CCM+.

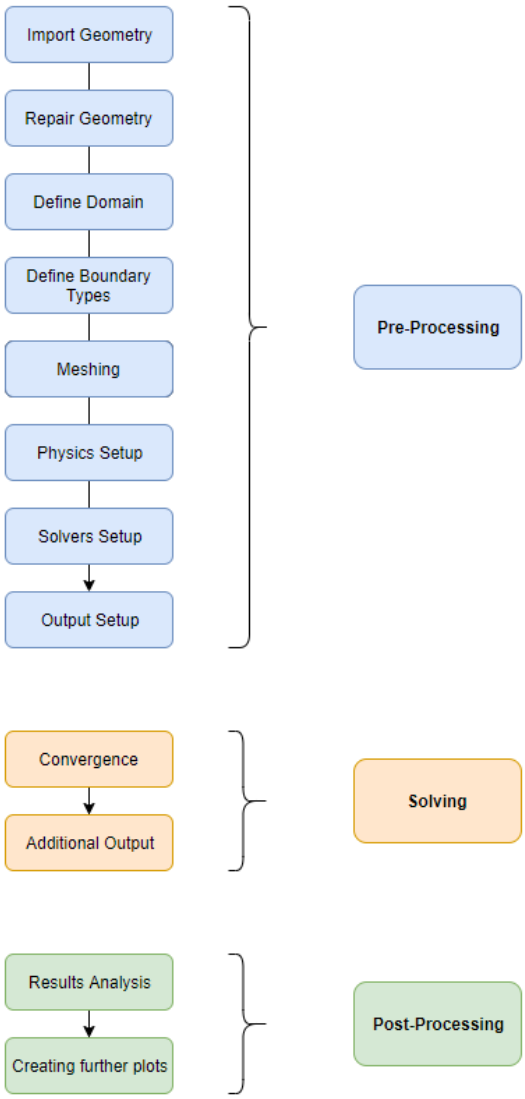

Figure 3-14 General workflow of Star-CCM+

3.3.1 Governing equations

For incompressible flows without external body forces, the averaged equations of continuity and momentum are expressed in the tensor form in the Cartesian coordinate system as follows by Eq. (3.1) and Eq. (3.2) (Ferziger and Peric, 2002)

$$\frac{\partial\left(\rho\overline{u}_i\right)}{\partial x_i}=0 \tag{3.1}$$

$$\frac{\partial\left(\rho\overline{u}_i\right)}{\partial t}+\frac{\partial}{\partial x_j}\left(\rho\overline{u}_i\overline{u}_j+\rho\overline{u_i'u_j'}\right)=-\frac{\partial\overline{p}}{\partial x_i}+\frac{\partial\overline{\tau}_{ij}}{\partial x_j} \tag{3.2}$$

in which $\overline{u_i}$ is the averaged velocity vector of fluid, $\overline{u_i' u_j'}$ is the Reynolds stresses, $\overline{p}$ is the mean pressure and $\overline{\tau}_{ij}$ is the mean shear stress tensor which is expressed as Eq. (3.3)

$$\overline{\tau}_{ij} = \mu \left(\frac{\partial \overline{u_i}}{\partial x_j} + \frac{\partial \overline{u_j}}{\partial x_i} \right) \tag{3.3}$$

where μ is the dynamic viscosity.

A second-order upwind scheme is used for the discretization of convection and diffusion terms in the RANS equations. The semi-implicit method for pressure-linked equations (SIMPLE) algorithm is implemented in STAR-CCM+ to resolve the pressure-velocity coupling.

3.3.2 Turbulence Model

The standart k-ε turbulence model was used throughout this thesis as its applicability is proven by previous CFD workshops (Larsson et al. 2014) and many other studies in the literature such as Enger et al. (2010) and Tezdogan et al. (2015). This model is a two-equation model which introduces two additional equations to solve; one for the kinetic energy (k) and one for the dissipation (ε). Two-equation models are the most popular models used in ship hydrodynamics. According to the SIEMENS Star CCM+ user guide, the k−ε model is described as providing a good balance between robustness, computational cost and accuracy. The findings from Larsson et al. (2014) also show that there is no obvious difference in resistance predictions when compared against more complex models. It is described as a suitable choice for flows over complex geometries which represents the underwater hull form variations in this study (SIEMENS, 2017). Based these reasons, this model was selected for the current study.

3.3.3 Volume of Fluid (VOF)

In order to simulate a floating ship at the free water surface, multiphase flow needs to be modelled. In the present thesis, free surface was captured by the Volume of Fluid (VOF) method which was introduced by Hirt and Nichols (1981). VOF method is described as “a simple multiphase model that is well suited to simulating flows of several immiscible fluids on numerical grids capable of resolving the interface between the mixture’s phases” by STAR-CCM+ (2019). VOF method has been a standard approach in marine CFD for the

resolution of free surface and it has been proven as a suitable approach for flow involving hull shape and breaking waves (Muzaferija and Peric, 1999). This applicability makes it suitable for the scope of current study. A second-order discretization scheme was used in order to obtain the sharp interfaces between the phases for all simulations as recommended by STAR-CCM+. More details about the VOF model can be found in the user guide of STAR-CCM+.

3.3.4 Computational Domain and Boundary conditions

Selection of the boundary conditions and positioning of these boundaries is essential to obtain an accurate solution with the CFD method as boundaries define fluid flux in and out of the computational domain as physical conditions. Different computational domains were created throughout the thesis for the solution of each unique problem. Computational domains will be described in detail in each numerical investigation section. Boundaries that applied in the present thesis can be summarised as follows:

• Velocity inlet:

A velocity inlet boundary in the computational domain represents the inlet of a duct. Flow velocity is directly specified and the pressure is extrapolated from the adjacent cell with reconstructed gradients.

• Pressure outlet:

Pressure outlet boundary is a flow outlet boundary at which pressure is specified while velocity is extrapolated from adjacent cells.

• Symmetry boundary:

Symmetry boundary condition refers to an imaginary plane of symmetry in the computational domain. A solution obtained by using a symmetry boundary plane would be equal to half of the result of a full domain by mirroring the mesh around the symmetry plane.

• Wall boundary:

A Wall boundary with non-slip condition is used to represent the surface of a body.

3.3.5 Modelling Motion

In the present thesis, Dynamic Fluid Body Interaction (DFBI) model was employed in order to simulate the realistic ship motions. In the DFBI model, the motion of the ship is simulated according to the acting forces induced by the flow.

There are several ways to introduce a propeller effect to a marine simulation. Self-propulsion simulations were conducted using two different simulation approaches namely, sliding mesh with 3-D propeller geometry and body force method based virtual disk approach to introduce the propeller effect to the resistance simulation.

3.3.5.1 Body Force Propeller Method

In Body Force Propeller approach, marine propeller effects such as thrust and torque are computationally estimated without actually utilising the geometry of the propeller. In this method, a uniform volume force distribution over the cylindrical virtual disk is employed. The volume force varies in the radial direction. The method models the flow field interaction of the hull of a ship and the propeller. The flow that is induced by the propeller depends on the flow around the ship hull. Similarly, the hull flow is influenced by the propeller.

Using this method provides a clear advantage to reduce mesh size and, therefore, computational cost over performing a simulation including the propeller geometry. It is useful if one does not require the detailed flow field around the propeller, but more importantly need the correct propulsion specification.

The body force propeller method requires the following inputs:

- Definition of a virtual disk regarding position and direction in which thrust is produced
- Specification of a propeller performance curve (from experiments or simulations)
- Specification of an operating point (ie, rotational speed, thrust)
- Specification of an inflow method

As a result, the distribution of the axial and tangential forces of the modelled propeller and its effect on the flow is calculated. The integration of these forces over the disk gives the thrust and torque of the propeller, which can then be coupled with a DFBI simulation.

It is recommended to refine the mesh in the zone where the virtual disk is located, particularly in the radial direction. This way, it is possible to obtain a good distribution of the axial and tangential body force components of the virtual disk. If using the sampled velocity plane option, the grid on the upstream plane should match the grid on the virtual disk for optimal results.

The Body Force Propeller Method requires to define the inflow specification of the virtual disk. Based on the selected inflow specification method, you either set an inflow velocity vector and density, or these values are calculated from the flow field. The virtual disk method uses these inflow quantities for the computation of the advance ratio, in combination with the operation point of a propeller.

The Body Force Propeller Method provides various options for specifying the inflow velocity to the propeller. The inflow velocity vector is used to compute the advance ratio J. Computed J value is then used to determine the operating point from the propeller characteristics curve yielding the thrust coefficient K_T and the torque coefficient K_Q. With these two coefficients, the thrust and the torque are evaluated.

The body force propeller method can be used as part of a DFBI (Dynamic Fluid Body Interaction) simulation to allow the propeller to follow the ship motions.

3.3.5.2 Sliding Mesh (Rigid body motion)

In the sliding mesh approach, the propeller is fully simulated in transient flow with a rotating region/mesh moving a defined displacement per time step. It is considered as the most accurate method to simulate moving parts hence it is the most computationally expensive. DFBI Superposed rotation was employed in order to allow the rotation of the propeller following the other ship motions for free sinkage and trim cases.

The propeller is fully simulated, in the transient, with the time step adjusted to resolving the rotation. The standard recommendation is 1 degree per time-step and about one face per time-step on the interface – which means at least one face per degree on the circular interface. For each time step, the interfaced region slides the mesh to a new position according to the given movement. It is possible to investigate transient flow effects such as flow interaction with the free surface.

In order to reduce the computational time, simulations can be initiated with a non-rotating propeller (0 rpm) to allow the development of the flow field around the hull. After that, propeller rotation can be started slowly and increasing the rotation rate gradually until the desired value is reached.

3.4 Chapter Summary

This chapter presented two main methodologies that were used in this thesis. Firstly, experimental facilities and details of the experimental approach with the description of the tested model were presented. Then, the test procedure including ballasting and inclining of the model was illustrated. After that CFD approach was explained in general terms. Workflow of CFD process, turbulence method and boundary conditions were presented. Lastly, different motion modelling approaches that were adopted in this thesis were described.

Chapter 4 Trim Influence on Calm Water Resistance

4.1 Introduction

This chapter presents results from calm water resistance tests and numerical simulations to examine the impact of trim on vessel performance in calm water. Experimental investigation results are presented first. Numerical results are then validated with experimental data and further simulations are conducted. In order to find out scale effects on optimum trim, full scale numerical simulations are also carried out and differences between model scale and full scale findings are discussed. Finally, the conclusions are presented based on the overall findings obtained from this chapter.

4.2 Model Scale investigation

As proved by previous studies in literature it is crucial to predict resistance accurately and efficiently for trim optimisation studies. A series of model tests were conducted at different trim angles and speeds to investigate the trim influence on calm water resistance and also to provide data for validation of numerical computations.

In the experimental part of the study, the mean draft was kept constant at the design draft for the initial investigation of trim influence on resistance characteristics. Experiments were carried out at different trim angles for a range of speeds between 18 knots (Froude number 0.20) to 24 knots (Froude number 0.26). The speed range has been selected considering slow-steaming speeds (18-19 knots) and service speed (24 knots) of KCS. Selected trim angle

values range from 0.25 degree up to 1 degree for bow and stern trim conditions to ensure complete propeller immersion. These angles correspond to 1m to 4m trim in full scale. Figure 4-1 shows maximum trim by bow and aft conditions in comparison with level trim.

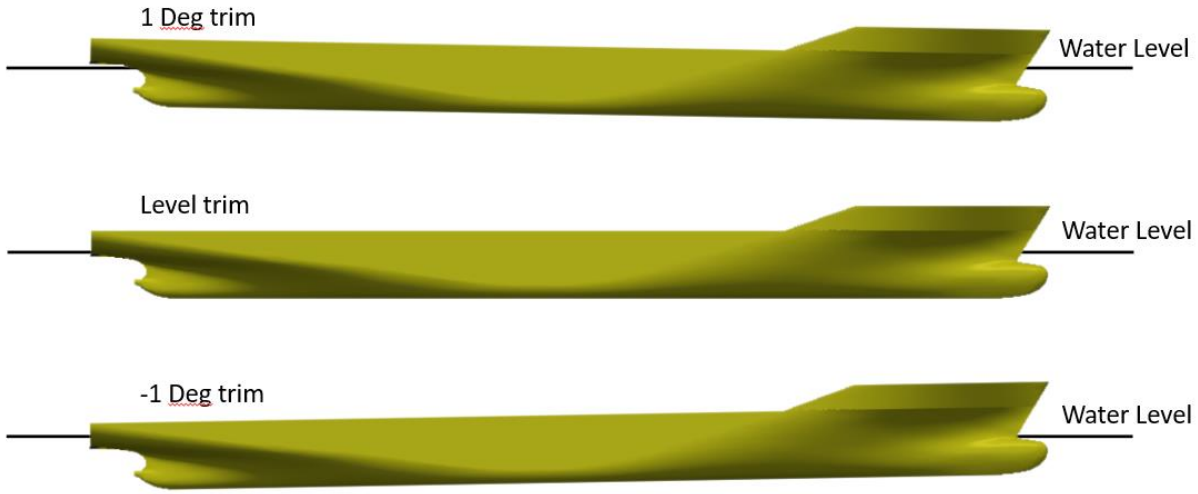

Figure 4-1 1 degree trim, level trim and -1 degree trim conditions

For the numerical trim optimisation study, two different draft values, namely, design draught (10.8 m) and ballast draught (9 m) conditions were investigated. First, the speed was fixed at the design speed of 24 knots (Froude number 0.26) and later slow steaming speed of 19 knots (Froude number 0.20) was investigated. Also in order to investigate the applicability of fixed motion simulations, further analyses were conducted without dynamic trim and sinkage motions. To assess the effect of ship motions on optimum trim numerical calculations were carried out for both ship fixed at rest position and dynamic sinkage and trim. Experiments were performed only for the free sinkage and trim model.

4.2.1 Experimental Investigation

Model tests were performed to obtain resistance curves in each trimmed condition. In this study, one draft of 0.144m and speeds corresponding to a Froude number between 0.19 and 0.26 was investigated. The test matrix for level trim is shown in Table 4-1. In total 6 different trim values were investigated ranging from 0.25 to 1 degrees.

Table 4-1 Test matrix for level trim

	Test01	Test02	Test03	Test04	Test05	Test06	Test07
Full Scale Speed in knots	18	19	20	21	22	23	24
Full Scale Speed in m/s	9.259	9.774	10.288	10.802	11.317	11.831	12.346
Model Scale Speed in m/s	1.069	1.129	1.188	1.247	1.307	1.366	1.426
Froude Number	0.19	0.21	0.22	0.23	0.24	0.25	0.26

Results from the towing tank experiments are post-processed by calculating the non-dimensional resistance coefficients for a corrected water temperature of 15°C following procedures proposed by the ITTC (ITTC 7.5-02-02-01). For the measured fresh water temperature that defined the water density ρ_M and kinematic viscosity ν_M, the monitored total resistance force of the KCS model R_{TM} at a carriage speed v_M was converted to its non-dimensional total resistance coefficient c_{TM} considering the hydrostatic wetted surface S_M (Eq. 4.1)

$$c_{TM} = \frac{R_{TM}}{0.5\,\rho_M\,S_M\,v_M^2} \tag{4.1}$$

The frictional resistance coefficient $c_{FM,ITTC}$ was calculated by the ITTC-1957 frictional correlation line as shown in Equation 4.3 for the model Reynolds number Re_M (Eq. 4.2), considering the static water line length $L_{M,WL}$.

$$Re_M = \frac{v_M\,L_{M,WL}}{\nu_M} \tag{4.2}$$

$$c_{FM,ITTC} = \frac{0.075}{(\log Re_M - 2)^2} \tag{4.3}$$

The wave making resistance can be found by,

$$c_W = c_{TM} - c_{FM,ITTC}(1+k) \tag{4.4}$$

The form factor k was determined by the performed Prohaska method as recommended by ITTC (ITTC 7.5-02-02-01) at level trim. In the Prohaska method, a series of low speed tests are conducted, and results of C_T/C_F versus Fr^4/C_F are plotted. A linear trendline is fitted to the plot and the y-intercept of the line equals the desired (1+k) value which is found to be 1.0118 as seen in Figure 4-2.

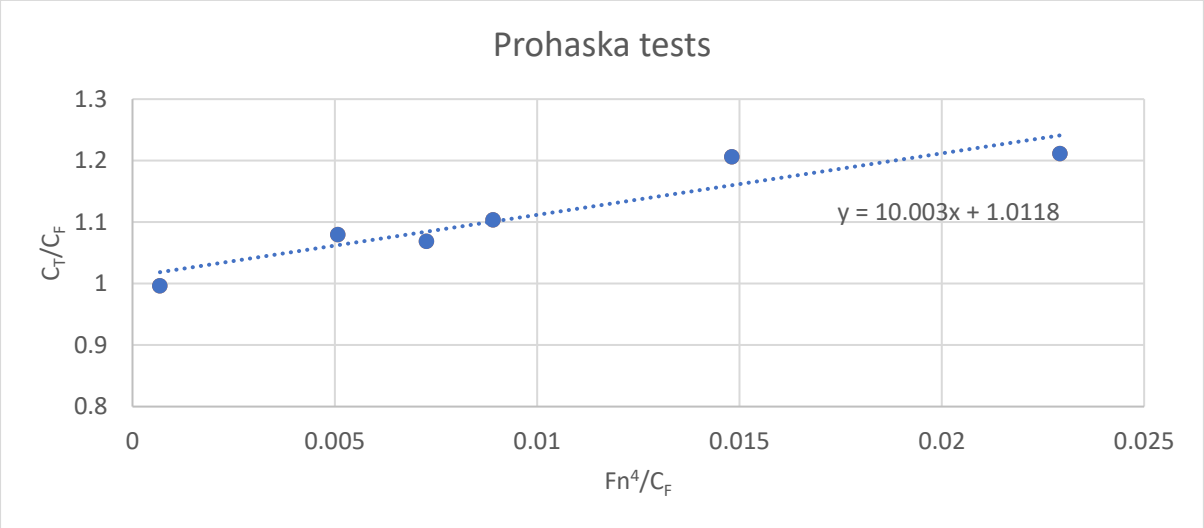

Figure 4-2 Form factor calculation based on Prohaska method

In order to correct the viscous effects of the measured results to a water temperature of 15°C, the frictional resistance coefficient $c_{FM,ITTC}^{15°C}$ was re-calculated by considering the model Reynolds Number $Re_M^{15°C}$ (Eq.4.5) for the kinematic viscosity $\nu_M^{15°C}$ at 15°C.

$$Re_M^{15°C} = \frac{v_M \, L_{M,WL}}{\nu_M^{15°C}} \tag{4.5}$$

$$c_{FM,ITTC}^{15°C} = \frac{0.075}{\left(\log Re_M^{15°C} - 2\right)^2} \tag{4.6}$$

Therefore, the temperature corrected total resistance coefficient $c_{TM}^{15°C}$ (Eq. 4.7) and the total resistance $R_{TM}^{15°C}$ at 15°C values are obtained as follows (Eq. 4.8).

$$c_{TM}^{15°C} = c_{FM,ITTC}^{15°C}(1 + k) + c_W \tag{4.7}$$

$$R_{TM}^{15°C} = 0.5\, c_{TM}^{15°C}\, \rho_M\, S_M\, v_M^2 \tag{4.8}$$

Experimental results are compared with other available data from FORCE (Simonsen et al., 2013) IIHR (Sadat-Hosseini et al., 2015) and NMRI, which was used in CFD workshop in Gothenburg 2010.

Table 4-2 Experimental values comparison for resistance tests in calm water at Fr:0.26

Facility	**Re**	**$C_T \times 10^3$**	**σ/L**	**τ°**
Force	6.51×10^6	4.31	-0.002	-0.1853
IIHR	3.61×10^6	4.69	-0.0015	-0.13
NMRI	1.26×10^7	3.71	-0.002	-0.169
KHL (Current Study)	3.87×10^6	4.41	-0.002	-0.162

Table 4-2 Experimental values comparison for resistance tests in calm water at Fr:0.26 compares total resistance coefficient (C_T), sinkage (σ/L) and trim (τ) results for tests in calm water at Fr:0.26. Current study results agree well with other experiments considering the scale differences. Trim values have larger differences between experimental facilities. This may be due to size differences and experimental uncertainty/facility bias.

4.2.1.1 Wetted Surface Area

The wetted surface area and the waterline length of the KCS was calculated for each trim angle. Variations in these values for trim angle are shown in Figure 4-3. Hull form variations in trimmed conditions can increase/decrease the waterline length up to 3% in trim by aft and bow conditions. Trim by aft increases wetted surface area up to 2% while in trim by bow conditions wetted surface area is up to 2.5% lower when compared against level trim.

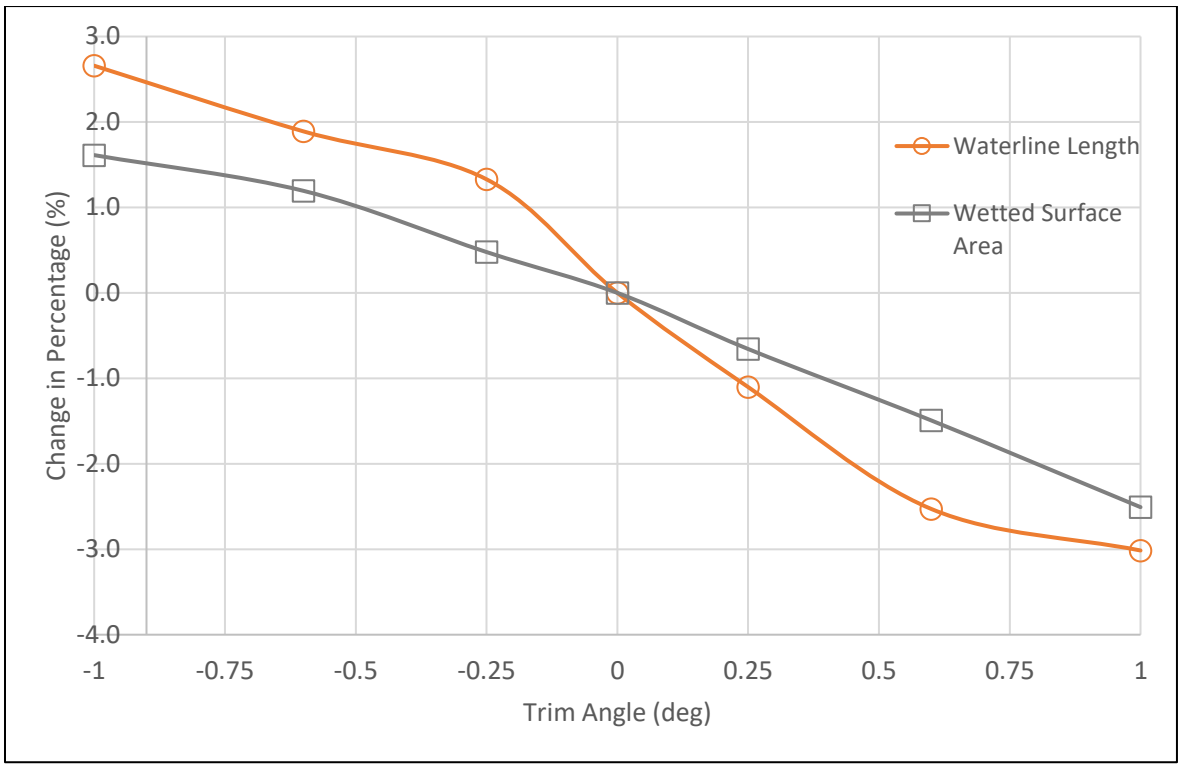

Figure 4-3 Waterline length and wetted surface area variation over the trim range

4.2.1.2 Trim Effect on resistance components

After obtaining temperature corrected values, total resistance values at trimmed conditions were compared to level trim and resistance curves are plotted for the whole speed range.

Figure 4-4 demonstrates resistance curves for 0.25 degree trim by stern and bow, and also level trim resistance curve for comparison purposes. A small trim angle of 0.25 degree by bow gave the optimum resistance for all speeds. Results indicated a 1% decrease in total resistance at this trim. This may be explained due to a small reduction in wetted surface area and improved bulb performance.

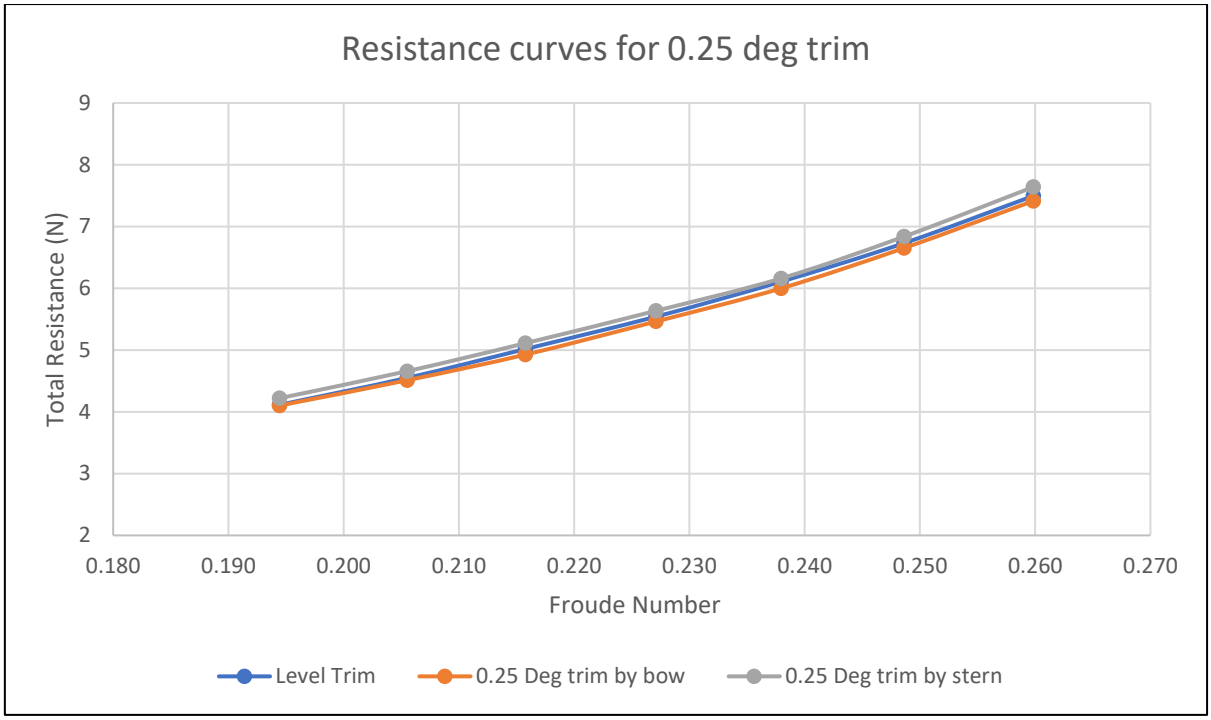

Figure 4-4 Total resistance curves comparison at 0.25 degree trim

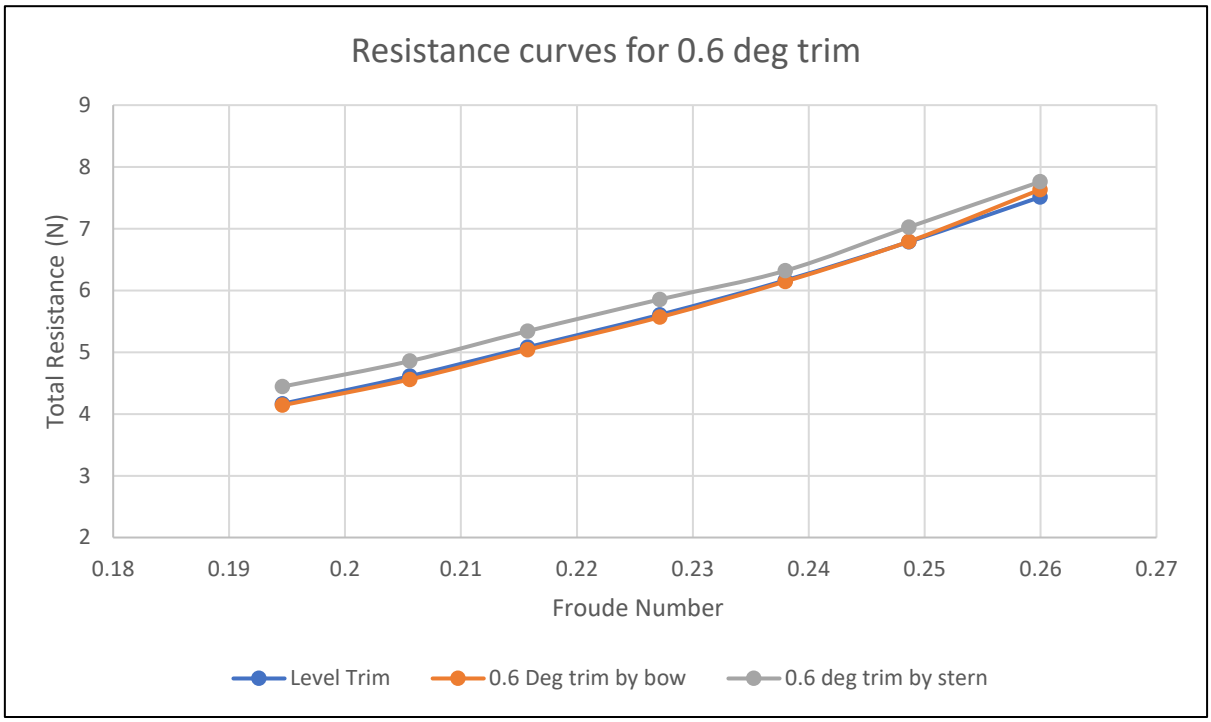

Figure 4-5 Total resistance curves comparison at 0.6 degree trim

Total resistance curves comparison at 0.6 degree trim are shown in Figure 4-4. While level trim and 0.6 degree trim by bow performed almost the same for slower speeds, at design speed of Fr = 0.26, 0.6 degree trim by bow and stern increased the total resistance with respect to level trim by 1.8% and 3.3% respectively.

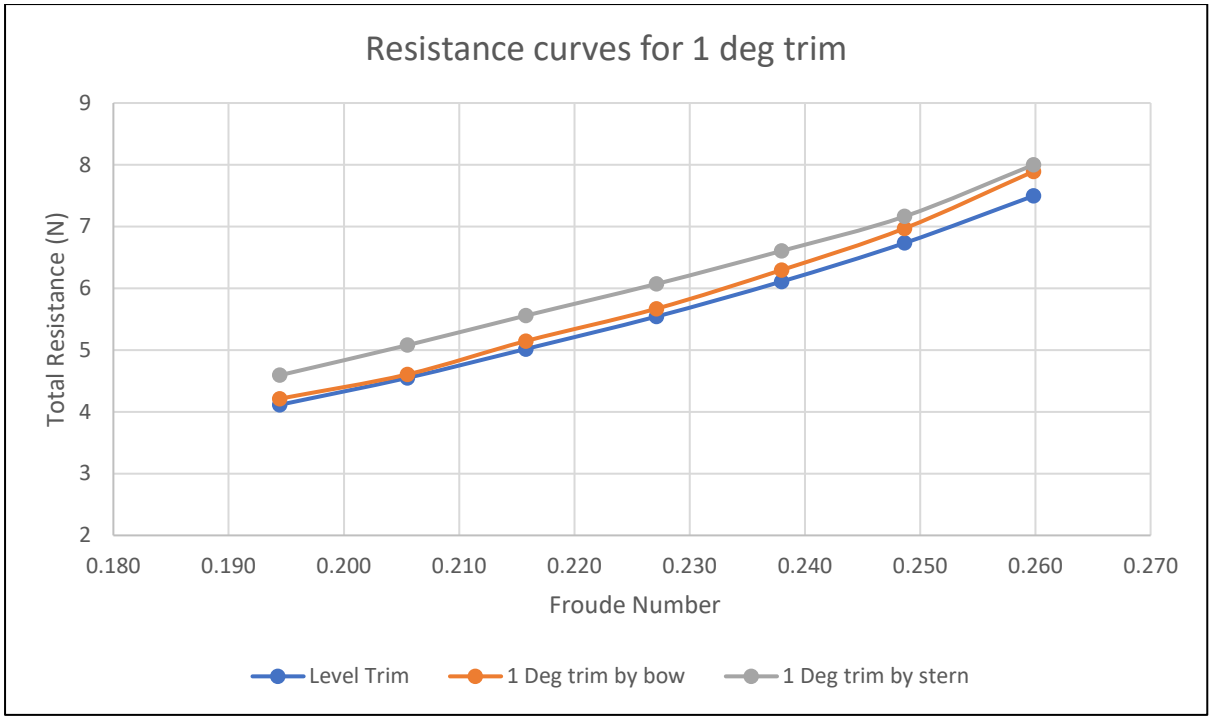

Figure 4-6 Total resistance curves comparison at 1 degree trim

As can be seen from Figure 4-6, 1 degree trim by bow increase the total resistance with increasing speed. In contrast, 1 degree trim by stern increased the total resistance significantly due to submergence of transom and increased water line length for whole speed range. In total, 1 degree trim by stern and bow increased total resistance by 8% and 6% respectively at the design speed.

In order to investigate the reasons behind the changes in detail, resistance components are compared against trim angle for each speed. The frictional resistance trend is similar for the whole speed range and it is shown in Figure 4-7 and Figure 4-8. Frictional resistance decrease in trim by bow conditions up to 2% in the largest trim angle. This is in line with the reduction in waterline length in trim by bow conditions. In trim by stern conditions, frictional resistance increases up to 1.5%.

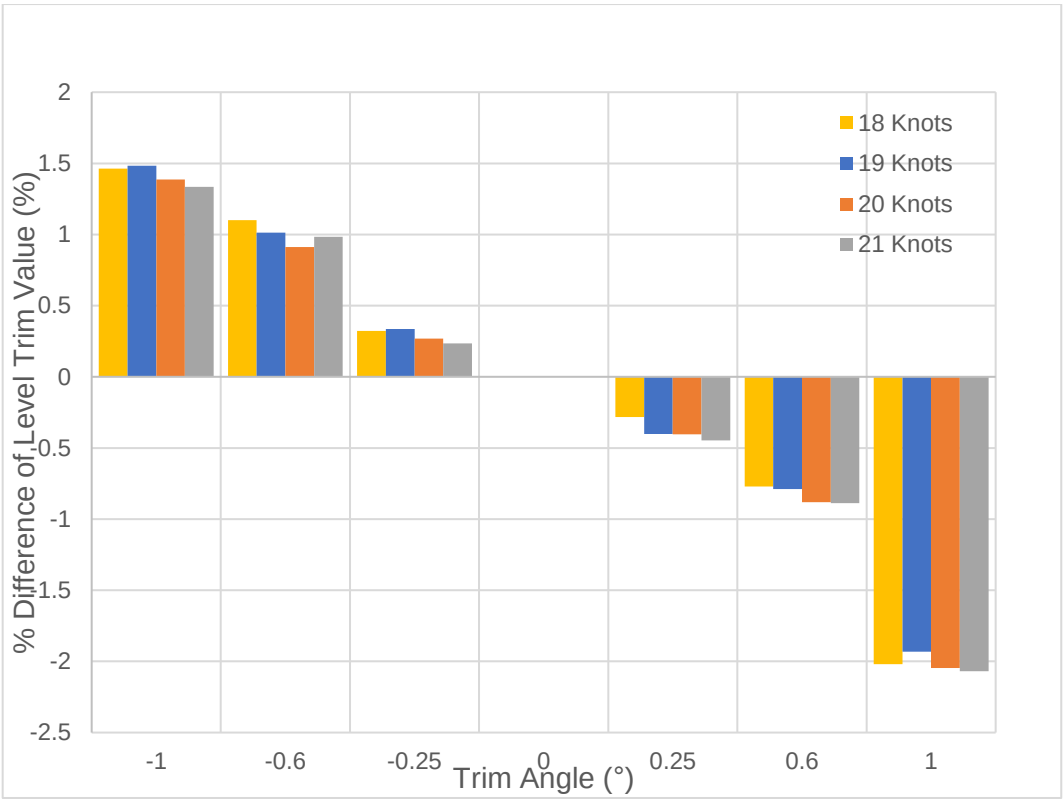

Figure 4-7 Frictional Resistance variation over trim range for 18 – 21 Knots

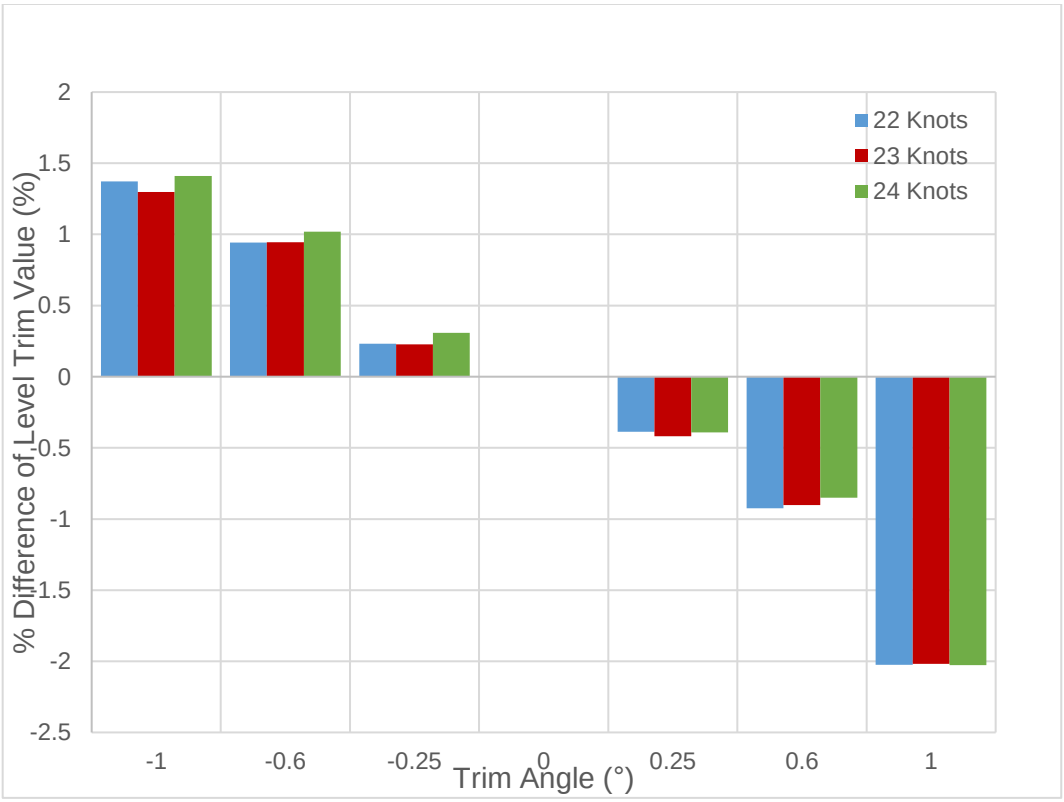

Figure 4-8 Frictional Resistance variation over trim range for 18 – 21 Knots

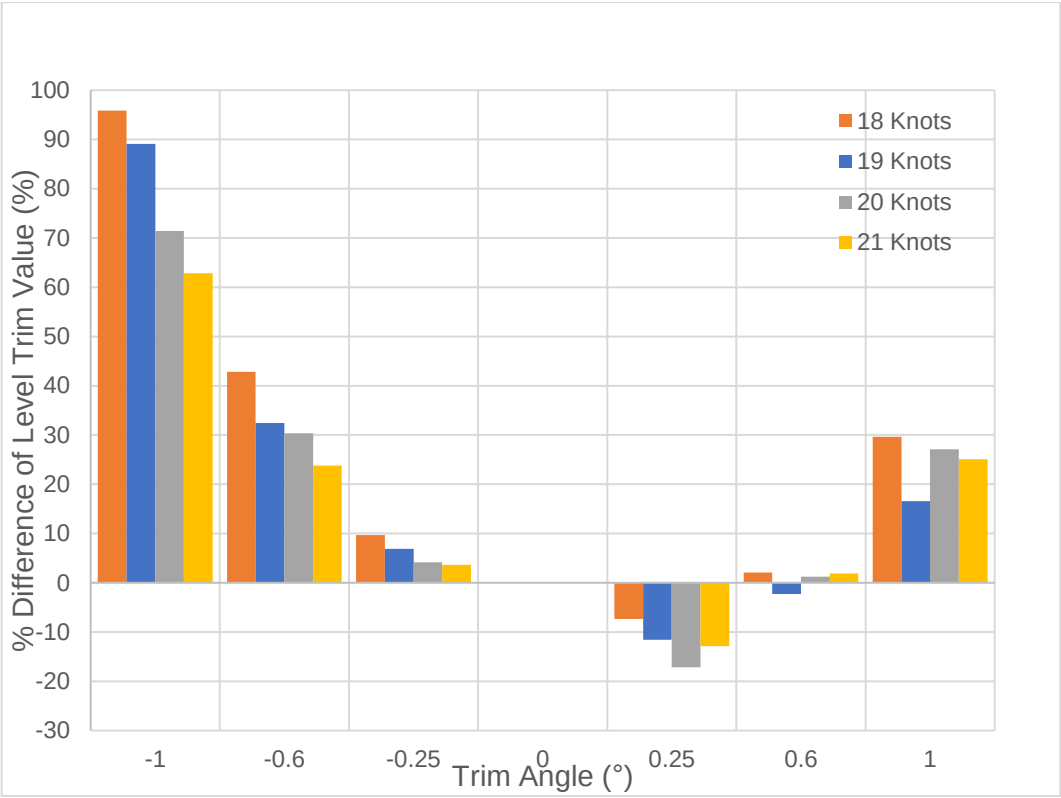

Figure 4-9 Wave making resistance variation over trim range for 18 – 21 Knots

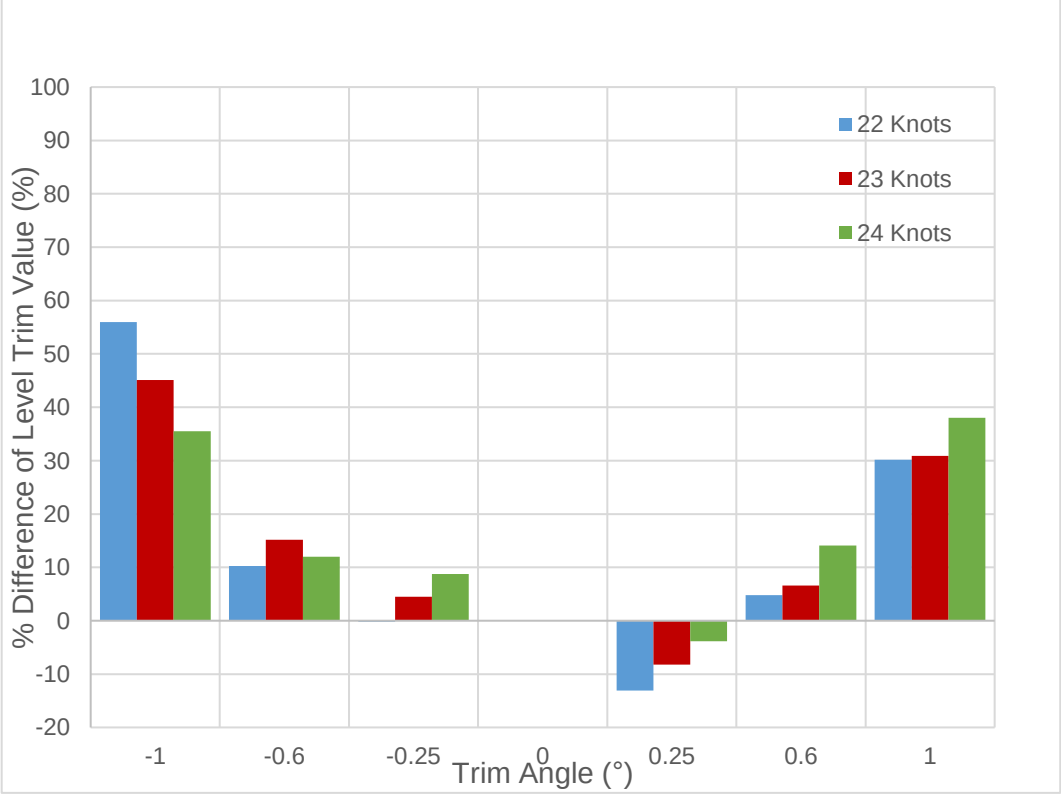

Figure 4-10 Wave making resistance variation over trim range for 22 – 24 Knots

Figure 4-9 and Figure 4-10 compares the wave making resistance at each trim angle against the level trim measurements for 18 to 21 knots and 22 to 24 knots, respectively. For trim by stern conditions, the wave making resistance shows a large increase of up to 90% at slower speeds. For medium to design speed range, trim by stern increases wave making resistance by up to 50% in line with increasing trim angle. Wave making resistance finds its lowest value at 0.25 degree trim by bow with a decrease of up to 15 per cent when compared against level trim. This saving magnitude decreases slightly with the increasing speed of the hull. Larger trim by bow and stern increases wave making resistance.

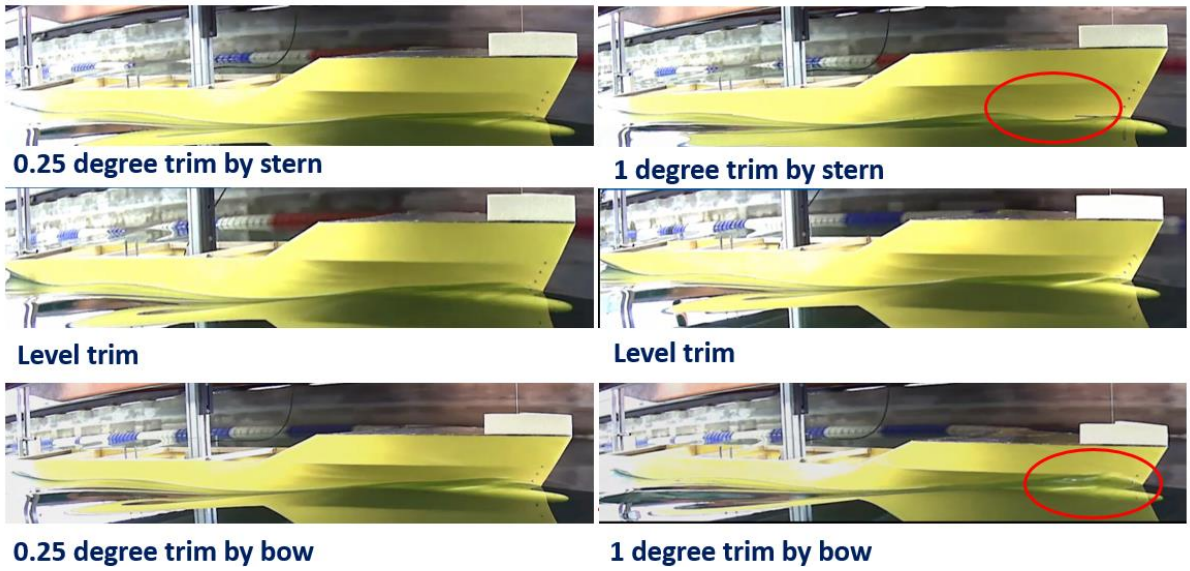

Figure 4-11 Formation of bow wave at different trim angles

Unfavourable bow wave at large trim angles can be clearly seen from the experiments as shown in Figure 4-11. This may explain the large increases in wave making resistance at large trim by bow and stern conditions.

4.2.2 Numerical Investigation

Numerical simulations were set up to investigate the effect of trim on resistance at design and ballast draft values in both model and full scale. Model scale calculations were carried out first and full scale simulations were conducted later. Commercial CFD software STAR-CCM+ was used and Reynolds Averaged Navier-Stokes (RANS) approach was adopted. The standard k-ε turbulence model was chosen for turbulence modelling. Free surface was

captured by the VOF method. Details of the numerical approach are discussed in Chapter 3 of this thesis.

In free case simulations, the ship was allowed to move freely in the pitch and heave directions with two degrees of freedom similar to experiments. Dynamic Fluid Body Interaction (DFBI) model was employed for free cases in order to predict the realistic ship behaviour. Further investigations were carried out by fixing ship motions, as fixed case simulations are computationally faster. Differences between free and fixed case simulations for all trim angles were discussed.

4.2.2.1 Mesh Generation and Boundary Conditions

The construction of the volume mesh has a direct influence on the accuracy of fluid flow simulation and turbulence. The rate of convergence and the accuracy of the final solution depends on the volume mesh. Trimmed mesh technique was employed due to the computational cost and accuracy of complex mesh generating problems. Half of the model was simulated due to the lateral symmetry condition.

Selection and positioning of initial and boundary conditions are also crucial to ensure the right simulation approach. The initial conditions and boundary conditions are defined to represent the KCS ship being towed in deep enough water to avoid shallow water effects. A velocity inlet boundary condition was set at 1.5LPP ahead of the vessel and a pressure outlet was selected at 2.5LPP behind. The top and bottom boundaries were both modelled as velocity inlets. A symmetry plane was used to reduce the number of cells and computational demand using a symmetry boundary condition at the vertical center plane. Therefore only half of the domain was modelled. These boundary conditions were selected by following best practices for similar simulations as recommended by SIEMENS (2017) and from similar studies in the literature (Tezdogan et al. 2016). Figure 4-12 shows an overview of the computational domain with KCS model and selected boundary conditions.

Artificial wave damping is applied along the inlet, outlet and side boundaries with a constant damping length of about 0.75LBP to prevent reflections from the boundaries and not to interfere with the results.

The domain size and location of boundaries are summarized in Table 4-3.

Table 4-3 Locations of the boundaries in the computational domain

	Min	*Max*	*Note*
X	-1.5 LPP	2.5 LPP	AP is set to 0
Y	0	1.5 LPP	Centre line is set to 0
Z	1.5 LPP	1.5 LPP	AP is set to 0

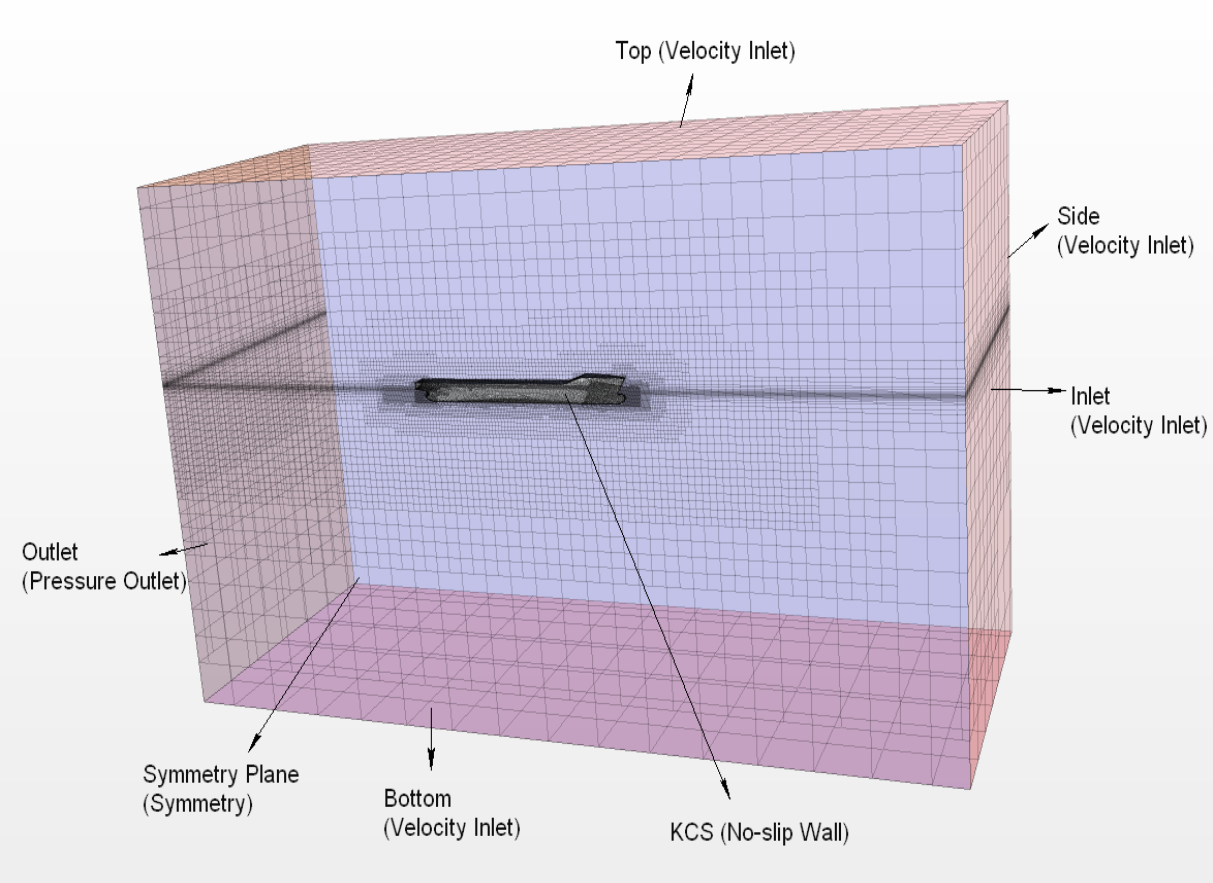

Figure 4-12 Overview of the computational domain for calm water simulations

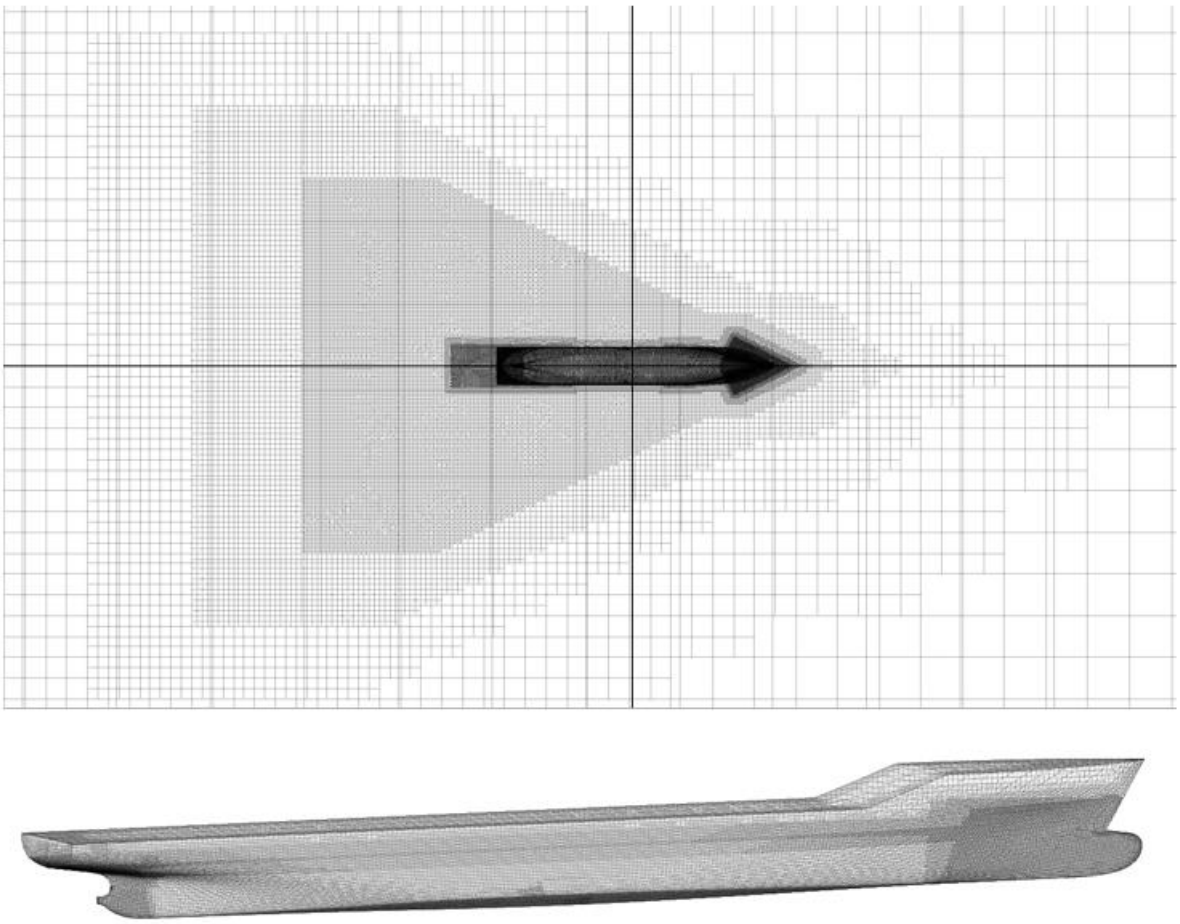

Figure 4-13 Computational mesh around the hull

Defining refinement regions around the hull and free surface allows the mesh size to be kept as small as possible while capturing relevant areas of interest. This was done through the use of volumetric controls in the expected wake areas. Figure 4-13 demonstrates the refinement areas around the ship hull to capture the free surface and Kelvin wake. The computational mesh was regenerated at each trim condition. Refinements around the bow and stern were adapted according to the trimmed ship position.

The boundary layer was modelled using all y+ wall treatment option in Star CCM+. Wall functions are used to avoid limitations related to fully resolved near wall modelling which are computationally expensive and may create grid resolution issues. All-y+ treatment approach emulates both the Wall Function law approach for y+ values (y+ is a non-dimensional wall distance for a wall-bounded flow) greater than 30 and the near-wall turbulence for y+ values lower than 5 to resolve the viscous sub layer. Grids resulting in the buffer zone (5<y+<30). should be avoided in solving any turbulent flow problem. Eca et al. (2015) stated that y+

values within the buffer zone may result in an error of 10% when calculating the frictional resistance. Prism layers are placed along the hull surface in order to resolve the boundary layer accurately and to achieve the required wall y+ values. As shown in Figure 4-14, the dimensionless wall distance y+ was around 45 for each mesh size which is considered as an appropriate size for the standard k-ε model with all y+ boundary treatment. (Peric, 2016)

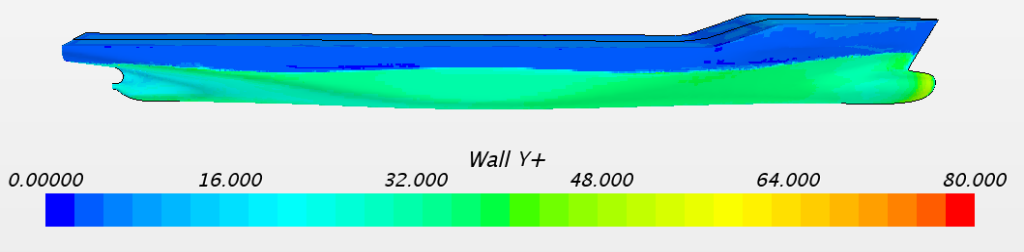

Figure 4-14 Wall y+ value on the hull

4.2.2.2 Grid Convergence Study

In order to investigate the numerical simulation uncertainty, grid uncertainty analysis was conducted using Grid Convergence Index (GCI) the method of Roache (1998).

Three different meshes, namely fine (N_1) consisting of 1.3 million cells, medium (N_2) consisting of 0.6 million cells and coarse (N_3) consisting of 0.28 million cells, were created with a constant refinement ratio of $\sqrt{2}$ as recommended by ITTC procedures. In order to assess the grid convergence, the convergence ratio is used as written in Eq. (4.9) below:

$$R=\varepsilon_{21}/\varepsilon_{32} \tag{4.9}$$

In Eq. (8) $\varepsilon_{21}=S_2-S_1$ and $\varepsilon_{32}=S_3-S_2$ are the differences between medium-fine and coarse-medium solutions, where S_1, S_2, S_3 correspond to the solutions of fine, medium, and coarse grid systems, respectively. A minimum of three solutions are required to evaluate the convergence. (Stern et al. 2006)

Four different types of convergence and divergence conditions are possible (Stern et al. 2006):

(i) monotonic convergence ($0<R<1$),

(ii) oscillatory convergence ($R<0$; $|R|<1$),

(iii) monotonic divergence ($R>1$)

(iv) oscillatory divergence ($R<0$; $|R|>1$)

For divergence conditions, errors and uncertainties cannot be calculated.

Grid Convergence Index (GCI) Method based on Richardson extrapolation (Richardson, 1910, Richardson and Gaunt, 1927) was used in this chapter for estimation of discretisation errors. Details of the method are fully described by Celik et al. (2008).

Grid uncertainty test results in a monotonic convergence for all three variables. As shown in Table 4-4, numerical uncertainties for sinkage, trim and CT are predicted as 1.85%, 1.45% and 0.77%, respectively, based on the Grid Convergence Index (GCI) method.

Table 4-4 Grid Convergence Study for calm water simulations

	Sinkage(m)	**Trim (deg)**	**C_T*10^3**
S_1 (1.3M cells)	-0.00555	0.196	4.29
S_2(0.6M cells)	-0.00568	0.199	4.23
S_3(0.28M cells)	-0.0064	0.204	4.10
R	0.35	0.64	0.43
GCI_{fine}	3.80%	2.75%	1.25%

Simulations took 88, 133 and 324 CPU hours for coarse, medium and fine meshes respectively. Based on these results it was decided to carry out the trim optimisation study with fine mesh approach.

4.2.2.3 Validation

Total resistance and dynamic motions of the KCS hull are validated against the experimental data before investigating the effect of trim on calm water performance. Table 4-5 compares total resistance coefficient, trim and sinkage values obtained from CFD simulations and experiments for design speed condition of 24 knots.

Table 4-5 Numerical and experimental results comparison for validation study

Parameters	***CFD***	***EFD***	***E % D***
C_T*10^3	4.29	4.41	2.72
Trim (Deg)	0.189	0.162	16.6
Sinkage (m)	-0.00598	-0.0069	15

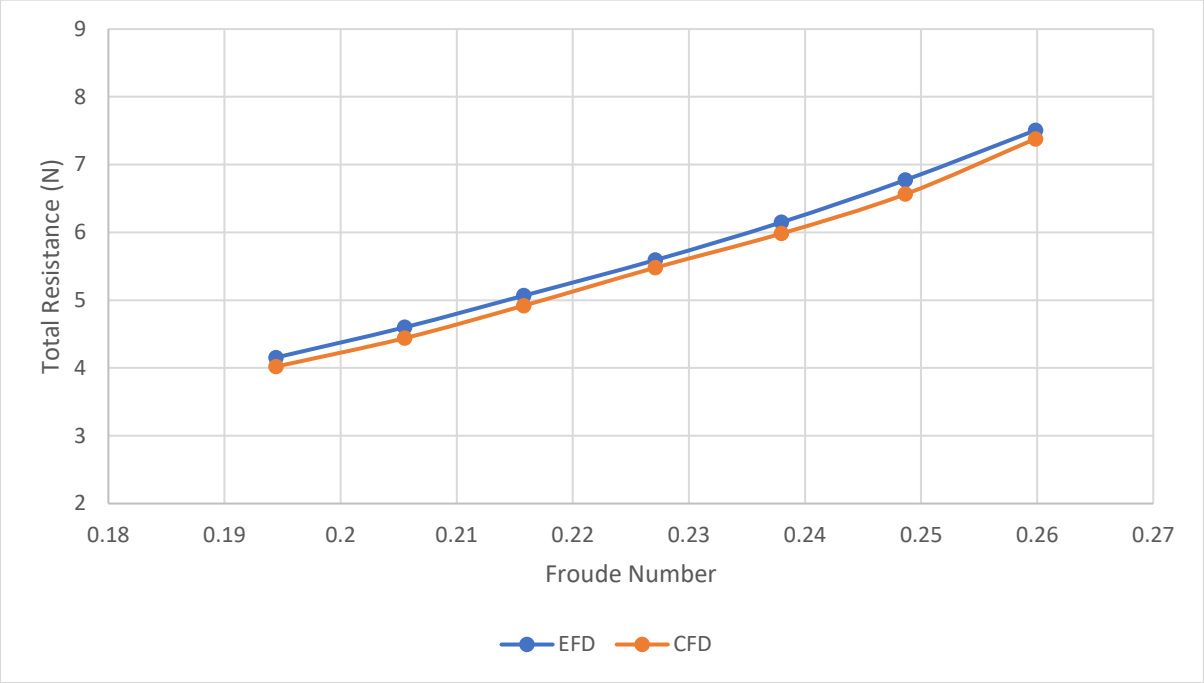

Figure 4-15 Total resistance curves for level trim case, CFD vs. EFD comparison

Figure 4-15 shows the comparison between experimental results and CFD calculations for different speeds. It can be seen that CFD results are in good agreement with experimental results with the maximum error being 2.7% for the total resistance. Percentage errors for dynamic sinkage and trim show larger differences however the actual difference in the magnitude of measured and calculated values are very small. Sinkage is predicted by E=15% difference, and trim is predicted with E=16.6% difference. Comparison of numerical and experimental results for dynamic sinkage and trim are found to be in reasonable agreement over the whole speed range as shown in Figure 4-16 and Figure 4-17.

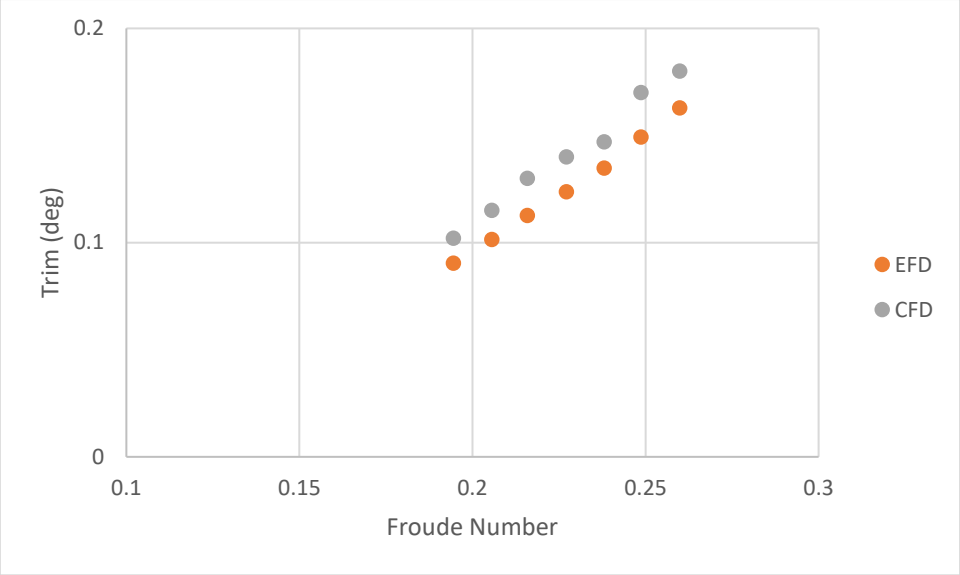

Figure 4-16 Dynamic trim, level trim case, CFD vs. EFD

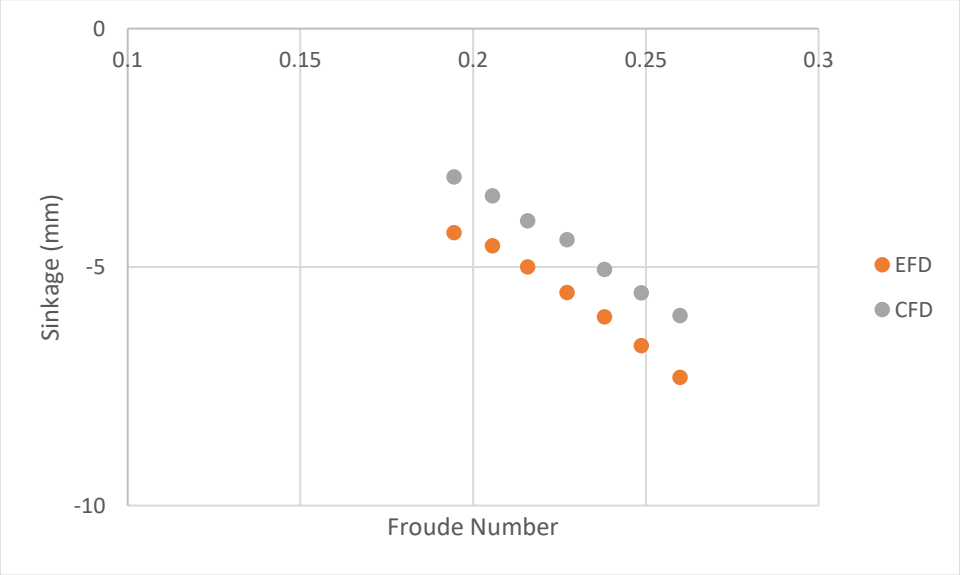

Figure 4-17 Dynamic sinkage, level trim case, CFD vs. EFD

4.2.3 Results and Discussion

After verification and validation of the numerical approach, the next step is to calculate the resistance values at different trim angles. Numerical calculations were carried out for slow steaming condition at 19 knots (Fn:0.20) and the design speed condition at 24 knots (Fn:0.26) for two different draft values, namely, design draft and ballast draft.

4.2.3.1 Design Draft

Based on resistance simulations, changes in total resistance, pressure resistance and frictional resistance are analysed for each trim angle in order to investigate the trim influence on resistance components.

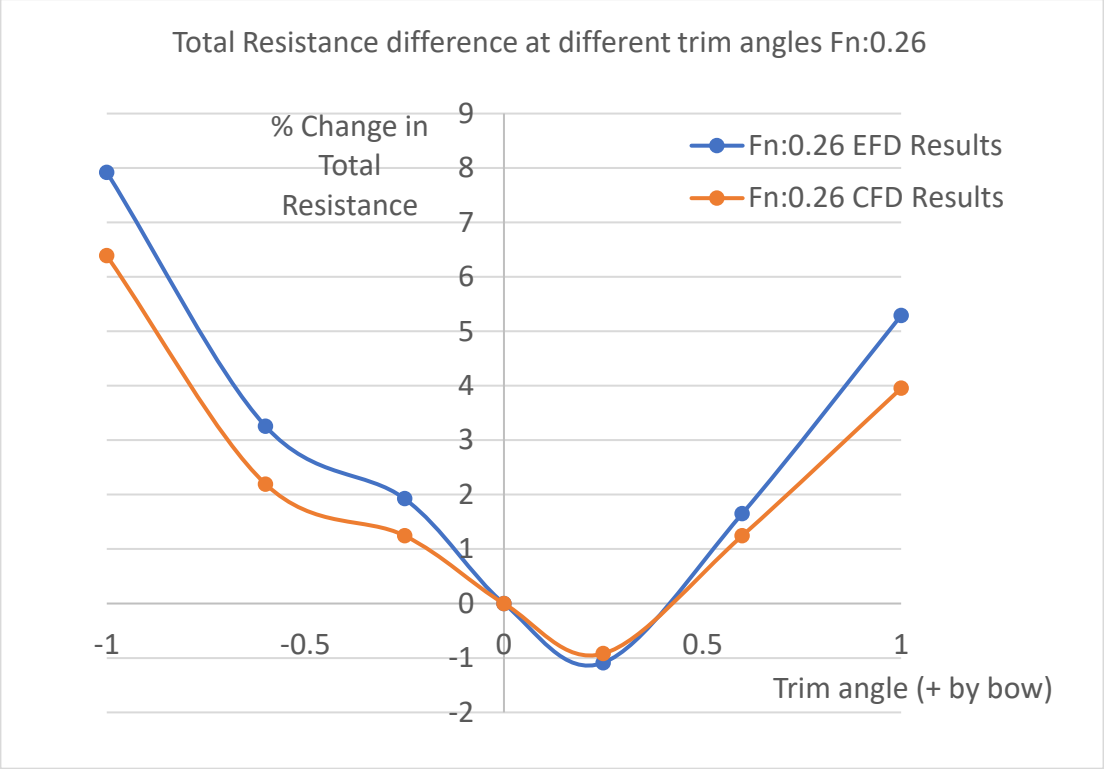

Figure 4-18 Changes in total resistance at different trims for design speed

Figure 4-18 compares the differences in total resistance at different trim angles from experimental results and numerical results for design speed of 24 knots (Fn:0.26) at the design draft condition. The difference of total resistance at trimmed conditions with respect to even keel operation is defined by $(R_\theta-R_0)/R_0*100$ where R_θ is resistance value at the trimmed condition and R_0 is resistance value at even keel condition. Figure 4-19 shows experimental and numerical predictions of changes in total resistance at trimmed operating conditions for slow steaming speed condition. It can be seen that the tendency of changes of total resistance at different trims between numerical and experimental results are similar for both speeds. Therefore, it is possible to say that the numerical calculation method adopted in the simulations is suitable for total ship resistance prediction of KCS model in various operating conditions such as different speed and trim angles.

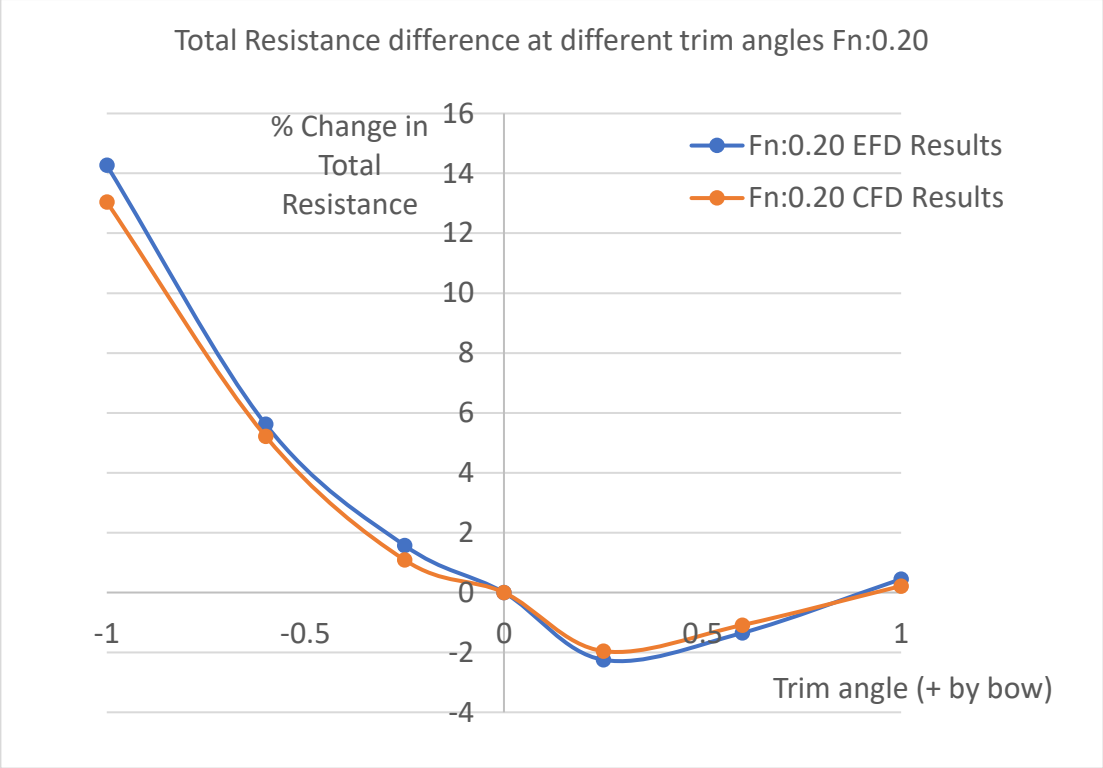

Figure 4-19 Changes in total resistance at different trims for slow steaming speed

Numerical predictions of percentage differences of total resistance for both speeds at different trims with respect to total resistance at level trim condition are given in Table 4-6.

Table 4-6 Numerical predictions of total resistance difference at different trim angles compared to level trim at design draft (10.8 m)

	Fn: 0.20	**Fn: 0.26**
	R_T difference in % with respect to level trim	
Trim (deg) (Positive by bow)		
-1	13.235	6.0234
-0.6	5.2622	2.3458
-0.25	1.2713	1.2941
0	0	0
0.25	-1.9216	-0.9876
0.6	-0.6660	1.4594
1	0.3612	4.0828

It can be seen that 0.25 degree by trim can provide up to 2% reduction in total resistance at 19 knots while reduction potential is around 1% at 24 knots. It is possible to say that slow steaming also affects the performance of the ship in the trimmed condition. It is clearly seen that trim by stern increases the total resistance for all trim angles. When the ship is trimmed 1 degree by stern total resistance increase by 13% at slow steaming condition compared to 8% increase at the design speed. Trimming the vessel by bow performs much better at the slow steaming condition with almost no difference in total resistance even at larger 1 degree trim compared to a 5% increase in design speed.

Changes in resistance components are investigated to better understand the influence of trim on total resistance. Figure 4-20 compares pressure resistance at each trim angle against the level trim predictions. For bow-up trim conditions, pressure resistance shows a large increase of up to 90% above level trim at the slow steaming speed of 19 knots. For 0.25 degree trim by bow, pressure resistance finds its lowest value for both speeds with a reduction of 10% and 4% for 19 knots and 24 knots, respectively.

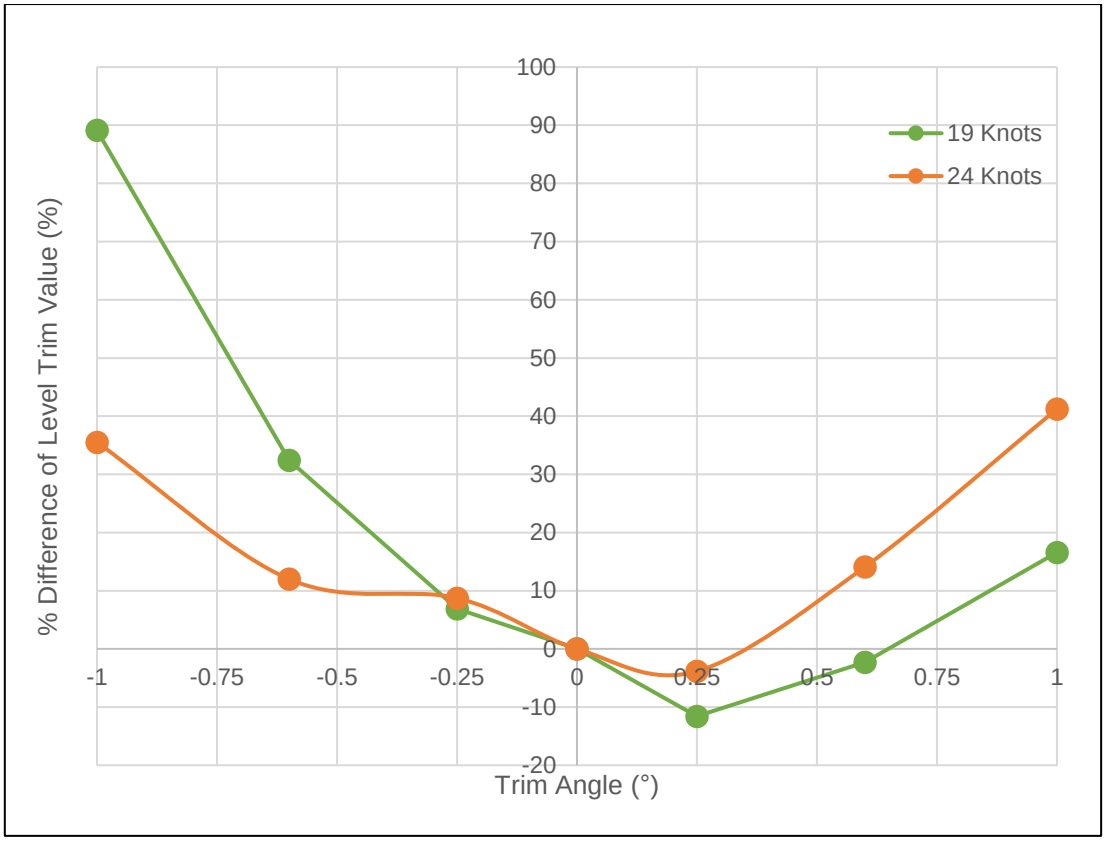

Figure 4-20 Pressure Resistance Variation over Trim Range at design draft

Figure 4-21 presents changes in frictional resistance component at different trim angles. Frictional resistance at design draft decreases slightly with trimming by bow and increase slightly for trim by stern conditions. Frictional resistance trends are almost the same for both slow steaming speed and design speed. The largest reduction is seen at 1 degree trim by bow in line with the reduction in waterline length. Frictional resistance increase by up to 1% in trim by stern conditions for both speeds.

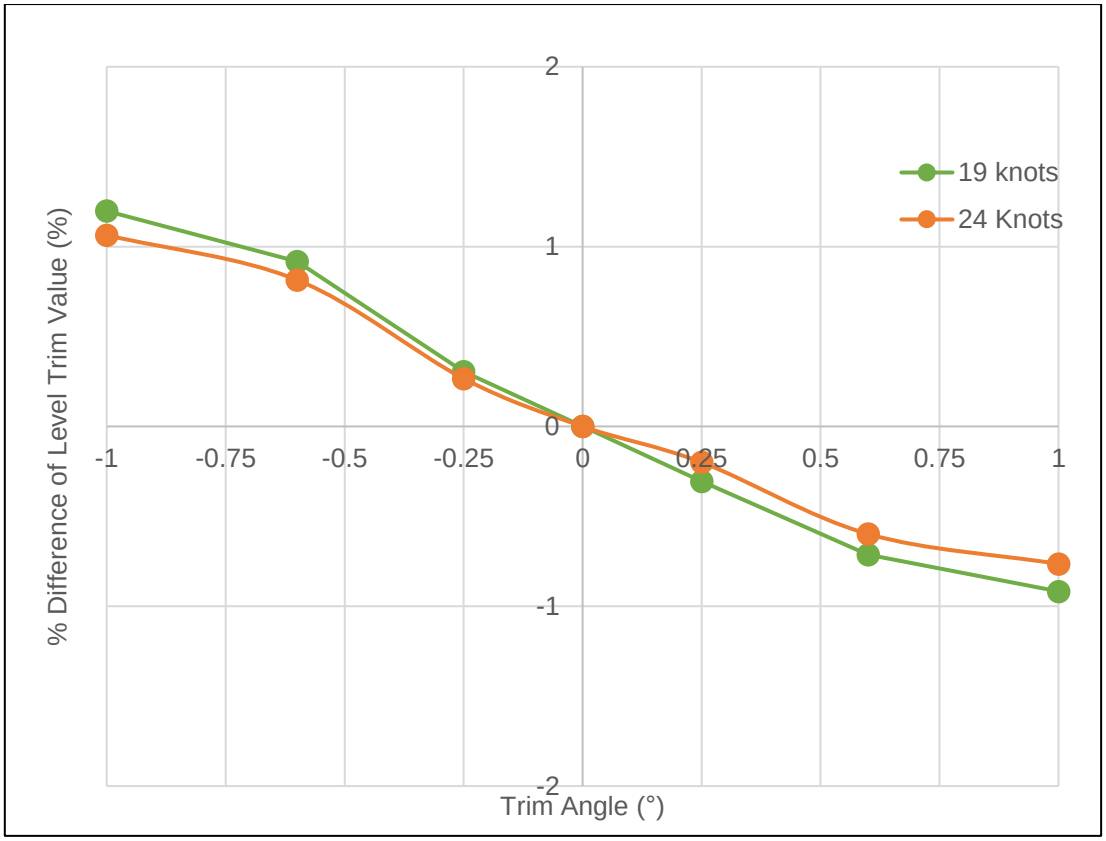

Figure 4-21 Frictional resistance variation over trim range at design draft

Table 4-7 Total resistance components of model scale KCS at design draft

	Frictional Resistance	*Pressure Resistance*
24 Knots	83.43%	16.56%
19 Knots	87.15%	12.85%

Table 4-7 shows the contribution of each resistance component to the total resistance. Frictional resistance is the major contributing resistance component which accounts for 83.43% and 87.15% of the total resistance for design and slow steaming speeds while pressure resistance accounts for the remaining 16.56% and 12.85% of total resistance, respectively.

The pressure resistance component which is related to wave making resistance is the most affected component by trim with larger increases and reductions in its value. However, as it accounts for less than 20% of the total resistance, overall changes are minimal. Even though changes in trim seem to influence pressure resistance greatly, total resistance changes are

much less. The largest reduction in total resistance seen at 0.25 degree trim by bow with 1.9% and 1.1% reduction for 19 knots and 24 knots respectively. Both frictional resistance and pressure resistance values are reduced at trimmed operating condition.

In order to further validate the applicability of the numerical model at different trim angles, experimental results are compared against numerical results for each trim angle at both slow steaming and design speed condition. As seen in Figure 4-22, numerical results are in good agreement with the experimental results. At design speed, predictions errors increase at larger trim angles with a maximum error of 3.5% at 1 degree by bow and 3.2% at 1 degree trim by stern. At the slow steaming speed of Fn:0.20, numerical predictions agree well again with experimental results with maximum error of 3%.

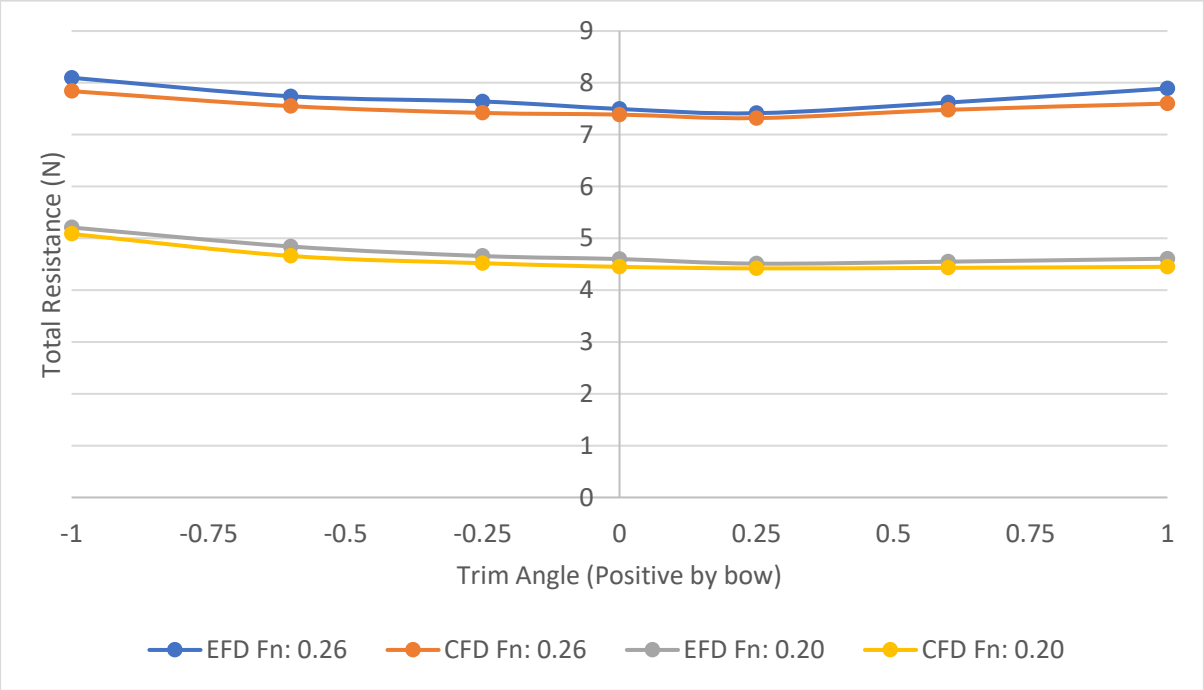

Figure 4-22 Total Resistance comparisons between experimental and numerical results at different trims

Bow wave formation comparison between experiments and calculations are shown in Figure 4-23. It is possible to say that CFD method can capture wave formation along the hull accurately at different trim angles as seen in photos in Figure 4-23. One can see that unfavourable bow wave conditions at larger trim angles are clearly captured in CFD method.

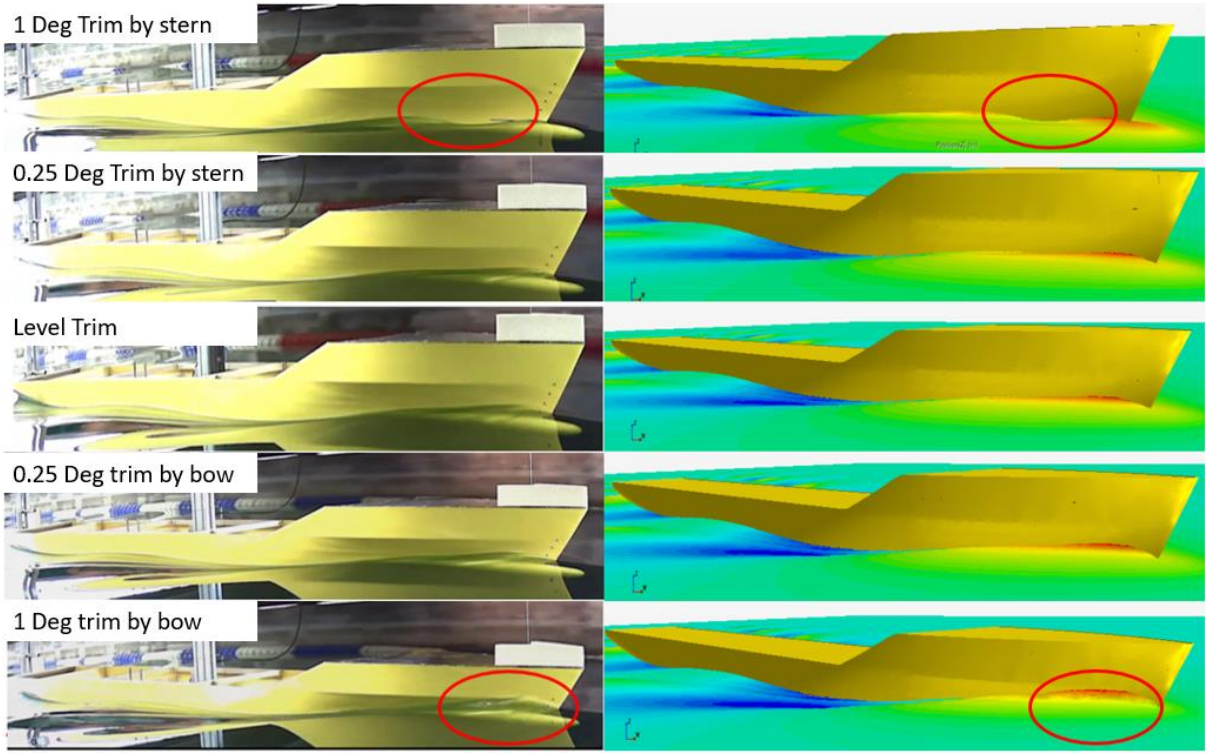

Figure 4-23 Bow wave comparison between EFD and CFD at different trim angles

4.2.3.2 Ballast Draft

The impact of trim on resistance is also investigated for ballast draft condition in the same way as in the design draft. As shown in Figure 4-24, in ballast draft conditions, trim by bow prove a significant reduction in total resistance at slow steaming conditions. At design speed, trim by bow does not provide the same reduction. Trim by stern causes the bulbous bow to emerge above the free surface and thus creates unfavourable bow wave which leads to an increase in ships resistance at both speeds.

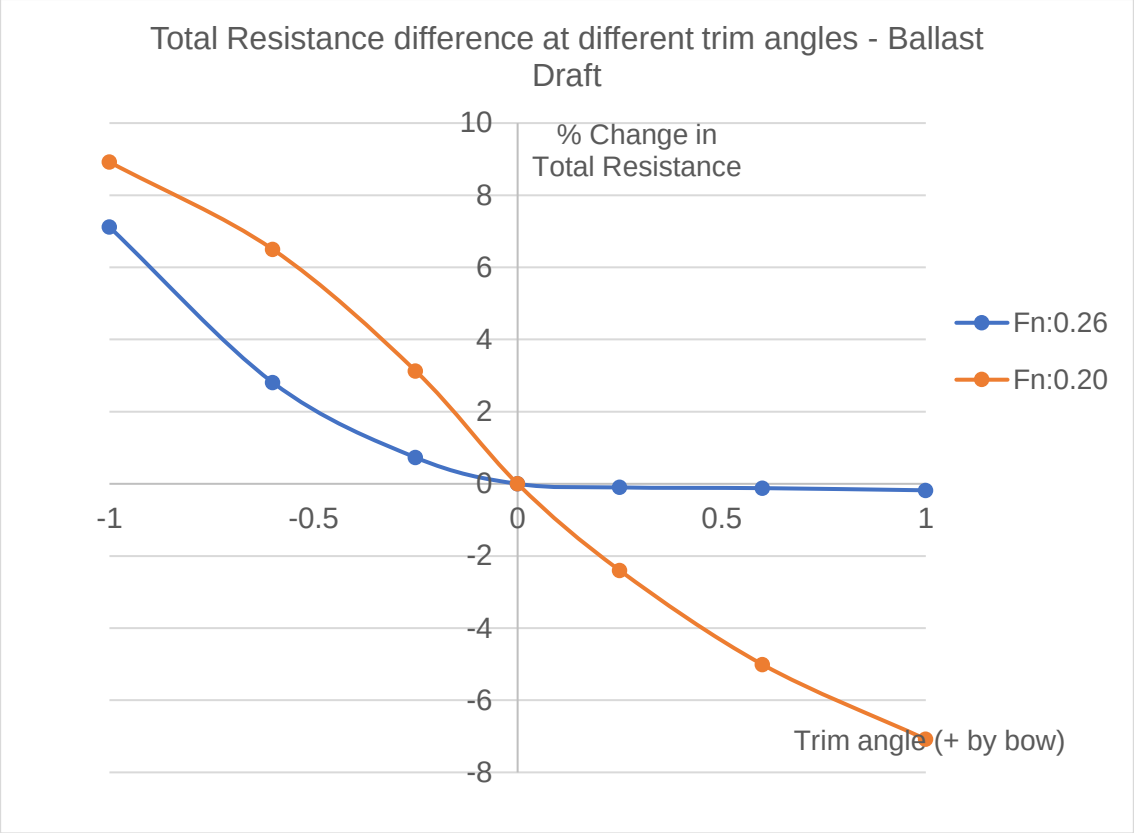

Figure 4-24 Changes in total resistance at ballast draft

Table 4-8 summarises total resistance differences for the ballast trim condition. It can be seen that 0.25 degree by trim can provide up to 2% reduction in total resistance at 19 knots while reduction potential is around 1% at 24 knots. It is possible to say that slow steaming also affects the performance of the ship in the trimmed condition. It is clearly seen that trim by stern increases the total resistance for all trim angles. When the ship is trimmed 1 degree by stern total resistance increase by 13% at slow steaming condition compared to 8% increase at the design speed.

Table 4-8 Total resistance difference at different trim angles compared to level trim at ballast draft (9 m)

	Fn: 0.20	**Fn: 0.26**
	R_T difference in % with respect to level trim	
Trim (deg) (Positive by bow)		
-1	8.92	7.12
-0.6	6.5	2.81
-0.25	3.13	0.73
0	0	0
0.25	-2.4	-0.1
0.6	-5.01	-0.12
1	-7.08	-0.18

Changes in resistance components are investigated to understand the influence of trim on total resistance in ballast draft condition. Table 4-9 presents weights of frictional and pressure resistance components in total resistance. Frictional resistance accounts for 83.70% and 84.45%, while pressure resistance makes up the remaining 16.7% and 15.55% of total resistance at 24 knots and 19 knots respectively.

Table 4-9 Total resistance components of model scale KCS at ballast draft

	Frictional Resistance	*Pressure Resistance*
24 Knots	83.70%	16.70%
19 Knots	84.45%	15.55%

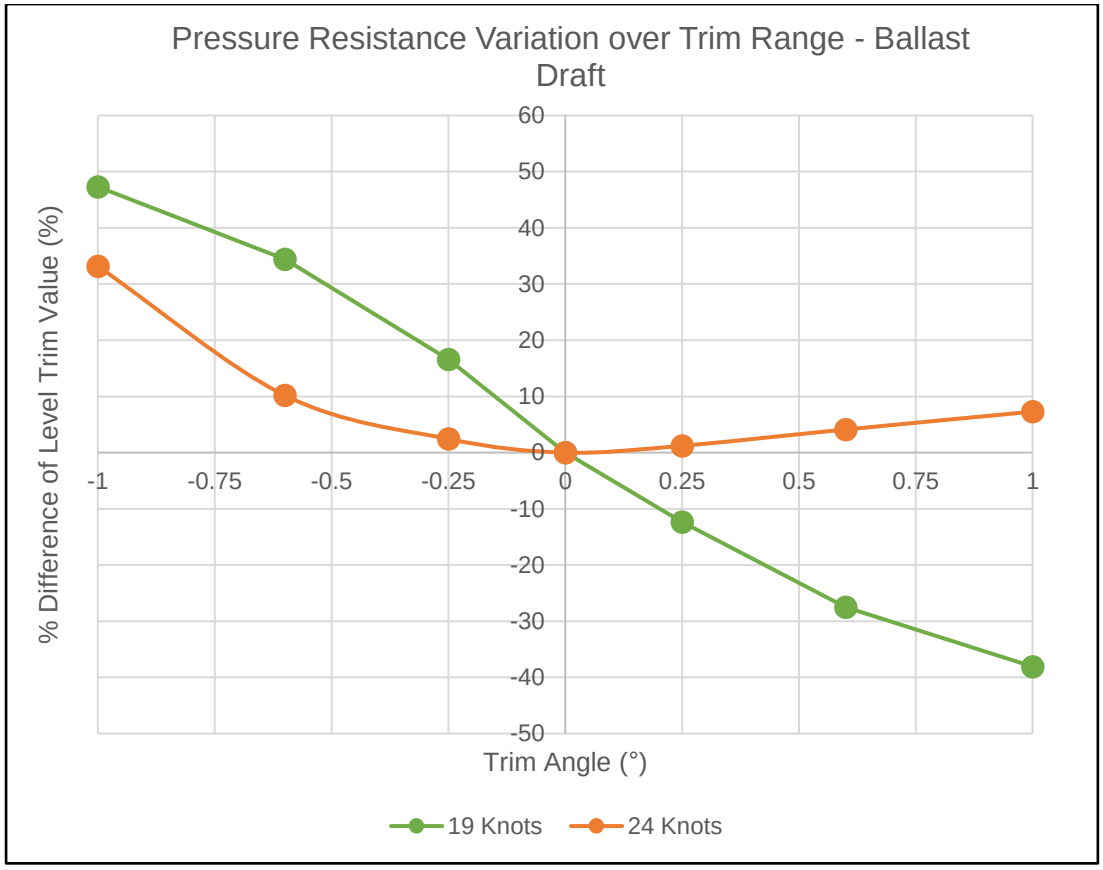

Figure 4-25 CFD prediction of pressure resistance variation over the trim range at ballast draft

In ballast draft, trim influence on pressure resistance varies significantly between slow steaming and design speed as shown in Figure 4-25. Pressure resistance shows a slight increase for trim by bow conditions at design speed while it decreases significantly for slow steaming speed of 19 knots when compared against even keel operation. For trim by stern operating conditions, pressure resistance increases for both speeds. 1 degree trim by stern results in 35% and 48% increase for 19 knots and 24 knots, respectively.

Bow wave formations at different trim angles are shown in Figure 4-26 and Figure 4-27 for design and slow steaming speed. Unfavourable bow wave can be seen clearly for trim by stern conditions at both speeds. Trim by bow results in a smoother bow wave at 19 knots while it creates a slightly bigger bow wave at 24 knots. This can explain the differences in pressure resistance at trimmed conditions which are related to wave making resistance.

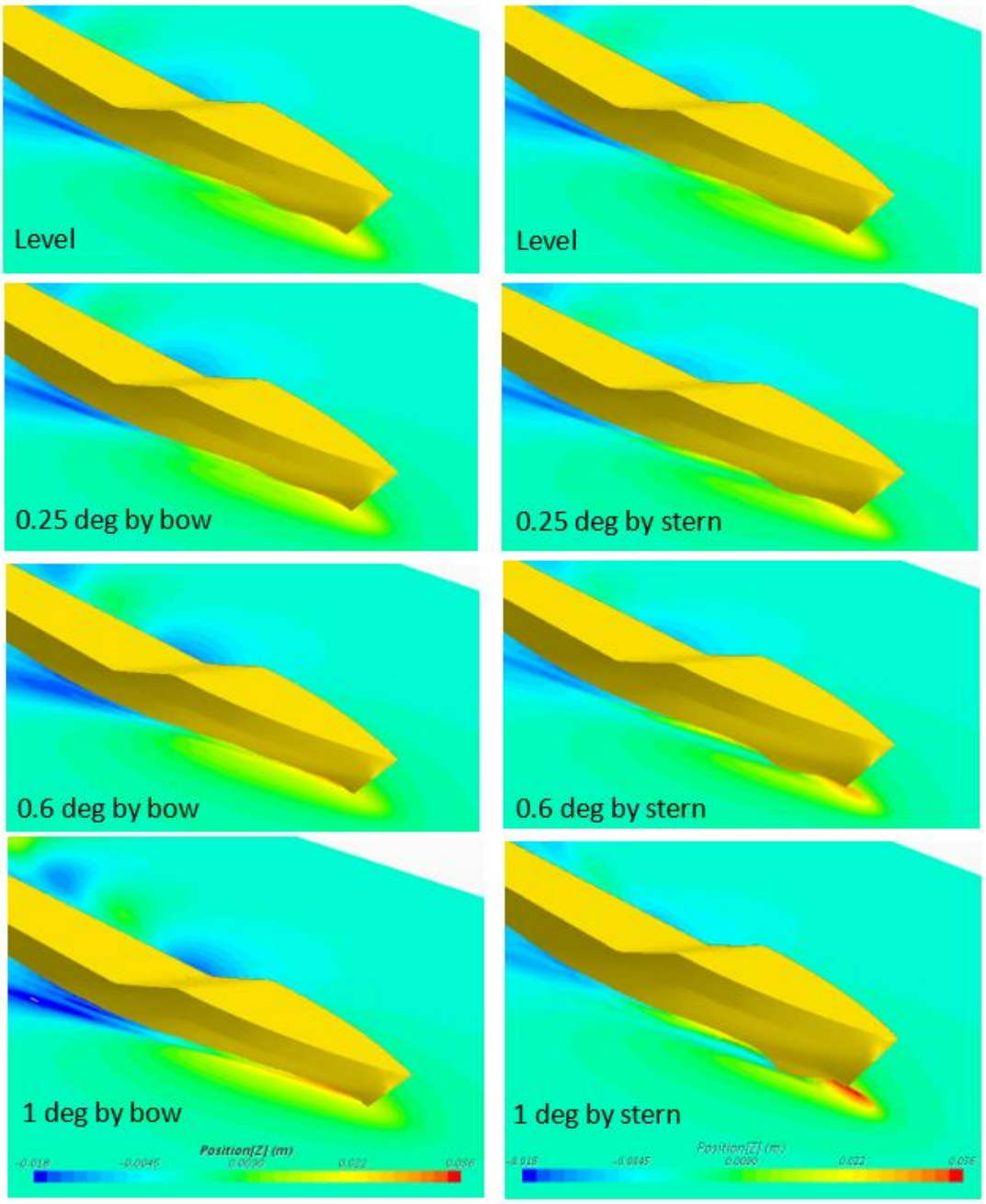

Figure 4-26 Bow wave at ballast draft 24 knots

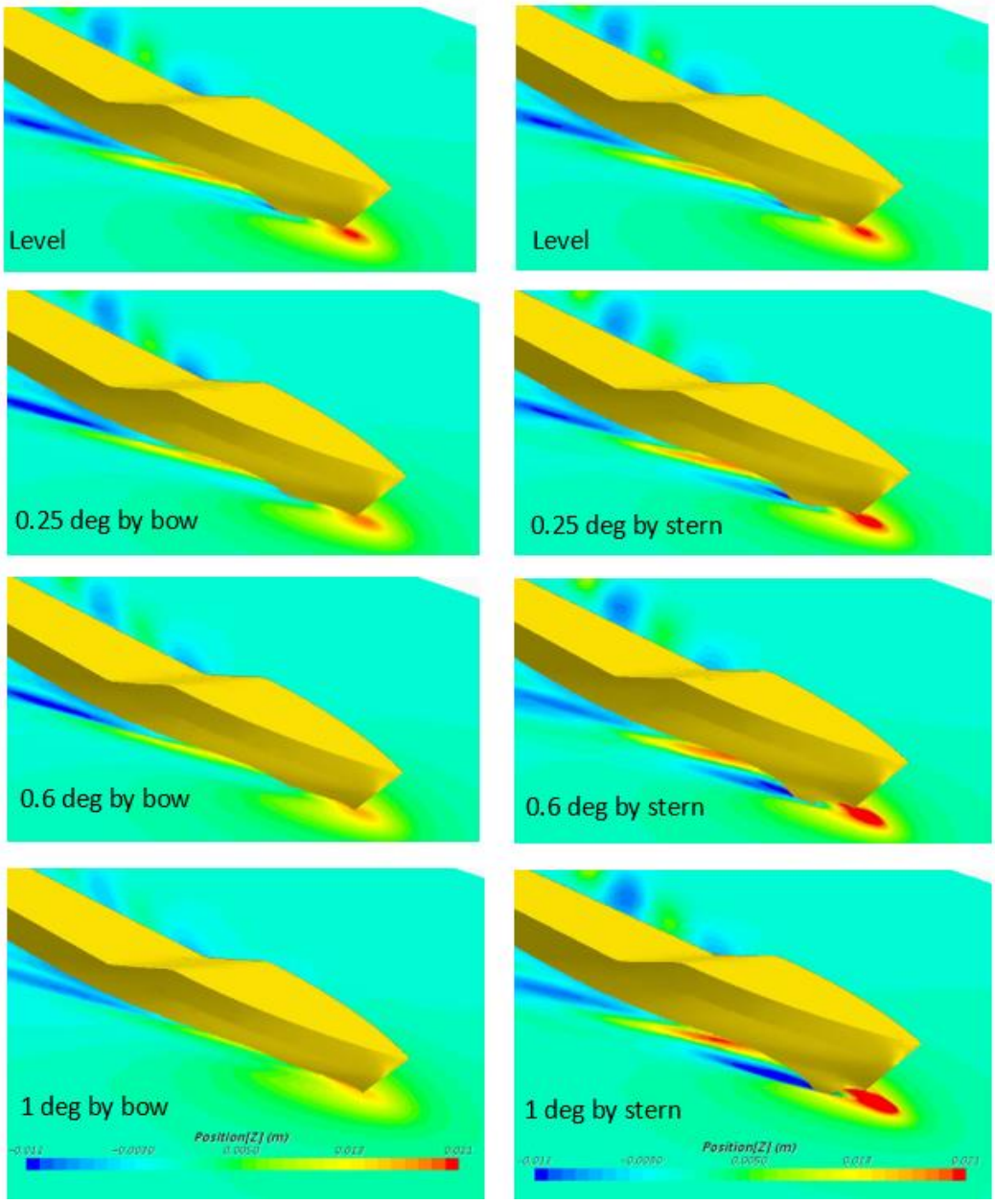

Figure 4-27 Bow wave at ballast draft at 19 knots

Wave pattern comparisons at the free surface for slow steaming condition are shown in Figure 4-28. Differences in bow wave formation and aft submergence can be clearly seen for different trim angles. The emergence of bulbous bow and aft submergence is visible for trim by stern condition and hence total resistance increases significantly. On the other hand, for bow trim condition bulbous bow submerges to the near optimum position which is similar to the design condition and performs much better as expected.

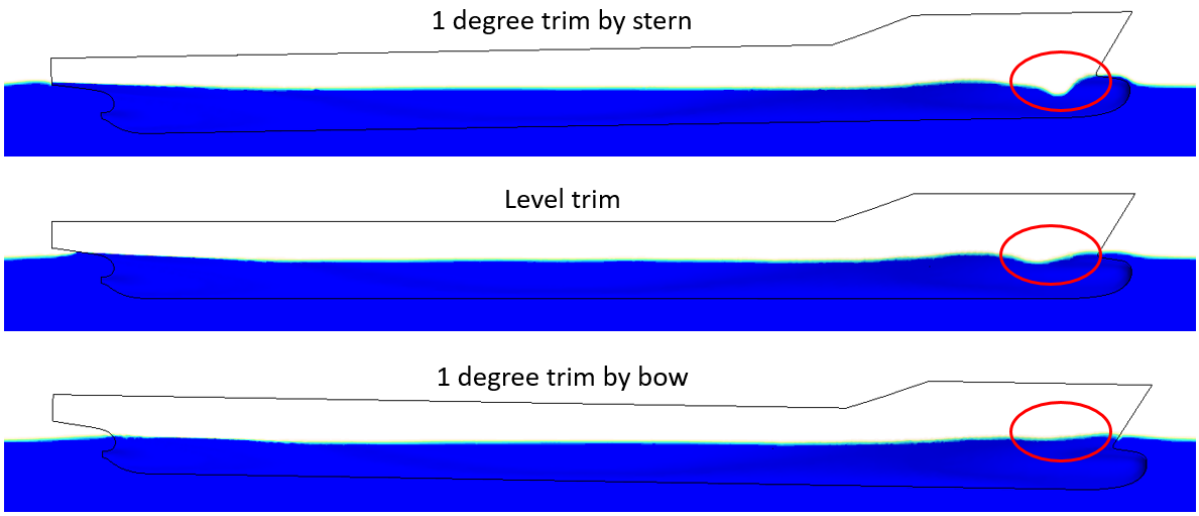

Figure 4-28 Wave pattern at free surface

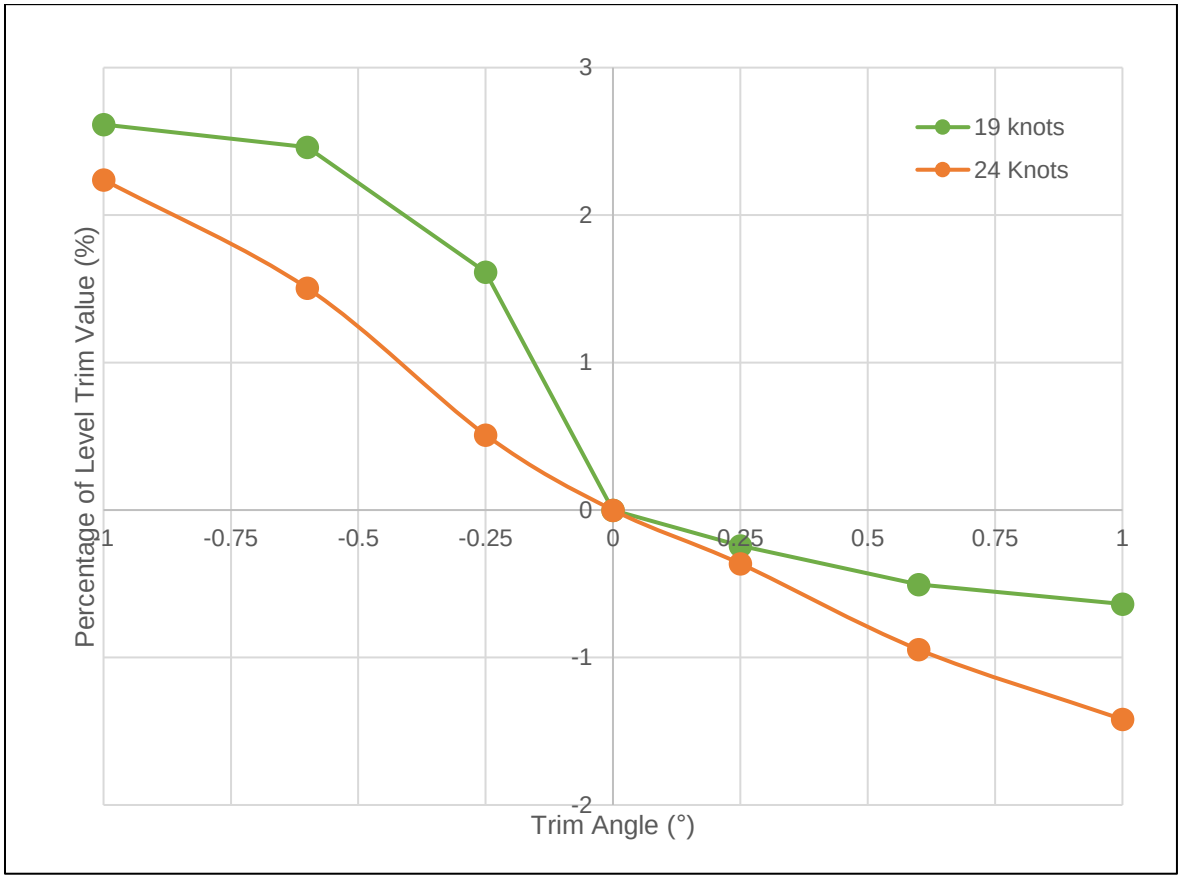

Figure 4-29 Frictional resistance variation over the trim range at ballast draft

Frictional resistance trends at ballast draft are similar to design draft condition with a slight decrease in trimming by bow and increase in trim by stern conditions. Slight differences with the design draft condition can be seen due to changes in length of waterline and Reynolds number in ballast draft condition.

The above results prove that the effects of trim on ships resistance depend on the vessel speed and the mean draft. The underwater hull form is one of the most important factors in this regard especially in conditions where bulbous bows partially protrude above the water or transom sterns partially immerse.

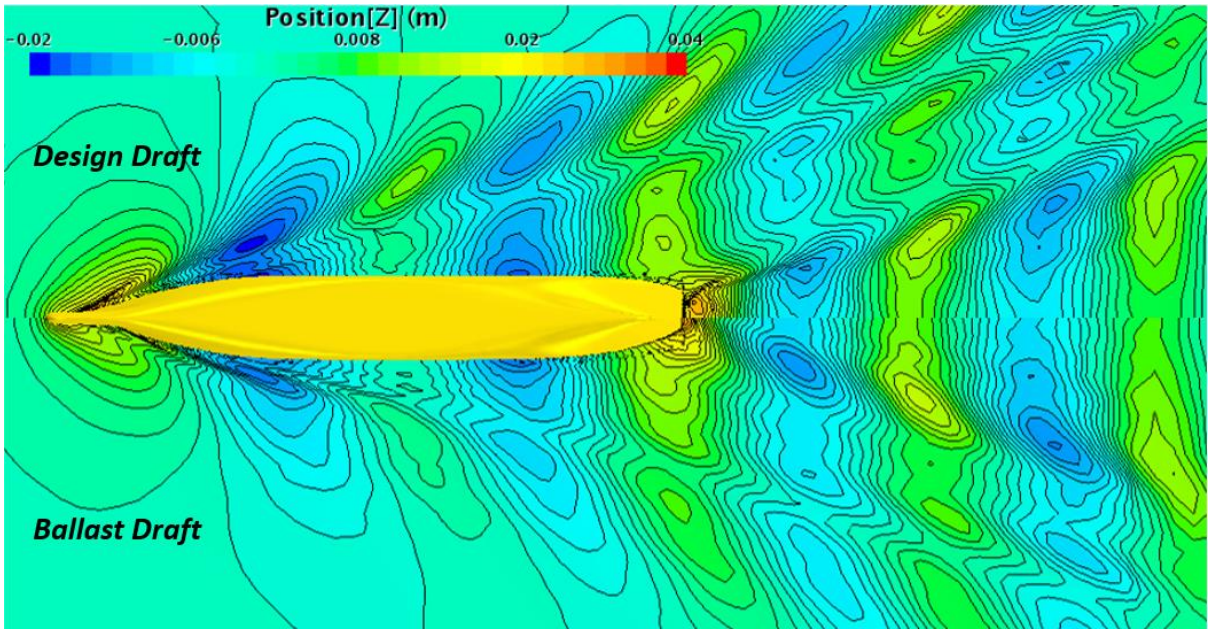

Figure 4-30 Wave elevation comparison between design draft and ballast draft

Figure 4-30 shows the differences in wave elevation for design draft and ballast draft conditions. The differences in wave elevation can be seen clearly as the ballast draft condition shows a smaller wave system. Underwater hull form changes with varying draft and trim and hence differences in wave form can be observed.

4.2.3.3 Fixed Simulations

Further simulations were conducted without dynamic trim and sinkage motions in order to investigate the feasibility of fixed simulations for trim optimisation applications. Consideration of dynamic sinkage and trim is important, as dynamic sinkage and trim add to the computational cost and thus may slow the optimisation process.

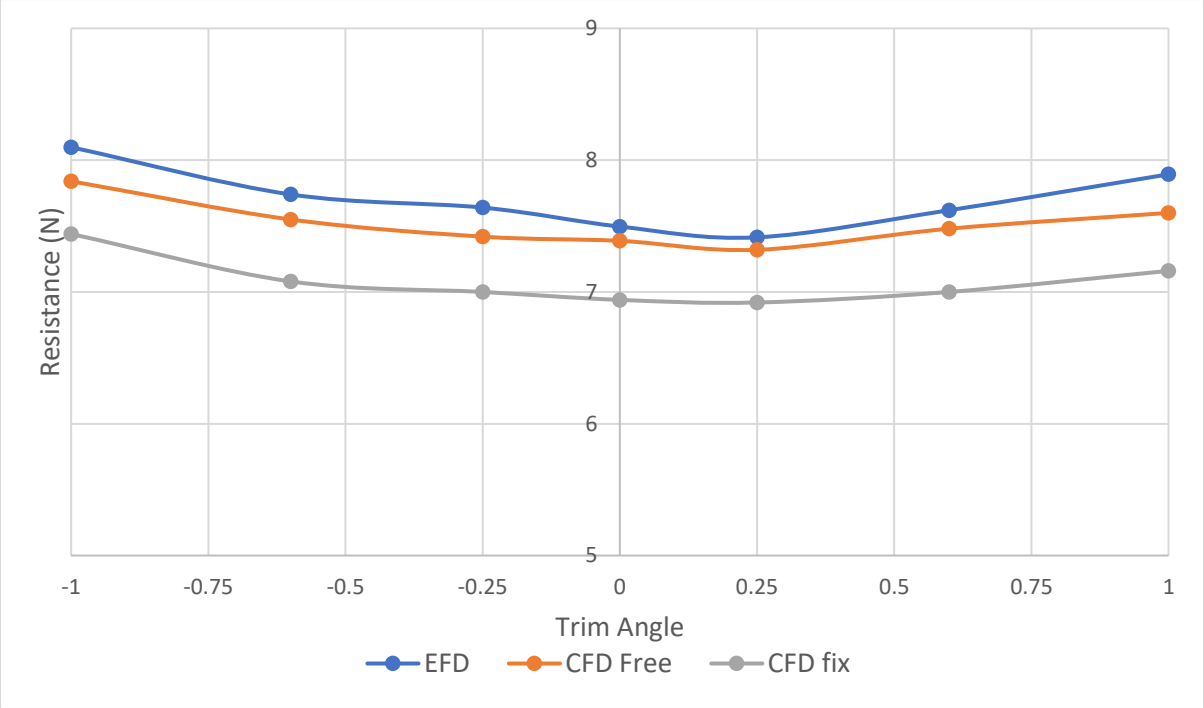

Figure 4-31 Comparison of free and fixed CFD simulations with experiments

Results from the simulations of fixed and free cases are presented along with the experimental results in Figure 4-31. The free model can accurately predict the 1 % reduction in total resistance when the ship is trimmed 0.25 degree by bow. The fixed model also predicts a reduction; however, its magnitude is not predicted as accurately. Comparing the three resistance curves, one can say that both fixed and free trim/sinkage model could predict the trend of resistance with the variation of trim angles; however, the fixed model fails to measure the absolute values as accurately as the free model did. The fixed model was tested as it is computationally faster and cheaper, but results prove that this is an inaccurate approach and it may lead to poor decision making regarding the optimum trim. Therefore, the free sinkage and trim method is found to be a more appropriate technique for trim optimisation.

4.3 Full Scale Investigation

4.3.1 Numerical Investigation in Full Scale

In order to find out scale effects on optimum trim, full scale numerical simulations are carried out. As CFD enables to simulate realistic behaviour of a full scale ship, numerical sea trial

approach was adopted to investigate the scale effects on optimum trim. Similar to the model scale experiments and simulations, the ship was free to heave and pitch but fixed in yaw, roll, surge and sway motions. In full scale simulations, the same approaches were used to create the numerical domain and the mesh structure as in model scale investigation. As in model scale simulations, trimmed mesh technique was employed and only half of the model was simulated due to the lateral symmetry condition. The boundary conditions for the full-scale KCS simulations are also identical to those used in model scale investigation. As fluid properties are not scaled, prism layer thickness was adapted accordingly in full scale simulations which resulted in average y+ values of around 300.

The details of the model scale investigation can be found in Section 4.2.2. The principal particulars of the KCS in full-scale are given in Table 3.1 in Chapter 3.

4.3.1.1 Grid Convergence Study

A grid convergence study was performed to assess the numerical uncertainty of the full-scale simulations as it was performed for model scale simulations. Further details of the adopted grid verification study are given in Section 4.2.2.2 of this thesis. Grid uncertainty test results are presented in Table 4-10 below.

Table 4-10 Grid Convergence Study for full scale simulations

	C_T*10^3
S_1 (1.9M cells)	2.197
S_2(1.05M cells)	2.170
S_3(0.6M cells)	2.133
R	0.56
GCI_{fine}	1.60%

Grid uncertainty test results in a monotonic convergence for the total resistance coefficient C_T with R = 0.56 and the grid uncertainty with U_G = 1.60%S_1 based on the Grid Convergence

Index (GCI) method. Fine mesh system with 1.9M cells was employed in the CFD simulations.

4.3.1.2 Comparison Study

Experimental results are extrapolated to full scale in order to make a comparison with the full scale simulation results. It should be noted that ITTC 7.5-02-02-01 guidelines are adopted during the extrapolation of the results from model scale to full scale. The total resistance coefficient of the full scale ship is:

$$C_{TS} = (1+k)C_{FS} + C_W \tag{4.10}$$

In which k is the form factor as determined in the previous section. The frictional resistance coefficient C_{FS} was calculated by the ITTC-1957 correlation line (Eq. 4.12) for the ship scale Reynolds number Re_S (Eq. 4.11), considering the hydrostatic water line length of the full scale ship $L_{S,WL}$.

$$\mathrm{Re}_S = \frac{v_S L_{S,WL}}{\nu_S} \tag{4.11}$$

$$C_{FS} = \frac{0.075}{(\log_{10}\mathrm{Re}_S - 2)^2} \tag{4.12}$$

As wave making resistance coefficient C_W is the same at both model scale and full scale, full scale resistance coefficient can be calculated. After that total resistance of the full-scale ship can be obtained as:

$$R_{TS} = 0.5 C_{TS} \rho_S S_S v_S^2 \tag{4.13}$$

Total resistance coefficient values at level trim condition from the CFD simulations are compared against the extrapolated experimental data. As seen in Table 4-11 full scale simulation results agree well with experimental results with discrepancies of -3.21% and -0.9% for 19 knots and 24 knots respectively.

Table 4-11 Comparison of full scale simulation results with experimental values

Full Scale KCS	***EFD***	***CFD***	***E%D***
C_T*10^3 (19 Knots)	1.99	1.92	-3.21%
C_T*10^3 (24 Knots)	2.21	2.19	-0.90%

4.3.2 Results and Discussion

Total resistance values for each trim angle are calculated for design speed and slow steaming speed at both design draft and ballast draft. Differences in total resistance at full scale are compared against model scale results. Figure 4-32 and Figure 4-33 show comparisons at design for 24 knots and 19 knots respectively. As can be seen from the figures, trends of total resistance differences at trimmed conditions are similar for full scale and model scale results. However, magnitudes of increases and decreases show significant differences between full scale and model scale. At design speed, optimum trim angle of 0.25 degree trim by bow results in 2% reduction in total resistance at full scale while saving potential was found to be around 1% for model scale investigation. For trim by stern conditions, increase in full scale resistance is higher for all three trim angles when compared against the increase in model scale results. Similar observations can be made for slow steaming speed ballast draft condition. At ballast draft condition, a similar trend can be observed again with potential reductions and increases in total resistance are higher for full scale simulations. Figure 4-34 and Figure 4-35 presents results for ballast draft operation.

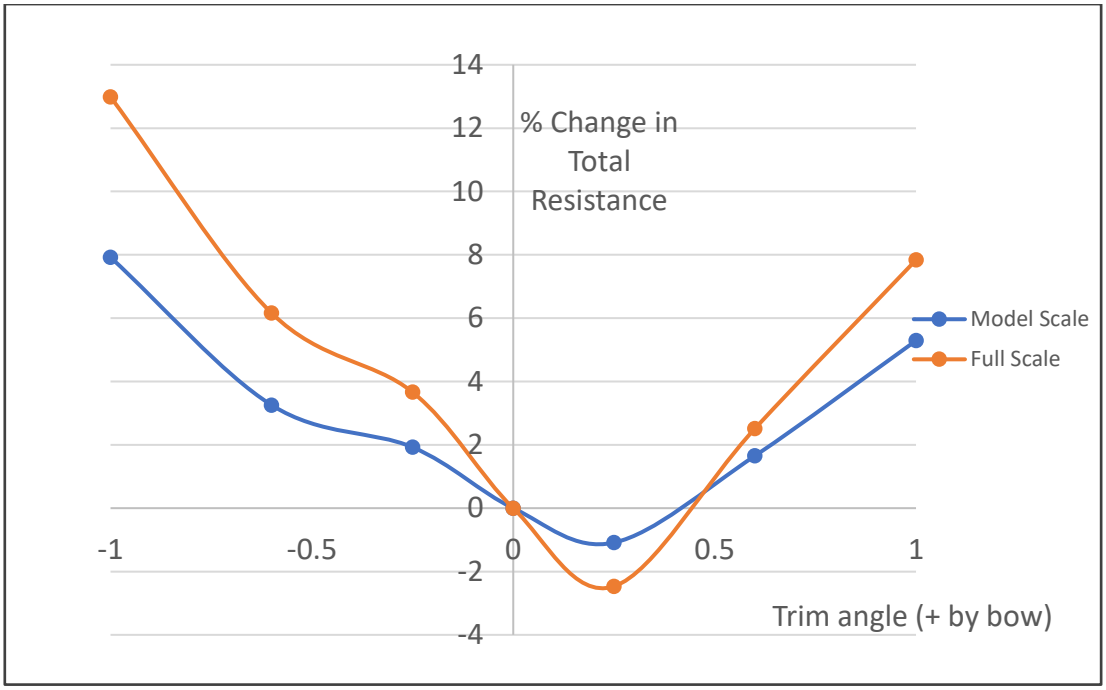

Figure 4-32 Total Resistance differences at Model and Full Scale KCS for different trim angles at 24 Knots at design draft

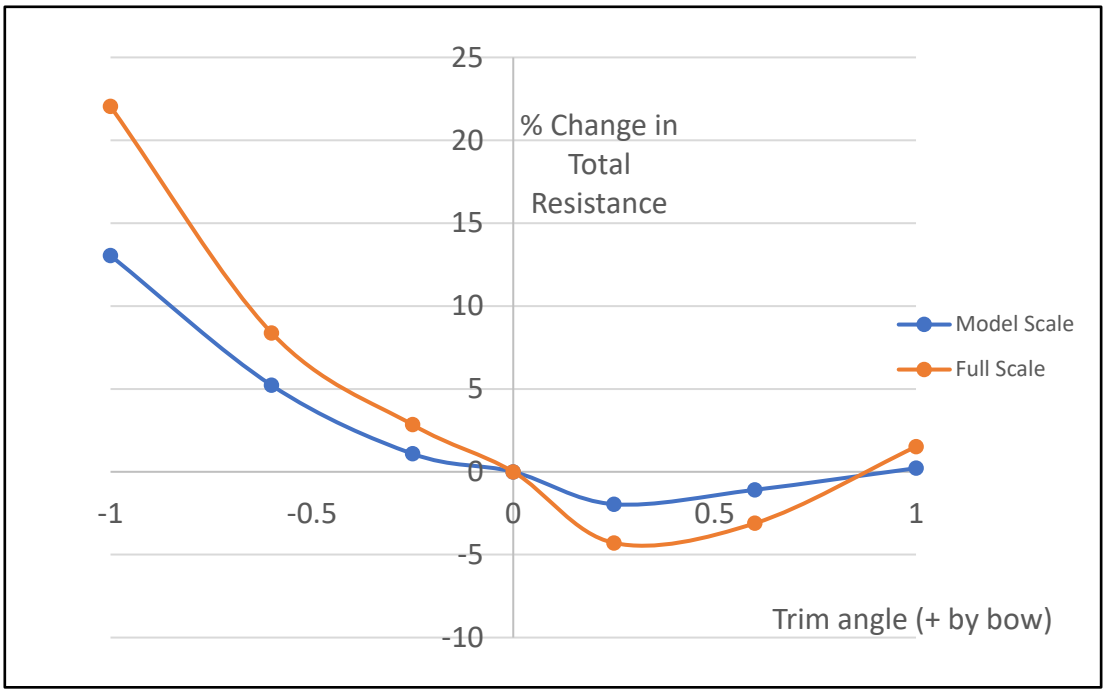

Figure 4-33 Total Resistance differences at Model and Full Scale KCS for different trim angles at 19 Knots at design draft

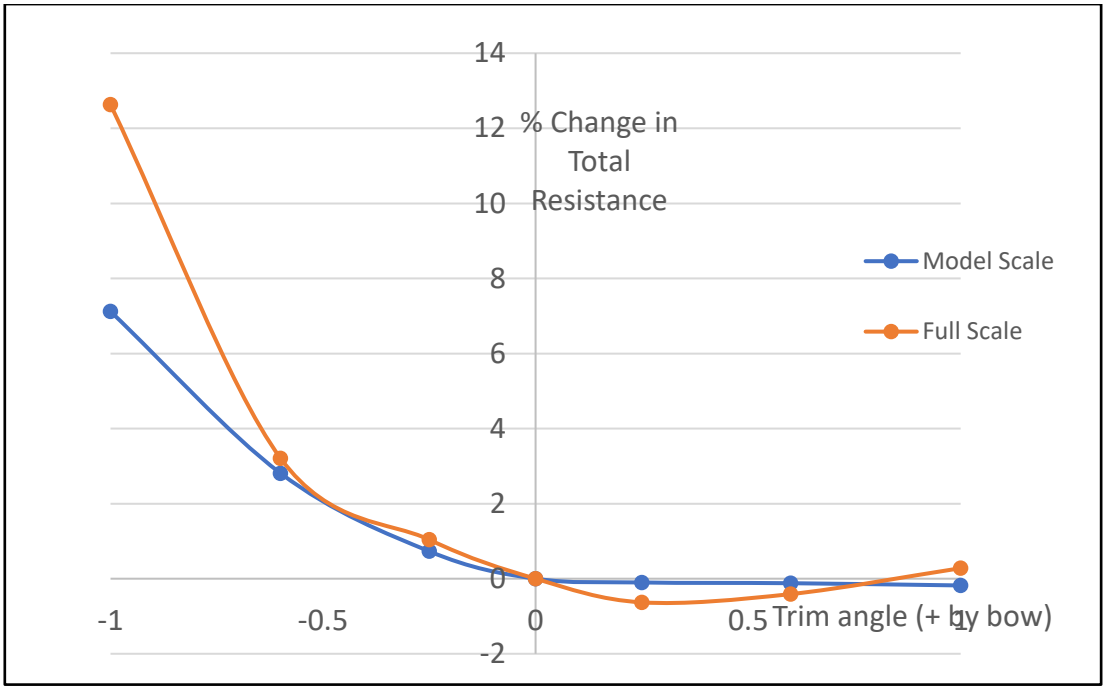

Figure 4-34 Total Resistance differences at Model and Full Scale KCS for different trim angles at 24 Knots at ballast draft

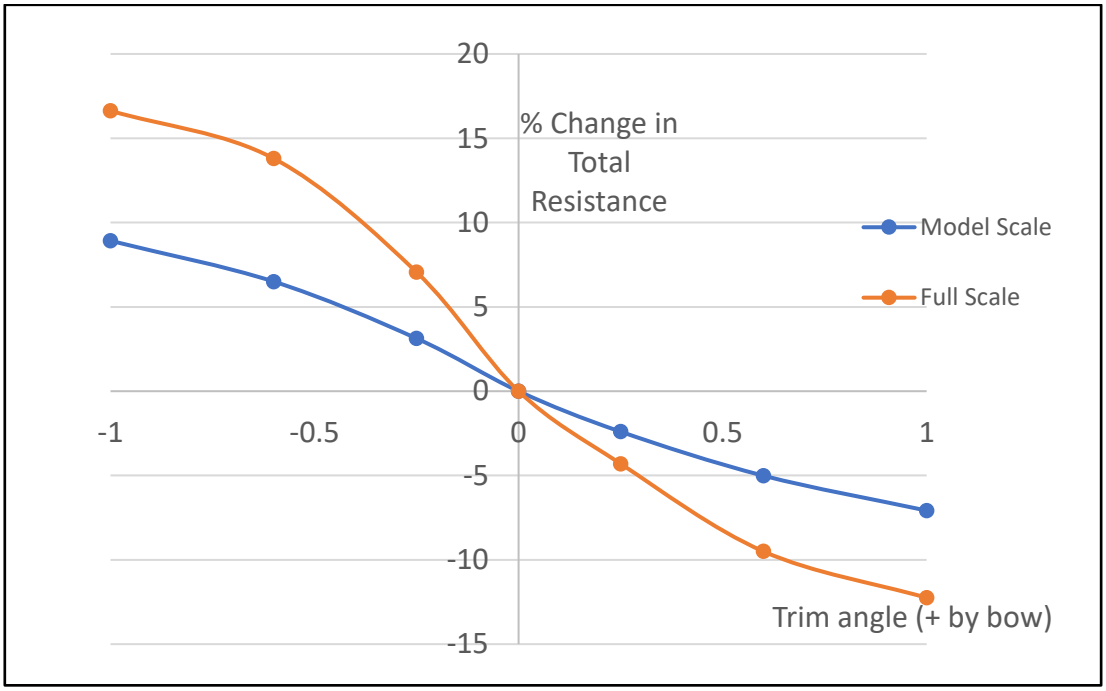

Figure 4-35 Total Resistance differences at Model and Full Scale KCS for different trim angles at 19 Knots at ballast draft

In order to investigate these differences between full scale and model scale results, resistance components at model scale and full scale are compared and discussed.

Table 4-12 Resistance components for full scale and model scale KCS

	Frictional Resistance	*Pressure Resistance*
Model Scale (24 Knots)	83.43%	16.57%
Full Scale (24 Knots)	71.72%	28.28%
Model Scale (19 Knots)	87.15%	12.85%
Full Scale (19 Knots)	77.60%	22.40%

Table 4-12 presents the contribution of individual resistance components at model scale and full scale for design speed. In full scale simulations, frictional resistance contribution decreases from 83% to 71.72% while pressure resistance contribution increases from 16.5% to 28% when compared against model scale simulations at the design speed of 24 knots. As discussed in the previous section, trim influences wave making resistance significantly, therefore it is possible to say that the differences between model scale and full scale resistance components become even more important for trim optimisation studies.

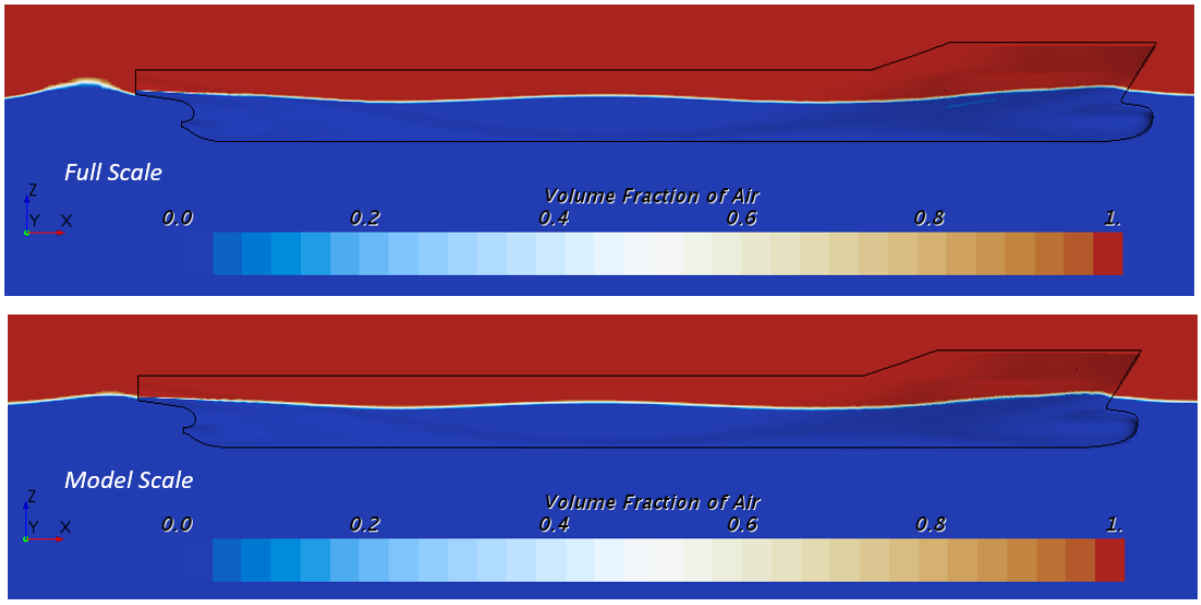

Figure 4-36 Side view of waterline for full scale and model scale KCS

Figure 4-36 shows the free surface elevation on the hull surface in model and full scale. Stern of the ship is slightly wet in model scale simulation while it is dry in full scale. Higher tail wake can be seen clearly for full scale ship. Differences in stern wave formation can be observed and it becomes even more significant with trim due to changes in stern shape. This

confirms the findings from wave pattern analysis as higher wave elevations seen for full scale ship increases the percentage of pressure resistance which is related to wave making resistance. Therefore, full scale investigation could be more beneficial for trim optimization of ships especially with transom sterns, where transom sterns partially immerse. Full scale simulations can also be beneficial for the simulation of physical fluid phenomena that are difficult for experiments.

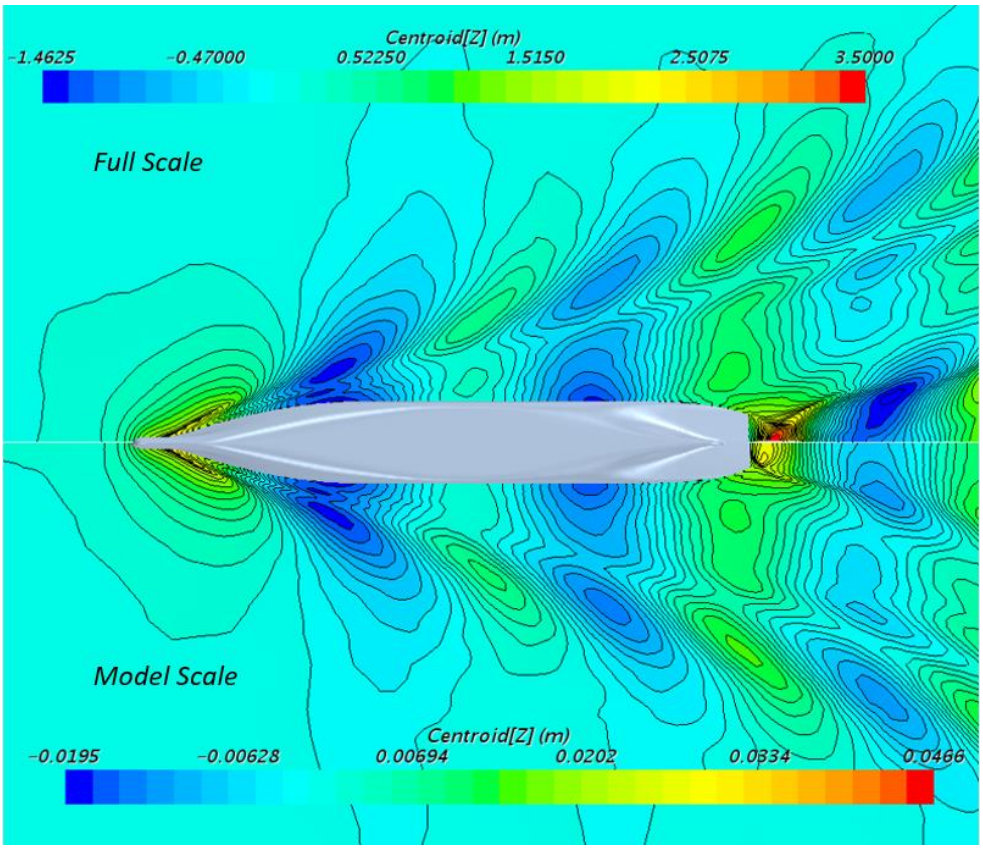

Figure 4-37 Wave profile around the hull at design draft

The wave profile around the hull is shown in Figure 4-37. There is not a significant difference between model scale and full scale ship wave field apart from the stern part where the viscous wake is present. This confirms the general assumption of equal wave resistance for model and full scale ships is correct. The geometrical similarity is achieved when performing model scale simulations independent of Reynolds number.

4.4 Conclusions

In this chapter, the influence of trim on ship resistance was investigated by model tests and numerical computations at model scale and full scale. The numerical results at different trims were compared with ship model experiments.

The experimental investigation was conducted first to investigate the trim influence on calm water resistance and to provide validation data for numerical simulations.

A grid convergence study was performed to validate the numerical approach and comparisons showed good agreement.

Another aim of the study was to assess the suitability of different CFD techniques in trim optimisation. The study showed that using a simpler technique of fixed trim and sinkage, although reducing computational cost, cannot accurately predict the magnitude of the saving at optimum trim. The model test and CFD method agreed well in the prediction of the total resistance trend with respect to trim. It was also confirmed that significant reductions in total resistance are achievable by operating the ship at optimum trim.

It was also observed that the resistance can be accurately predicted using a relatively small number of cells (1.3M mesh size) with local refinements around the areas of interest. This is especially important for comprehensive trim optimization studies which require high numbers of CFD simulations. Model tests are valuable in the sense they provide reliable information about the influence of trim on vessels resistance performance. However, the creation of a dense knowledge base that includes different speed, trim and draft values within the operational profile of the vessel may take more time and cost than computational methods.

It was shown that draft, speed and trim all influence the resistance of the vessel. Trim optimisation can help to obtain savings and also to avoid certain operating conditions which can increase the fuel costs significantly. Analysis of vessel operating profile becomes important to define the most popular operating points such as draft and speed in order to realise the gains from trim optimisation.

Changes in total resistance components analyses showed that pressure resistance is the most affected component by trim. Pressure resistance value can vary up to 90% at trimmed

conditions when compared against level trim value. Changes in frictional resistance were minimal at trimmed conditions in line with the changes in length of waterline.

Model scale investigation can capture the effect of trim on total ship resistance accurately regarding the prediction of increase, decrease in resistance at trim by stern, and bow respectively. However, the magnitudes of prediction values are different from full-scale investigation. Model scale investigation can provide initial information about trim effects however full-scale investigations would be more appropriate technique to understand the real potential savings.

Chapter 5 Trim Influence on Added Resistance

Chapter 5 is dedicated to the investigation of the trim influence on added resistance. The chapter starts with details of the experimental investigation. Following this, numerical model details are outlined. Finally, experimental and numerical results are presented and results are discussed.

5.1 Introduction

In this chapter, EFD, CFD and potential theory based methods are employed to investigate ship motions and added resistance in regular head waves at six different trim angles. As it is well-known, high fidelity CFD simulations require significant amount of computational power and time for the prediction of added resistance. Hence, potential theory based methods are also employed in this chapter in order to indicate ranges of ship speed, trim and wave conditions to which rapid linear potential flow calculations may be applicable. Numerical computations of ship motions and added resistance were validated against model scale experiments.

As discussed in Chapter 2 of this thesis, the majority of trim related studies have been performed at calm water and many of the added resistance studies have been conducted at level trim angles. Optimum trim attained at calm water may not have the same effect in real sea environment as waves restrict overall ship behaviour and lead to speed loss. Therefore, added resistance in waves at different trim angles should be investigated in ship operational optimization to increase energy efficiency. In that regard, this study aims to provide an understanding of the seakeeping behaviour and performance of the KCS model at different trim angles.

In this chapter, added resistance and motion responses of KRISO Container Ship (KCS) were evaluated experimentally and numerically in six different trim angles.

5.2 Experimental Investigation

A series of towing tank experiments were performed for six different trim angles at design speed in regular head waves. The principal particulars of KCS can be found in Table 3.1. Details of the experimental setup can be found in Chapter 3.

The experiments are carried out at Fr=0.26 in calm water and in head waves with λ/L=0.5~2.0 covering short wavelength $\lambda/L < 0.8$, mid-range wavelength $0.8< \lambda/L<1.4$ and large wavelength $\lambda/L >1.4$ region, for design draft condition.

Seven different regular head waves were carefully selected following ITTC recommendations for seakeeping experiments covering the wave-ship length ratio λ/L=0.5, 0.65, 0.75, 0.85, 1.15, 1.37, 1.95 with $H/\lambda = 1/60$, as shown in Table 5-1. Accuracy of wave amplitude is of critical importance as added wave resistance is proportional to wave amplitude squared. Wave probes were used to measure incident wave amplitudes. Wave probes were located in the middle of the tank and one ultrasonic wave probe close to the model. The details of the wave probe calibration are given in section 3.2.4.3 The difference between measured and target wave amplitude values do not exceed 3% of the target wave amplitude value.

Table 5-1 Test matrix

λ/L	**Wave length (m)**	**Wave height (m)**	**Wave amplitude (m)**	**Wave steepness**
0.5	1.533	0.0256	0.0128	1/60
0.65	1.993	0.0332	0.0166	1/60
0.75	2.300	0.0383	0.0192	1/60
0.85	2.607	0.0434	0.0217	1/60

1.15	3.527	0.0588	0.0294	1/60
1.37	4.201	0.0700	0.0350	1/60
1.95	5.980	0.0997	0.0498	1/60

Tests were conducted for three different trim angles by bow, three for aft trim in total six different trim angles and level trim condition at design speed. Selected trim angle values range from 0.25 degree up to 1 degree for bow and stern trim conditions to cover a wide range of trim conditions and to ensure complete propeller immersion. These angles correspond to 1m to 4m trim in full scale.

In the post-processing stage, the time-histories of the vessel's sinkage, bow motion, drag and amplitudes of generated waves were analysed using the commercial software package Spike. The details of the measurement instruments can be found in section 3.2 of this thesis.

5.3 Numerical Investigation

In the present study, the 3-D linear potential flow and URANS CFD methods are applied to predict the added resistance and the ship motions in regular waves.

This section aims to provide a brief overview about the main features of the adopted numerical approaches.

URANS CFD simulations were carried out using commercial software Simcenter STAR-CCM+. Details of the CFD approach was given in Chapter 3.

To indicate ranges of trim and wave conditions to which rapid linear potential flow calculations may be suitable for adoption, potential flow theory based method is also used in this study. 3-D linear potential theory results are obtained using PRECAL code, which is developed by the MARIN Cooperative Research Ships (CRS) and include a 3-dimensional potential code (Van't Veer, 2009). The planar panel method, which is able to calculate the

seakeeping performance of different hull forms such as monohulls, catamarans and trimarans, is adopted in PRECAL code. Since panel codes use a more detailed description of the hull, the diffracted and radiated waves can be accounted for in all directions. Furthermore, it has the capacity to calculate the deformation modes of a ship's hull girder, internal loads, pressure on the hull and added resistance in waves. The near-field approach based on direct pressure integration over the mean wetted hull surface is used for added resistance calculations. Only the mean values of forces and moments are taken into account in added resistance calculations. Calculations take only a short period of time since all computer cores are being used. Kim et al. (2017) and Hizir et al. (2019) have explained the code in more detail and they have presented results regarding the robustness of the code and provided a more detailed discussion of added resistance components.

5.3.1 Computational Domain and Boundary Conditions

5.3.1.1 Boundary Conditions

The initial conditions and boundary conditions are defined to represent the KCS ship being towed in deep water. Selection of the boundary conditions and positioning of these boundaries are essential to obtain an accurate solution. A velocity inlet boundary condition was positioned at $1.5L_{BP}$ ahead of the vessel to decrease the free running length of incident waves and a pressure outlet was selected at $3L_{BP}$ behind to avoid wave reflections. This is different than the calm water simulation domain which was located 2.5LBP away from the ship body. Location of pressure outlet boundary was extended in wave simulations as wave reflection from the walls was more prominent. Velocity inlet boundary condition was also applied to top, side and bottom boundaries to prevent fluid reflections. A symmetry boundary condition was used to reduce the number of cells and computational cost. These boundary conditions were selected by following best practices for similar simulations as recommended by Simcenter and ITTC guidelines (SIEMENS, 2017). Artificial wave damping was applied at the outlet boundary with a damping length of $1.25L_{BP}$ to numerically reduce the wave amplitude and to reduce reflections. Figure 5-1 displays an overview of the computational domain showing the KCS model and selected boundary conditions.

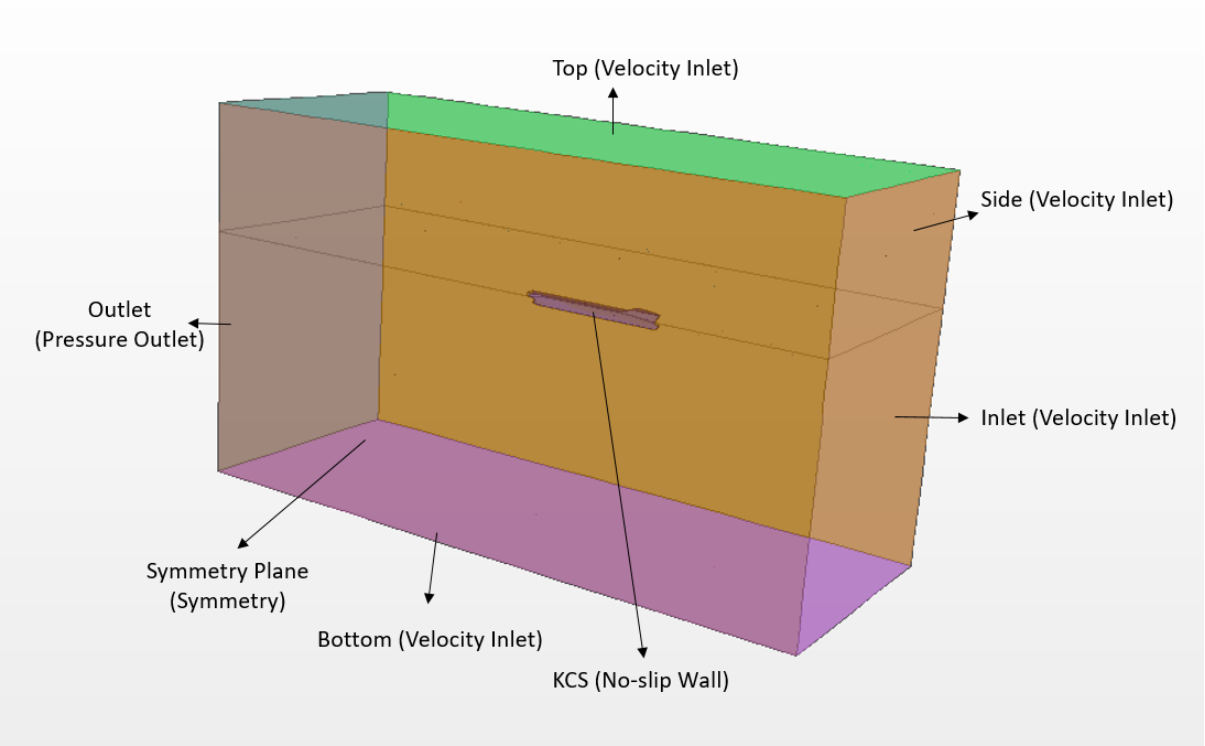

Figure 5-1 Overview of the computational domain and boundary conditions

The domain size and location of boundaries are summarized in Table 5-2.

Table 5-2 Locations of the boundaries in computational domain

Boundary	*Position*	*Boundary Condition*	*Note*
Inlet	2.5 LPP	Velocity Inlet	AP is set to 0
Outlet	3.0 LPP	Pressure Outlet	AP is set to 0
Symmetry	-	Symmetry	Centre line is set to 0
Side	2.0 LPP	Velocity Inlet	Centre line is set to 0
Top	1.5 LPP	Velocity Inlet	LWL is set to 0
Bottom	2.5 LPP	Velocity Inlet	LWL is set to 0

5.3.1.2 Mesh Generation

Volume mesh generation is crucial as it has a direct influence on the accuracy of fluid flow simulations. Mesh construction defines the rate of convergence and it also has a strong influence on the accuracy of the final solution. Volume mesh was created by using the automatic meshing tool in Star CCM+. The trimmed cell mesher technique was employed as it provides a robust and computationally efficient solution for complex meshing problems. Only half of the flow domain was simulated due to the lateral symmetry condition in order to reduce computational effort. Local mesh refinements were applied in the areas of interest such as the area nearby the ship hull, bulbous bow and stern, expected free surface and in the wake field that was created by the ship, in order to capture the complex flow features. The computations were performed at the same scale and same conditions as in the physical tests to ensure the best comparability.

Accurate resolution of the wave shape is one of the main goals in seakeeping simulations. It is necessary to create a good mesh that is refined in the correct regions. According to Star CCM+ user guide, a minimum of 80 cells per wave length and 20 cells per wave height should be used on the free surface in order to resolve the wave shape. (SIEMENS, 2017). Based on these recommendations, a base mesh system was created for seakeeping simulations. Cross sections of the volume mesh are presented in Figure 5-2.

The boundary layer was modelled using the “All Y+ wall treatment” method in Star CCM+. Prism layers were placed near boundary walls along the hull surface in order to resolve the boundary layer accurately and to achieve the desired wall Y+ values. It is important to keep the dimensionless wall distance Y+ value within the range of boundary layer treatment. The aim should be to have either $Y+<5$ or $30<Y+<50$. The all-Y+ wall treatment should give results within this range. As shown in Figure 5-3, it was kept around a value of 45 at the underwater hull for each mesh size. This value can be considered as an appropriate size for the standard k-ε model with all Y+ boundary treatment.

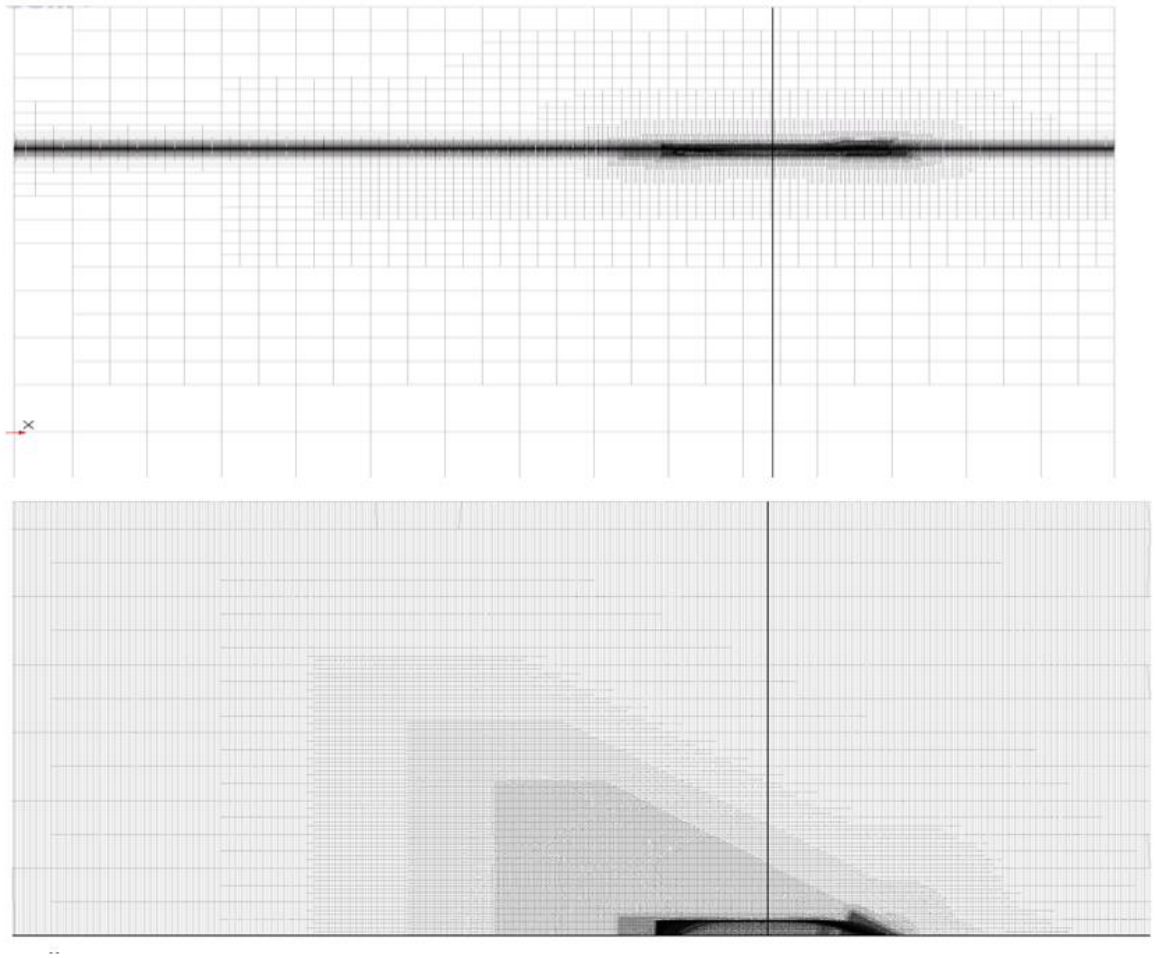

Figure 5-2 Computational mesh around the hull Profile view and Top view

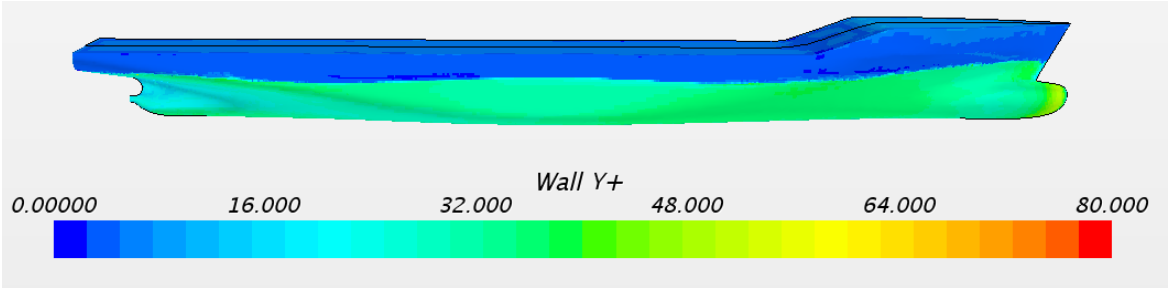

Figure 5-3 Wall Y+ on the underwater hull

5.3.1.3 Choice of time step

It is essential to use an appropriate time-step size when simulating waves as cell size and time step size go hand in hand to resolve the wave shape. The time step used in the simulations is

determined by ITTC guidelines and Courant number. Courant number is defined as the ratio of physical time step to the mesh size and it should be less than 1 for numerical stability. It is advised to use at least 100 time steps per encounter period. Therefore, the time step size was adapted to simulated wave condition. It should be noted that a second-order temporal scheme was applied to discretise the unsteady term in the Navier-Stokes equations as the first order can be too dissipative. (SIEMENS, 2017)

5.3.2 Grid Convergence Study

In order to investigate the numerical simulation uncertainty on wave added resistance and ship motions, grid uncertainty analysis also conducted using the Grid Convergence Index (GCI) method of Roache (1998). The resonant case ($\lambda/L=1.15$) wave condition was selected for grid convergence study as large motions and accelerations are likely to cause higher numerical errors (Weymouth et al. 2005). The computational mesh was refined by multiplying the mesh base size by $\sqrt{1.7}$ in all directions as this value provides a sufficiently high refinement ratio for grid convergence studies. (Sigmund and el Moctar, 2018) Three different mesh systems namely, a coarse, medium and a fine mesh comprising from 1.2 M to 5.4M control volumes were created. The non-dimensional wall distance Y+ on the underwater hull was kept constant at a value of approximately 45 in order to minimize the effect of turbulence modelling and wall functions.

In order to assess the grid convergence, the convergence ratio is used as written in Eq. (5.1) below:

$$R=\varepsilon_{21} / \varepsilon_{32} \tag{5.1}$$

In Eq. (18) $\varepsilon_{21}=S_2-S_1$ and $\varepsilon_{32}=S_3-S_2$ are the differences between medium-fine and coarse-medium solutions, where S_1, S_2, S_3 correspond to the solutions of fine, medium, and coarse grid systems, respectively. A minimum of three solutions are required to evaluate the convergence. The subscript k refers to the k^{th} input parameter (i.e. grid-size or time-step) (Stern et al. 2006)

Four different types of convergence and divergence conditions are possible: (i) monotonic convergence ($0<R<1$), (ii) oscillatory convergence ($R<0$; $|R|<1$), (iii) monotonic divergence ($R>1$), and (iv) oscillatory divergence ($R<0$; $|R|>1$) (Stern et al. 2006)

Table 6-3 presents the results of uncertainty analysis for heave and pitch transfer functions and added resistance coefficient. Grid uncertainty test results in a monotonic convergence for all three variables. As shown in Table 6-3, numerical uncertainties for TF_3 TF_5 and C_{AW} are predicted as 3.21%, 2.52% and 3.02%, respectively, based on the Grid Convergence Index (GCI) method.

Table 5-3 Grid Convergence Study for TF_3 TF_5 and C_{AW}

	TF_3	**TF_5**	**C_{AW}**
S1	0.857	0.718	10.03
S2	0.871	0.725	10.25
S3	0.897	0.735	10.68
R	0.538	0.7	0.511
GCI_{fine}	3.21%	2.52%	3.02%

Considering the computational time, CFD simulations took around 2200 CPU hours for one wave condition using the fine mesh system while the 3-D potential flow method took around 30 seconds for each wave frequency on a single CPU. Therefore, it is possible to obtain results much faster using the potential flow method.

5.4 Post Processing Procedure

This section explains the post-processing procedure of the obtained results.

It should be noted that Fourier Series analyses were performed to obtain the force and ship motions for the selected time history range.

The ship motions in waves were quantitatively analysed with the use of transfer functions. The definition of heave and pitch transfer functions, respectively, are given by:

$$TF_3 = \frac{x_{31}}{\zeta_{I1}} \tag{5.2}$$

$$TF_5 = \frac{x_{51}}{k\zeta_{I1}} \tag{5.3}$$

where x_{31}, x_{51} are the Fourier Series first harmonic amplitudes of heave and pitch, ζ_{I1} is the incident wave amplitude and $k=2\pi/\lambda$ is the wave number. Computed and measured heave and pitch motion time histories at λ/L=1.95 are shown in Figure 5-4. The solid line indicates computed motions; while the dotted line shows measured motions from the experiments.

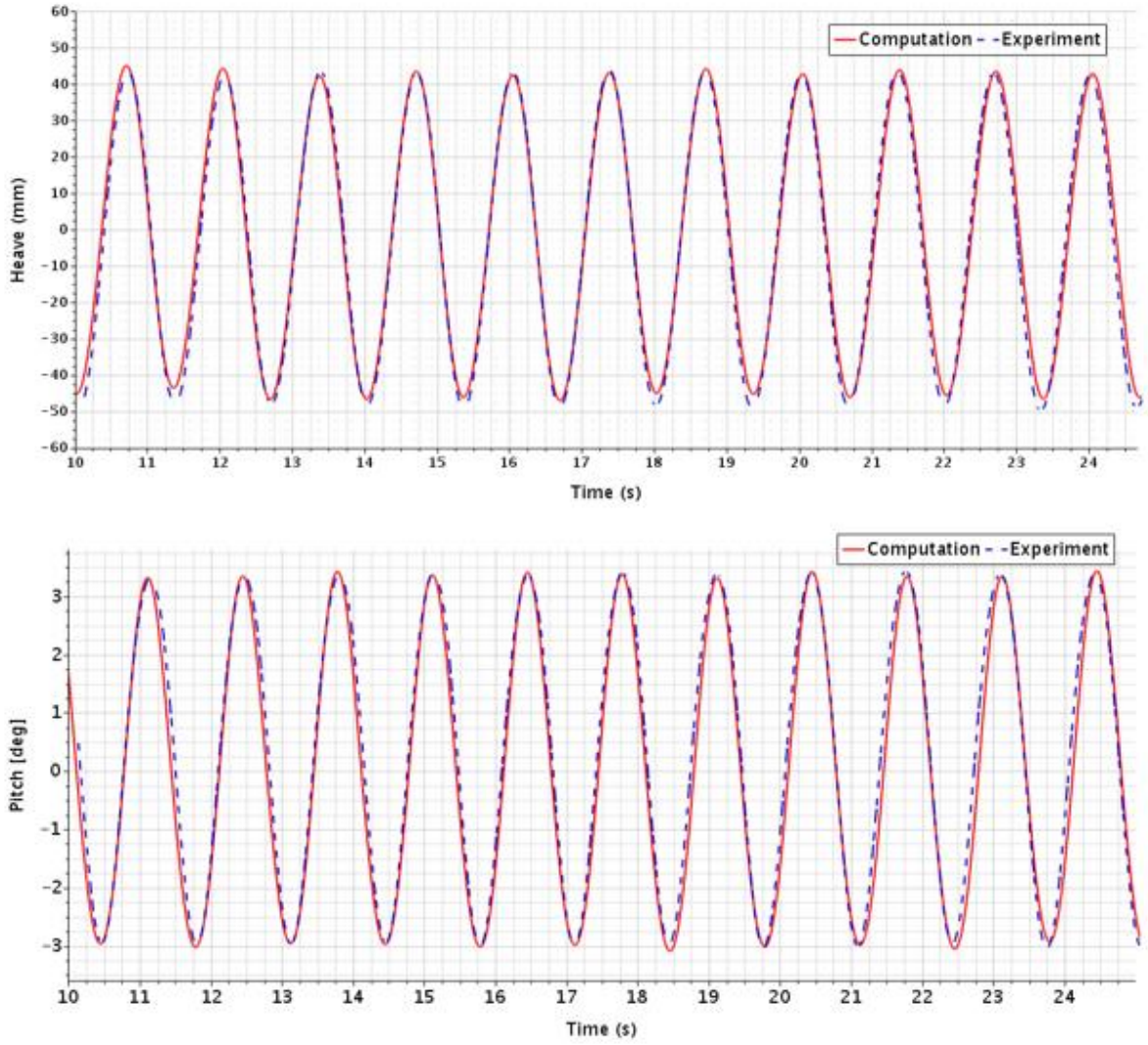

Figure 5-4 Computed and measured heave and pitch motion time histories at λ/L=1.95

Measured and computed values of resistance amplitudes were normalised by using non-dimensional total resistance coefficient C_T both in calm water and waves at different trim angles.

For calm water conditions C_T is calculated by:

$$C_T = \frac{F_X}{\frac{1}{2}\rho U^2 S} \tag{5.4}$$

where F_X is the time averaged longitudinal force (the total drag), ρ is water density, U is ship speed and S is the wetted surface area of the ship in calm water.

In order to find the added wave resistance, calm water resistance (*Fx,calm*) is subtracted from the time averaged longitudinal force in waves (*Fx,wave*) for the same trim angle and speed. It was then normalized as follows:

$$C_{AW} = \frac{(Fx, wave - Fx, calm)}{\rho g \zeta_{I1}^2 B_{WL}^2 / L_{BP}} \tag{5.5}$$

A typical sample of computed longitudinal force time history is shown in Figure 5-5. In this figure oscillating solid red line represents the total resistance in waves, blue line time-averaged value of total resistance in waves and green line calm water resistance values.

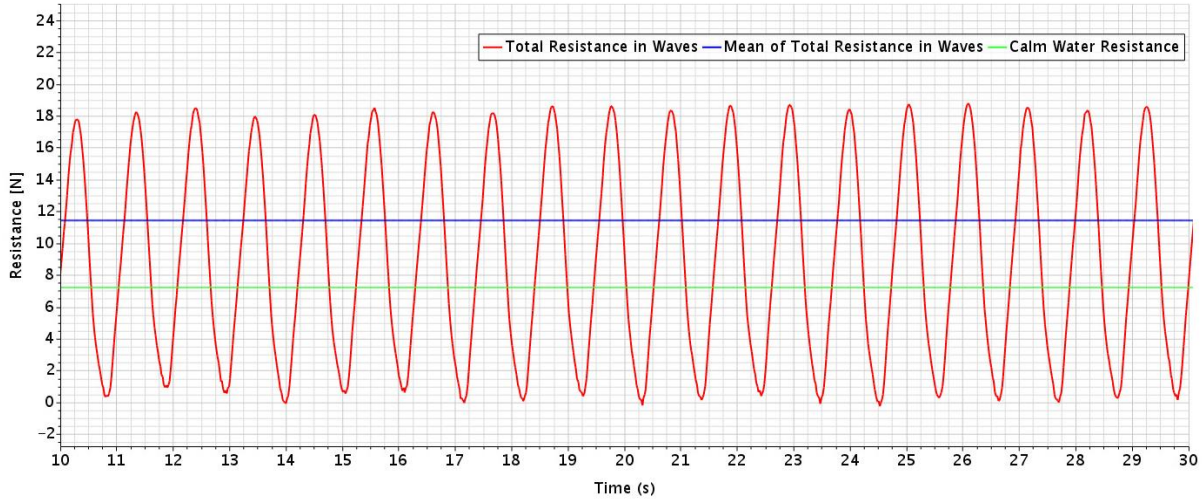

Figure 5-5 Time history of the total resistance in waves and mean values of total resistance

As added wave resistance is proportional to the square of the wave amplitude, the accuracy of used wave amplitude is of critical importance. Therefore, it is necessary to note that actual measured wave amplitude values were used instead of target values. Wave amplitudes were

measured in both experiments and simulations. Figure 5-6 shows time history of simulated and measured wave profile at the wave probe for wave length λ/L=0.75 with ship present.

Waves were generated using 5th-order Stokes waves in the computational domain. Stokes 5th order wave theory based on the work of Fenton (1985) is used as this wave more closely resembles a real wave than one generated by the first order method according to StarCCM+ user guide. It was also successfully used by other researchers (Tezdogan et al., 2016).

It should be noted that the response data presented is based on the amplitudes of sinusoidal functions fitted to the measured time histories for motions and waves. Fitting the sine functions utilises the data efficiently, and effectively acts as a noise filter to eliminate any high frequency effects. Wave amplitudes were calculated by applying Fourier Series on time histories of wave elevation covering last ten encounter period.

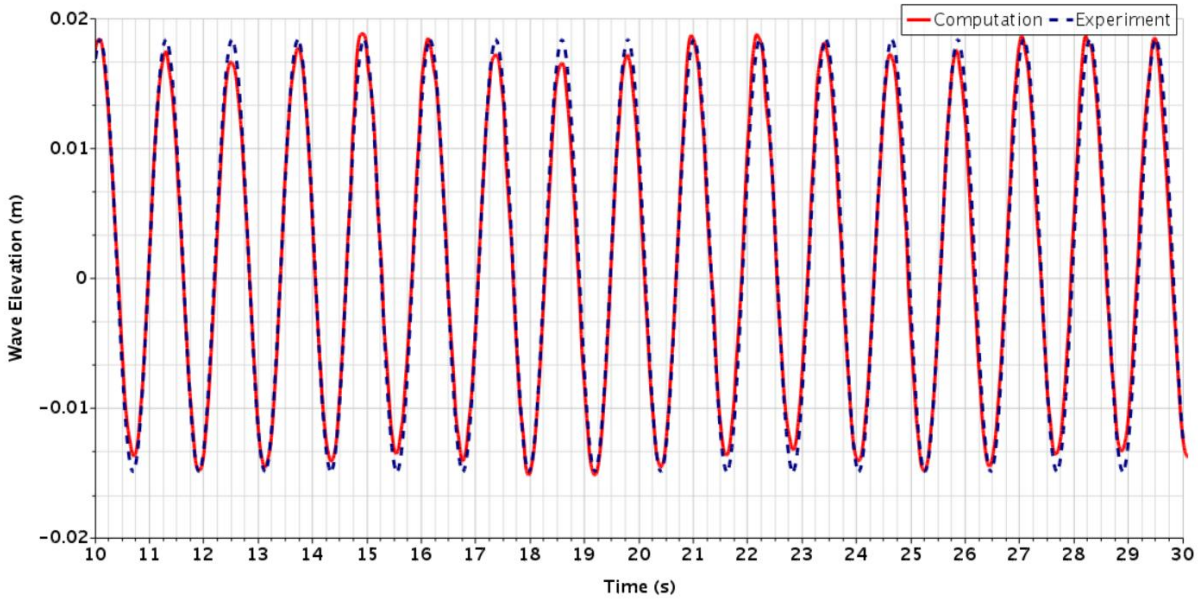

Figure 5-6 Computed and measured wave profile at the wave probe for λ/L=0.75

5.5 Results and Discussion

In this section, experimental and numerical results are presented. Simulation results from CFD and 3D Potential flow methods are later discussed and compared against experimental findings.

5.5.1 Experimental results

In this section, experimental results are discussed to investigate the effects of trim on motion responses and added resistance of the vessel.

5.5.1.1 Effects of Trim on Motion Responses

In order to investigate the motion response of the ship at different trim angles results of the experimental study are discussed in this section.

Accurate prediction of ship motions is important as the added resistance is dominated by radiation in moderate to long wave range. The motions are very small for the short waves which covers $\lambda/L=0.5\sim0.75$ as the wave radiation force is not dominant in this range. Motion responses for each trim angle are calculated and comparative response amplitude operators (RAOs) of heave and pitch motions obtained from the experiments at different trim angles are shown in Figure 5-7and Figure 5-8 respectively.

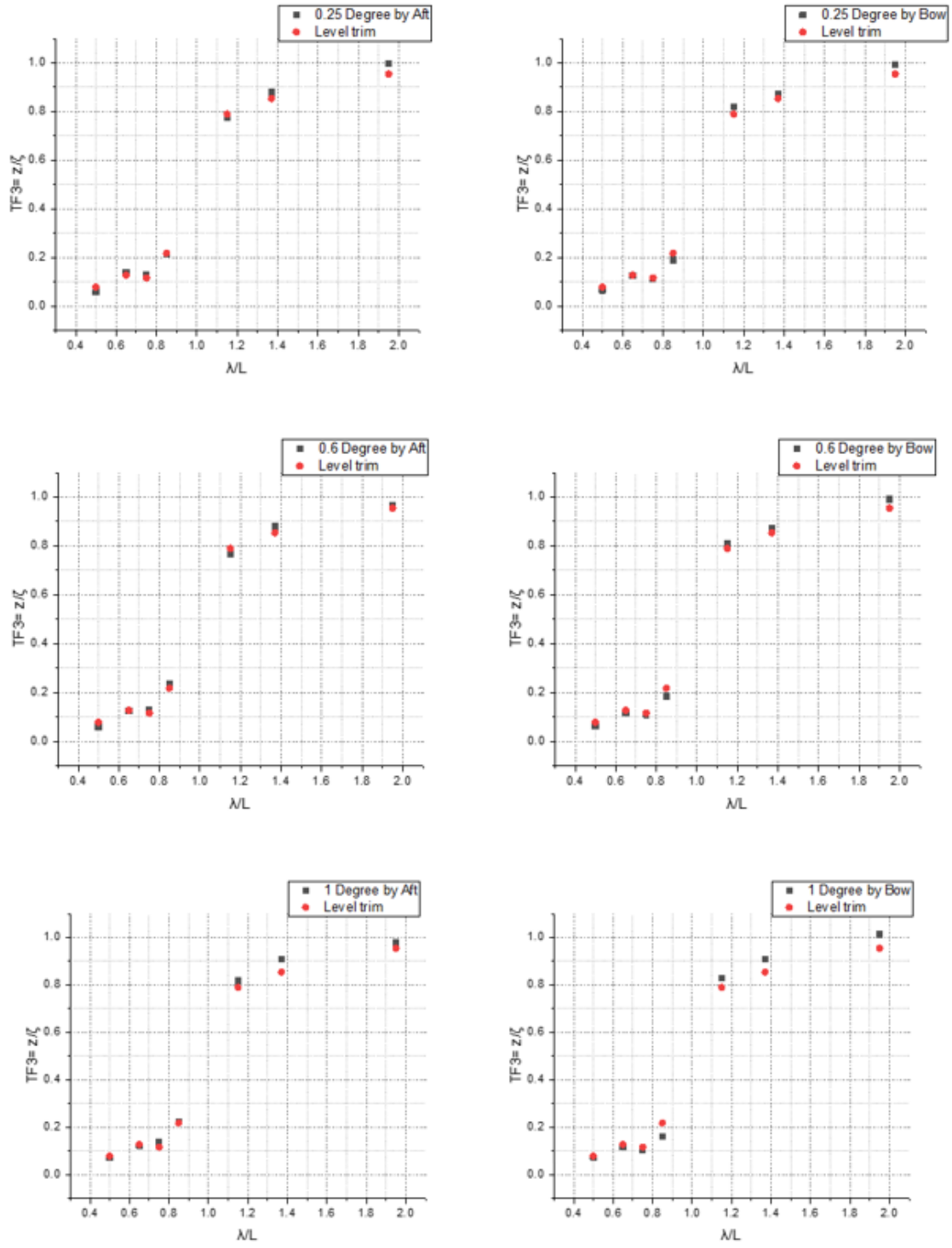

Figure 5-7 RAOs of Heave Motion

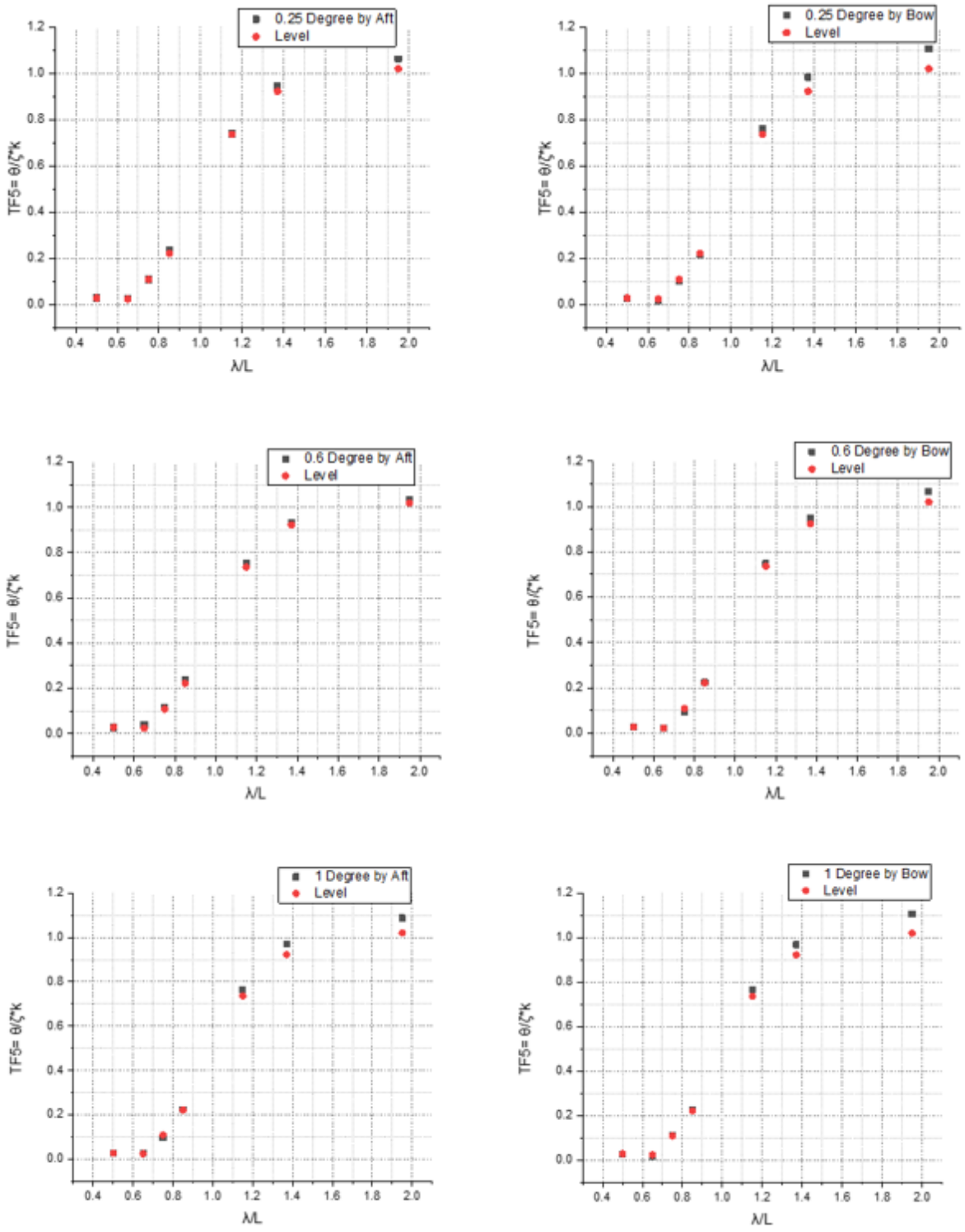

Figure 5-8 RAOs of Pitch Motion

The results show that operating at different trim angles have little influence on ship motions and that trend of ship motions are similar to operating at level trim especially in the short wave region. The motions are very small for the short waves which cover λ/L=0.5~0.75 as

the wave radiation force is not dominant in this range and there is low energy which is not enough to oscillate the vessel. For all trim angles, heave and pitch motion responses had a higher value at the long wave range (λ/L>1.15) at trimmed condition. Operating at level trim have a slightly smaller pitch and heave response value at all wave conditions. Small trim angle of 0.25 degrees has no significant influence on motion responses. Heave response amplitudes decrease slightly at aft trim conditions at around the resonance period ($1.0 < \lambda/L < 1.4$) while pitch amplitudes vary insignificantly. At larger trim angles, motion responses increase slightly in long wave region. Maximum motion responses appear in the long wave region for all trim angles. As discussed by Lewis (1988), since the magnitude of the excitation force and the coefficient of motion equations are frequency functions, maximum responses may occur at long wavelength region rather than at the natural frequency.

5.5.1.2 Effects of Trim on Added Resistance in waves

Changes in added resistance at various trim angles are discussed in this section. Added resistance at trim by aft and trim by bow conditions are compared against level trim and results of the experimental study are plotted in Figure 5-9.

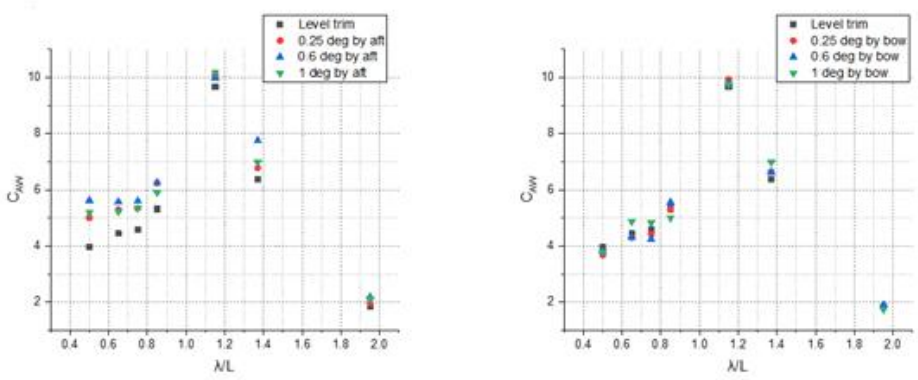

Figure 5-9 Added resistance comparisons at different trim angles

In short wave region, optimum trim trends are similar to calm water results as slight trim by bow results in the lowest added resistance value. The magnitude of savings are more significant compared to calm water results as 0.25 degree trim by bow can provide 7% reduction in added resistance coefficient compared to 1.25% reduction in calm water resistance coefficient. The added resistance in trim by aft conditions showed an increase in the short wave region which is in line with calm water predictions. However, the amplitude

of losses is much larger at around 20% in short waves when compared against 8% in calm water. In the short wave region, the diffraction component is dominant which is affected by the shape of the bow. Wave reflection creates a significant amount of added resistance in short waves. A blunt bulbous bow has typically very large wave reflection and the effective shape of the bow changes with trim angle. The large wave reflection creates a larger wave added resistance impact on the ship bow. Hence, the added resistance due to wave reflection effects is significant for trim optimisation studies. It can be said that the changes in the bow shape can be considered as a contributing factor to the added resistance in the short wave region for trim by aft conditions. Trimming the ship 0.6 degree by aft results in the highest added resistance in this region as motions are slightly higher compared to 1 degree trim by aft. Stern immersion at 1 degree trim by aft might be a reason for slightly reduced heave motions.

In the moderate wave length region, added resistance value reached its maximum when the wavelength was similar to the ship length ($\lambda/L=1.15$). In moderate-long wave range, added resistance is dominated by radiation which is related to the relative motion as mentioned earlier. Therefore, the increase in added resistance coefficient at trimmed conditions is in line with the increase in relative motions in this wavelength region.

5.6 Numerical Results

In this section, computational results will be compared to experimental results and the prediction capabilities of CFD methods at different trim angles will be discussed.

5.6.1 Numerical Prediction of Motions Responses and Added Resistance in Waves

Firstly, the numerical results of the heave and pitch motion predictions are compared with the experimental data. Using the transfer functions to compute the response amplitude operators of heave and pitch, motions are calculated. Results from experiments, CFD and 3D Potential Flow (PF) based methods are presented in Figure 5-10 and Figure 5-11. It can be seen that CFD predictions agree better with experiments than the potential theory based method. The

potential flow based method significantly over predicts heave motion at moderate to long waves. Heave RAO is decreasing as λ/L decreases and in short waves, it gets closer to zero value. In long waves, it becomes closer to one which means the ship vertically moves as the value of the wave amplitude. As discussed by Hizir et al. (2019), in the 3D PF method, forward speed corrections are applied to boundary conditions as well as to the Neumann-Kelvin (NK) approximation where the steady wave and unsteady wave interactions are linearized. NK approach is known to overestimate the heave and pitch motion responses when compared against the experimental data as discussed by Kim and Shin (2007).

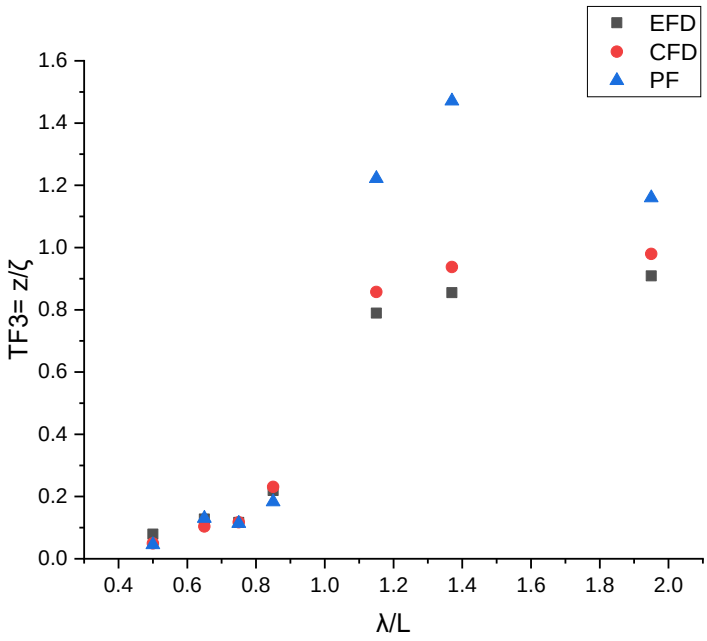

Figure 5-10 Comparison of computed and measured Heave motion RAOs

For pitch motion, CFD and EFD agree well except the long wave region. The error increases as λ/L get bigger than 1.15. Pitch motion prediction with the potential flow method showed good agreement with experiments and CFD calculations with slightly larger motion predictions at resonance period ($1.0 < \lambda/L < 1.4$) This may be due to the adapted NK approach as discussed above.

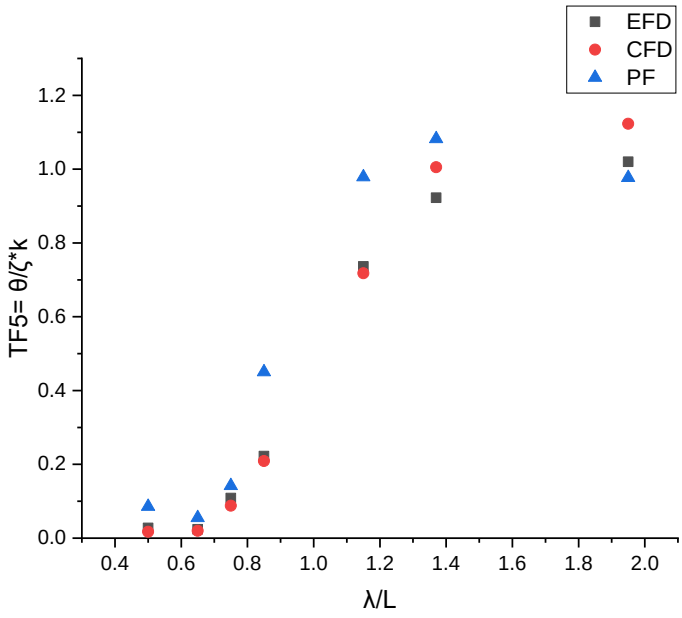

Figure 5-11 Comparison of computed and measured Pitch motion RAOs

Numerical results for the added resistance coefficient at level trim has been compared with EFD measurement of KHL as well as of FORCE (Simonsen et al. 2014) which conducted experiments for 6.1 m model of KCS for the same range of λ/L and presented in Figure 5-12. Considering the differences between EFD approaches, generally, a good agreement can be observed between the two experiments which show scaling isn't highly sensitive for added resistance. Overall trends are the same for EFD, CFD and PF based methods. Discrepancies between linear potential theory and CFD are larger especially at short waves due to intensified non-linear hydrodynamic effects (Kashiwagi et al., 2010).

Prediction errors of added resistance in head waves from the current study are also compared with other numerical studies that are available in the literature. (Sadat-Hosseini et al., 2015) Table 5-4 presents findings from CFD-Ship IOWA, Force Technology, and current study at the same wave conditions. Numerical prediction of added resistance values are compared against experimental values for each study and percentage errors are given in Table 5-4. Relatively large prediction errors for added resistance can be seen for all studies especially in short wave region.

Table 5-4 Prediction errors of added resistance for CFD studies in head waves

	CFD-Ship Iowa	Force (Star-CCM+)	Current Study
λ/L	**CAW E%D**	**CAW E%D**	**CAW E%D**
0.5	-5.5	33.4	-18.36
0.65	-9	11.3	-19.6
0.75	-14.2	2.1	-16.04
0.85	-35.7	-	-14.04
1.15	-72.7	0.1	2.59
1.37	-41.3	-3	9.65
1.95	-11.1	2.3	-4.95

As can be seen from Figure 5-12 and Table 5-5, CFD agrees better with EFD when compared to PF for all trim angles. Both numerical methods under-predict the added resistance coefficients compared to the EFD data except at the resonance period ($1.0 < \lambda/L < 1.4$). As viscosity cannot be included in the 3-D potential flow theory method, ship motions and added resistance are over predicted around the resonant frequency region. As discussed earlier, over estimation of heave and pitch motion can be the contributing factor to over estimation of added resistance in this region. Results also show that there is a tendency for the prediction errors for added resistance coefficient to increase with increasing trim angle. It is possible to say that, CFD simulation results agree well with the experimental data for all trim angles considering the highly non-linear nature of seakeeping analysis.

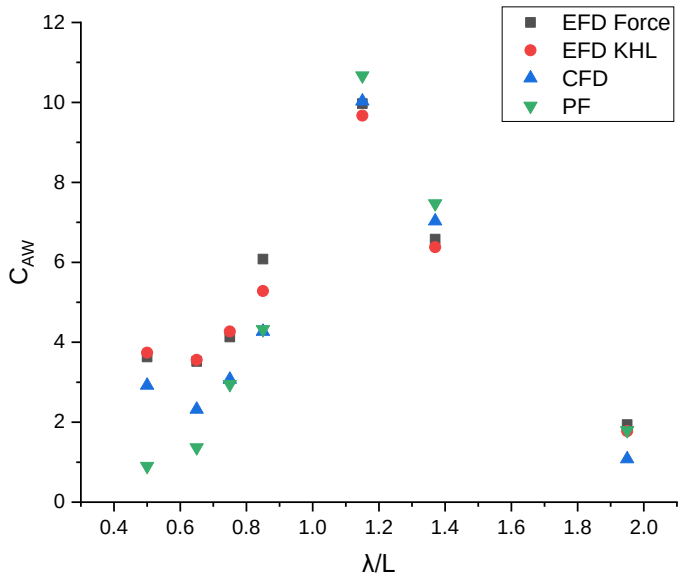

Figure 5-12 Comparison of CFD, PF and experimental data for added resistance coefficient in head waves for different wavelength conditions

Table 5-5 Prediction errors of added resistance coefficient for trim by bow conditions for CFD and PF simulations

	C_{AW} Level Trim			**C_{AW} 0.25 Deg trim by bow**			**C_{AW} 0.6 Deg trim by bow**			**C_{AW} 1 Deg trim by bow**		
λ/L	**EFD KHL**	**CFD E%D**	**PF E%D**	**EFD KHL**	**CFD E%D**	**PF E%D**	**EFD KHL**	**CFD E%D**	**PF E%D**	**EFD KHL**	**CFD E%D**	**PF E%D**
0.5	3.87	-18.36	-33.00	3.68	-15.48	-31.84	3.81	-16.23	-48.61	3.79	-16.58	-58.79
0.65	4.44	-19.60	-37.39	4.31	-20.24	-39.60	4.31	-19.99	-41.91	4.87	-14.94	-57.47
0.75	4.57	-16.04	-31.13	4.41	-16.85	-29.31	4.24	-12.48	-19.33	4.82	-11.50	-36.79
0.85	5.32	-14.04	-17.24	5.30	-13.78	-19.73	5.56	-16.90	-11.31	5.01	-11.70	-21.09
1.15	9.78	2.59	9.14	9.94	0.45	5.28	9.79	1.41	6.42	9.76	2.32	4.22
1.37	6.37	9.65	18.14	6.64	4.49	9.69	6.63	5.24	6.86	6.98	3.80	4.40
1.95	1.78	-4.95	-3.26	1.83	-11.93	-11.28	1.90	-9.89	-14.72	1.74	-5.40	-7.12

Table 5-6 Prediction errors of added resistance coefficient for trim by aft conditions for CFD and PF simulations

	Caw Level Trim			**C_{AW} 0.25 Deg trim by aft**			**C_{AW} 0.6 Deg trim by aft**			**C_{AW} 1 Deg trim by aft**		
λ/L	**EFD KHL**	**CFD E%D**	**PF E%D**	**EFD KHL**	**CFD E%D**	**PF E%D**	**EFD KHL**	**CFD E%D**	**PF E%D**	**EFD KHL**	**CFD E%D**	**PF E%D**
0.5	3.87	-18.36	-33.00	5.01	-19.21	-59.09	5.63	-25.53	-67.02	5.20	-29.08	-74.42
0.65	4.44	-19.60	-37.39	5.30	-19.92	-54.13	5.58	-23.45	-60.08	5.22	-23.80	-67.70
0.75	4.57	-16.04	-31.13	5.34	-18.84	-38.18	5.60	-18.43	-45.02	5.35	-10.71	-48.07
0.85	5.32	-14.04	-17.24	6.24	-19.04	-24.78	6.25	-18.09	-23.86	5.90	-17.17	-28.18
1.15	9.78	2.59	9.14	10.10	0.45	6.39	9.98	1.86	6.37	10.20	-1.75	-13.91
1.37	6.37	9.65	18.14	6.78	6.04	10.70	7.75	-5.68	-5.16	6.99	6.66	-17.70
1.95	1.78	-4.95	-3.26	1.97	-9.57	-17.37	2.18	-13.38	-33.66	2.11	-8.62	-38.96

When the ship is trimmed, the position of the bulbous bow and transom have an impact on the resistance of the ship. This effect is especially significant when bulbous bow partially come out of the water or transom stern partially immersed in water due to trim. As discussed by Kim et al. (2017), added resistance and relative wave height at the bow section have a strong correlation between them. This also proves the importance of the bow effect on added resistance. When the ship motions are maximum at around the resonance period, trim by bow cause an increase in the added resistance. One should also consider the bottom surface contribution to the added resistance. The bottom surface does not contribute to the added resistance at even keel condition as the directional normal has zero component in the longitudinal direction. Under trimmed conditions, these inclined bottom starts to contribute to the added resistance. Another point is the evaluation of non-linear effects. As can be seen in Table 5-6 prediction errors for the PF method is increasing with the increase in trim by aft. As the trim angle increases, the draft at the bow becomes smaller and the bulbous bow shape changes. Thus, non-linear effects caused by wave diffraction and the change in wetted surface become more significant. While CFD can capture these non-linear effects better, prediction errors of added resistance by the PF method increase especially when the trim angle is bigger. One can say that rapid linear potential flow calculations may not be suitable to predict the added resistance at large trim angles where keel contribution effects are more significant.

5.7 Increase in the effective power of the vessel due to added resistance at different trim angles

One of the most important considerations of energy efficient shipping operations is to determine the power requirement of a ship at adverse operating conditions. A ship with a higher power requirement will automatically require more amount of fuel during the voyage, which will increase fuel costs and carbon emissions.

Effective power (P_E) is the power required to move the ship through the seaway at a given speed. It is calculated as the product of the total resistance of the ship and ship speed. As the speed is constant, the difference between total resistance coefficients between wave and calm water conditions are considered and calculations can be performed for each trim angle similar to the equation that was used by Tezdogan et al. (2015) as given below.

$$\%\ \text{Increase in } P_E \text{ due to added resistance} = \frac{\Delta C_T}{C_{T,calm}} x100 = \frac{C_{T,wave} - C_{T,calm}}{C_{T,calm}} x100 \tag{5.6}$$

Experimental predictions of the total resistance coefficients were applied to Eq. 5.6 and a percentage increase in the effective power of KCS due to induced added resistance at different trim angles were obtained. Figure 5-13 and Figure 5-14 below present the obtained results comparing level trim predictions against trim by bow and trim by aft, respectively.

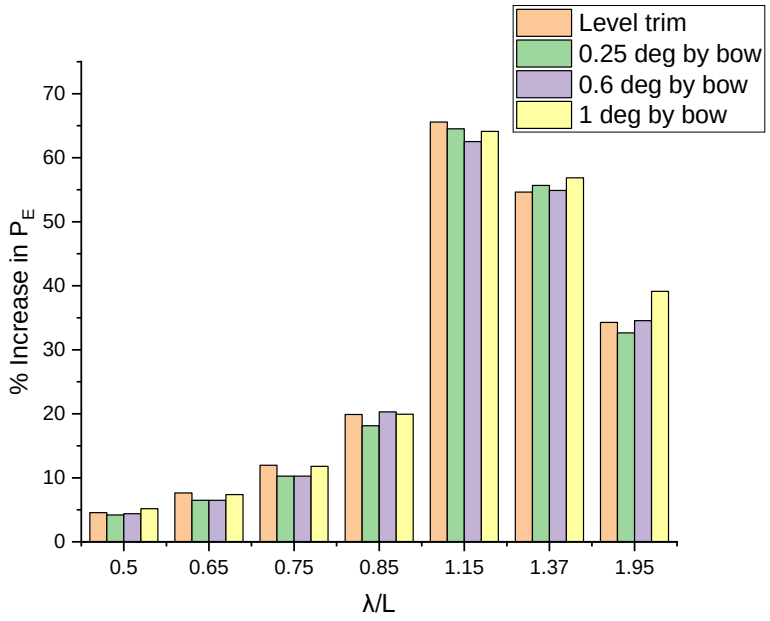

Figure 5-13 Percentage increase in effective power due to added resistance at different trim angles (Trim by bow)

In short waves, small and moderate trim by bow results in the lowest increase in the effective power. The trend is similar to still water but it can be seen that 0.6 degrees trim by bow performs better in waves as it results in a lower increase in effective power than level trim for almost entire wave conditions. Around the resonant period, moderate bow trim showed a lower increase in power compared to low bow trim case. This is due to the combined effect of higher calm water resistance and slight reduction on ship motions at moderate trim when compared to low bow trim.

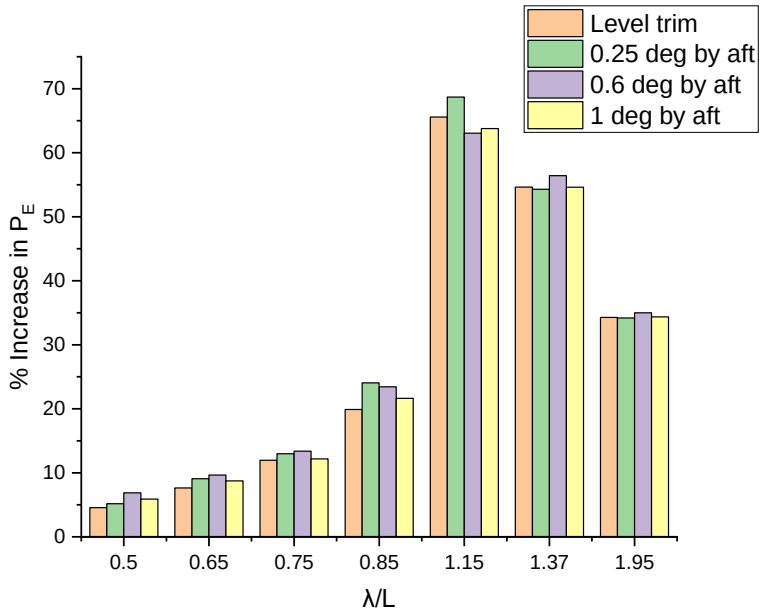

Figure 5-14 Effective power increase due to added resistance at different trim angles (Trim by aft)

Figure 5-14 show that trim by aft increase effective power requirement, especially in the short wave region. The highest increase in effective power for all trim angles is observed at λ/L=1.15 which is the resonance point. Compared to level trim operating condition, the increase in effective power in trim by aft conditions is slightly larger. These trends can be observed for all the wave range. Therefore, it is possible to say that level trim operation performs better compared to operating at trimmed by aft condition.

5.8 Conclusions

In this study, experiments and numerical simulations were performed for bare hull KCS in regular head waves at different trim angles. Effects of trim on the added resistance and ship motions (heave and pitch) in regular head waves were investigated. Numerical results from the unsteady RANS and the 3-D potential flow method simulations were compared with experimental data for a broad range of wave conditions at different trim angles.

In the experimental results, it was shown that the trends for added resistance at different trim angles are close to the calm water ones in the short wave region. Although the optimum trim trends at calm water and waves are similar for short waves, in long waves optimum trim

angle trends are not always the same with calm water results. It was also demonstrated that operating at different trim angles have little influence on ship motions and that trend of ship motions are similar to operating at level trim especially in the short wave region. Motion responses increase slightly in the long wave region at bigger trim angles.

In the numerical analysis part, initially, discretization errors were investigated to identify the optimum mesh structure for CFD analysis. After validating added resistance and heave and pitch motions with experimental data, computations and measurements correlated favourably. Motion response comparison for heave and pitch motions showed good agreement with experimental data. Added resistance coefficient was calculated for all trim angles and compared with experimental data. Both CFD and PF methods under-predict the added resistance coefficients compared to the EFD data except at the resonance period ($1.0 < \lambda/L < 1.4$)

The potential flow method can be applied in moderate wave range for small trim angles to achieve a quick estimation of the added resistance of ships at different trim angles in regular waves. In larger trim angles by aft and bow, however, the potential flow method provided poor results for the prediction of added resistance. Thus, this method may not be suitable for computing added resistance in various trim angles.

Prediction of wave added resistance and added power is still challenging for researchers and the industry. Although CFD methods can capture more relevant physics than traditional potential flow methods, improved accuracy may be costly as CFD simulations require powerful computers and are time-consuming. Especially short wave simulations are more computationally expensive than the long wave simulations due to the high number of cells required to resolve the wave pattern at the free surface. With increasing High Performance Computing (HPC) capacity and access, CFD methods can provide a very useful tool to compare vessel performance at different trim angles and define optimum trim at both calm water and waves. In each case, a balance between available resources and required accuracy has to be found.

Chapter 6 Trim Influence on Propulsive Performance

Chapter 6 is dedicated to the investigation of the trim influence on propulsion performance. The chapter outlines numerical details of the self-propulsion simulations. Model scale and full scale self-propulsion simulations are conducted at trim different angles and results are discussed.

6.1 Introduction

The aim of this chapter is to investigate trim influence on propulsion performance and the necessity of self-propulsion tests for trim optimisation studies. As reviewed in Chapter 2, although there are many studies on the self-propulsion performance of ships, the influence of trim on propulsion characteristics is rarely investigated. To the best of the author's knowledge, there is no study that investigated the trim influence on the self-propulsion performance of KCS.

KCS ship is utilised again for the self-propulsion study as experimental data is readily available for the self-propelled KCS model. Self-propulsion experiments were carried out by National Maritime Research Institute (NMRI) in Tokyo and results have been reported in the proceedings of the CFD Workshop Tokyo 2005 (Hino 2005) Due to available experimental data of self-propulsion case, 31.6 scale of KCS is used for model scale self-propulsion simulations. The current study is conducted for both model scale and full scale ship. Details of the KCS in full scale and model scale are given in Table 6-1.

Table 6-1 Principal particulars of the KCS in full-scale and model scale

Parameters	*Full scale*	*Model Scale*
Scale	1	31.6
Length between the perpendiculars	230	7.278
Beam at waterline	32.2	1.019
Depth	19	0.601
Design draft	10.8	0.341
Displacement	52030	1.649
Ship wetted area without rudder	9530	9.544
Block coefficient	0.651	0.651
Design speed		
U	24	2.196
Fr	0.26	0.26

In this chapter, numerical modelling of self-propulsion simulations are presented. Section 6.2 presents numerical modelling of self-propulsion in model scale. Details of the computational domain, mesh generation, mathematical formulations used to investigate propulsion characteristics and verification and validation are presented within this section. Results from model scale simulations are presented in Section 6.2.7, and the effect of the trim on ship self-propulsion characteristics are discussed. Simple resistance test results from numerical towing tank simulations are compared to self-propulsion test results and differences are discussed.

Section 6.5 presents full scale self-propulsion simulations. Differences between model scale and full scale results are discussed in this section.

6.2 Numerical Modelling of Self Propulsion at Model Scale

6.2.1.1 Propeller model

In this study, numerical model of the KP505 propeller was used in the self-propulsion simulations. The KP505 propeller was designed by the Korea Research Institute of Ships and Ocean Engineering (KRISO) to be used for the KRISO Container Ship (KCS). Table 6-2 and Figure 6-1 show the principal particulars and geometry of the KP505 propeller.

Table 6-2 Principal particulars of KP505 propeller

Parameters	*Full Scale*	*Model Scale*
Propeller Diameter	7.9 m	0.25 m
Number of Blades	5	
propeller Type	FPP	
P/D (mean)	0.95	
Ae/Ao	0.8	
Blade Section	NACA66	
Rotation	Right	

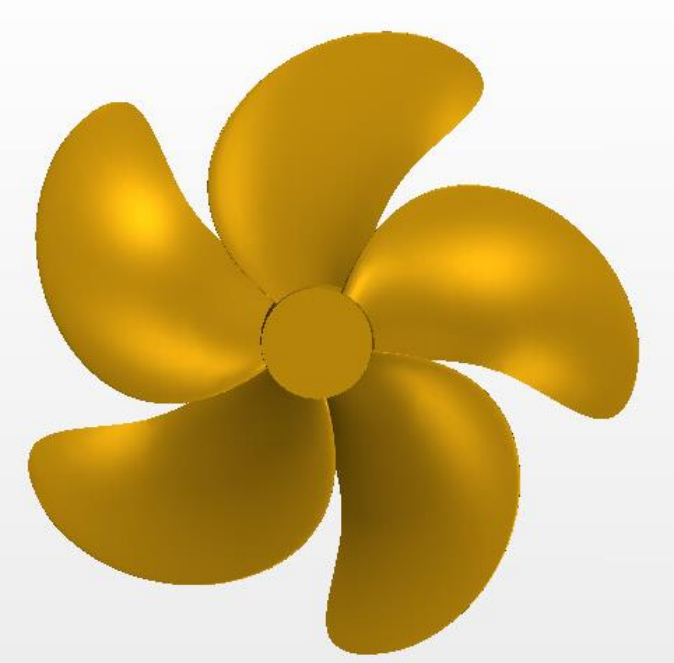

Figure 6-1 KP 505 Propeller Geometry

6.2.2 Computational Domain and Boundary Conditions

In self-propulsion simulations, the complete fluid domain was modelled as symmetry condition cannot be applied due to the rotating propeller. A velocity inlet boundary condition was set at 1.5LPP ahead of the vessel and a pressure outlet was selected at 2.5LPP behind to avoid wave reflections as similarly used by Song et al. (2020). The top, bottom and side boundaries were all modelled as velocity inlets. Side and bottom boundaries were located at 2.5LPP distance from the centreline of the ship while top boundary was located at 1.5LPP above the waterline. Figure 6-2 shows an overview of the computational domain and boundary conditions. Hull surface and propeller were defined as no-slip walls as in previous simulations.

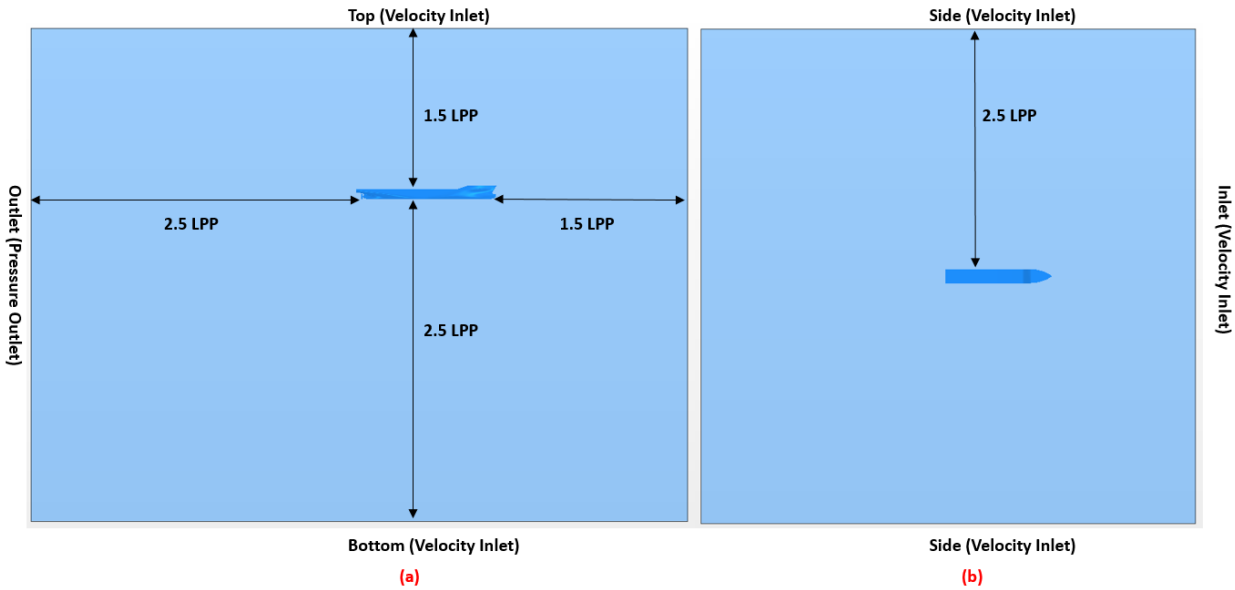

Figure 6-2 Computational Domain and boundary conditions for self-propulsion simulations (a) side view (b) top view

6.2.3 Mesh Generation

As mentioned earlier, self-propulsion simulations were performed using two different methods, namely, sliding mesh with 3-D propeller geometry and body force method based actuator disk approach. In the 3-D propeller method, in order to simulate the rotating propeller, a sliding mesh domain was created around the propeller to simulate the rotation. Hexahedral cells were used in the stationary domain and the polyhedral mesh was used at the rotating domain. Polyhedral cells allow better approximation of propeller geometry and as polyhedral cells have many neighbours so gradients can be much better approximated (SIEMENS, 2017) Rotating domain and polyhedral cells within this domain are shown in Figure 6-3. Local refinements were applied around the hull as in resistance simulations which were discussed in Chapter 4.

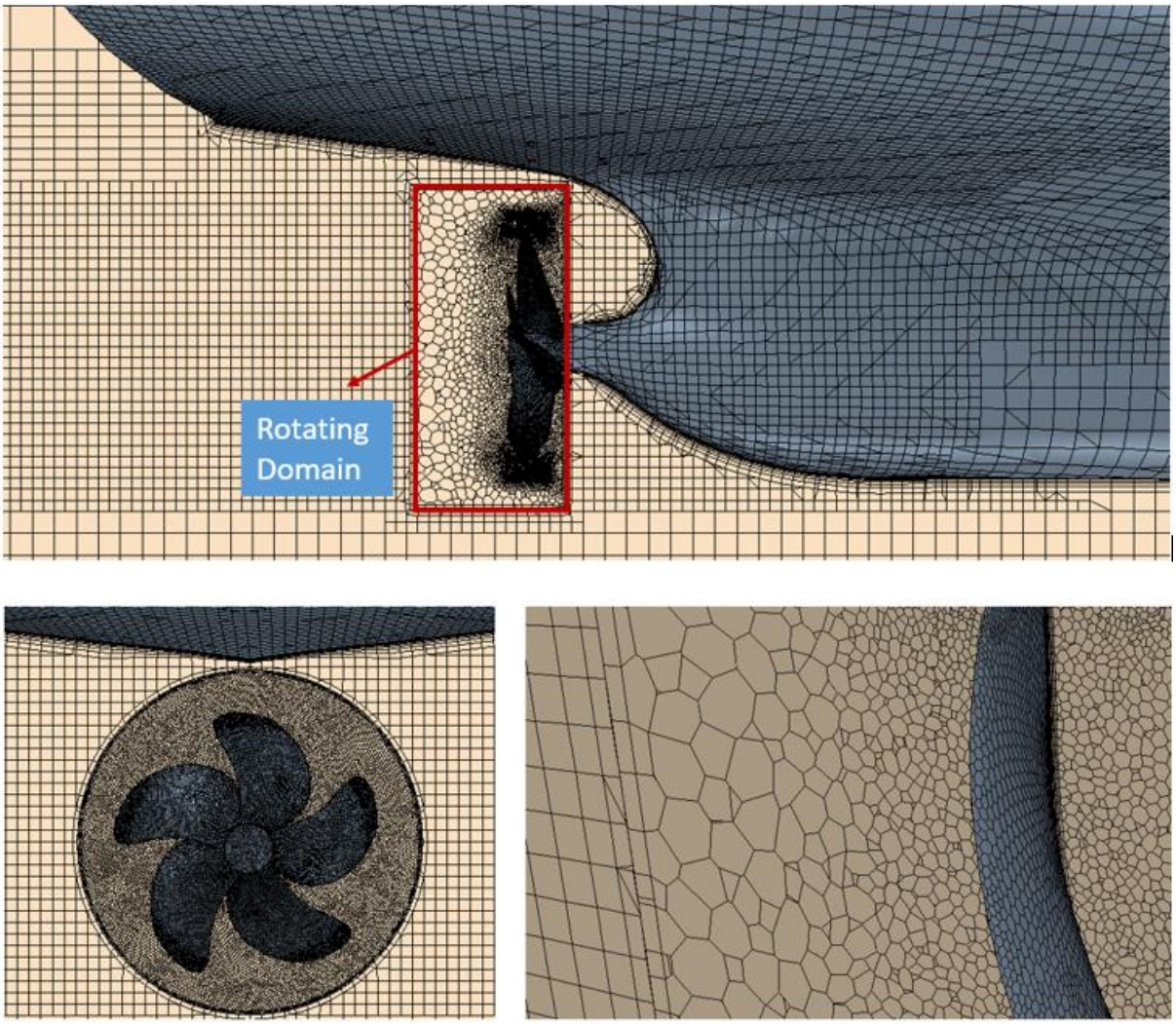

Figure 6-3 Generated mesh around the propeller in rotating domain

In Body Force based Virtual Disk approach, the mesh is refined in the area where the virtual disk located to obtain an accurate distribution of the axial and tangential body force components of the virtual disk as seen in Figure 6-4. In order to ensure that pressure jump is applied over the sufficient number of cells, minimum of four cells within disk thickness were applied by refining the mesh as recommended by Star CCM+ user guide. (SIEMENS, 2017)

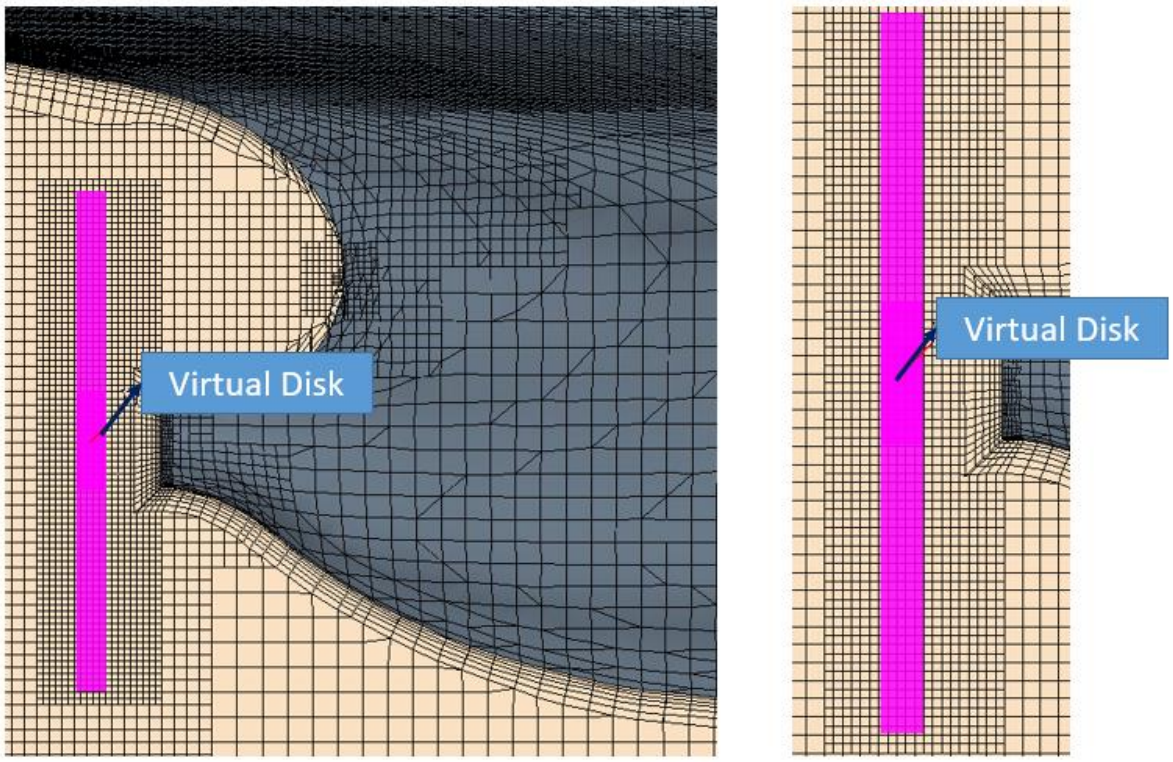

Figure 6-4 Local mesh refinement in the virtual disk area

6.2.4 Time step selection

For self-propulsion simulations with a rotating propeller, 1 whole rotation of the propeller was analysed in 180 time steps as recommended by ITTC (ITTC, 2014b).

$$\Delta t_{SP} = \frac{1}{rps \cdot 180} \tag{6.1}$$

It should be noted that simulations were initiated with 0 rps and a higher time step in order to achieve a faster result. This approach enabled the convergence of resistance value and flow field around the hull in a shorter time. After the initial flow field converged, propeller rotation rate was increased and the time step was reduced gradually to its final value to obtain the self-propulsion point.

6.2.5 Characteristics of self-propulsion

The forces and moments produced by the propeller are expressed in their most fundamental form in terms of a series of non-dimensional characteristics for a specific geometric configuration.

Thrust and torque coefficients which are the functions of thrust and torque values respectively and can be calculated as follows:

$$K_T = \frac{T}{\rho n^2 D^4} \tag{6.2}$$

$$K_Q = \frac{Q}{\rho n^2 D^5} \tag{6.3}$$

Here; ρ is the water density (kg/m^3), n is the propeller rotational speed (rps) and D is the diameter of the propeller (m), T is thrust (N) and Q is the torque ($N.m$).

Advance ratio is J defined by:

$$J = \frac{V_A}{nD} \tag{6.4}$$

Where V_A is the propeller inflow velocity, n is the propeller revolution and D is the propeller diameter.

6.2.6 Verification and Validation

6.2.6.1 Verification

Verification study is conducted for self-propulsion simulations with discretised propeller geometry using the Grid Convergence Index method. The reader can see the details of verification methodology in Chapter 4 Section 4.2.2.2. Three different meshes were created namely fine, medium and coarse mesh. Fine mesh was used for further analysis.

Uncertainty values were calculated for total resistance coefficient (C_T) and rotational speed of the propeller (n) for the level trim case. N_1, N_2, N_3 represents the total number of cells for fine, medium, and coarse grid systems. S_1, S_2, S_3 correspond to the solutions of fine, medium, and coarse grid systems, respectively. The results are presented in Table 6-3 below.

Table 6-3 Grid Convergence Study for C_T and n

	C_T	n
N_1	4520000	4520000
N_2	2330000	2330000
N_3	1250000	1250000
S_1	0.857	9.54
S_2	0.871	9.556
S_3	0.897	9.58
R	0.46	0.67
GCI_{fine}	1.82%	0.52%

6.2.6.2 Validation

Numerical results from both virtual disk and 3D propeller methods are compared with available experimental results and also with the average predictions from the participants of the latest CFD Workshop in Tokyo (L. Larsson et al. 2018).

Self-propulsion computations were conducted at ship point following the experimental procedure. In the experiments, the model ship was towed to account for the larger skin friction at model scale compared to full scale. The towing force, the Skin Friction Correction (SFC), was taken as 30.25 N from the tests (L. Larsson et al. 2018).

In the computations the thrust T, was balanced by varying the rotational speed of the propeller, n, to obtain force equilibrium in the longitudinal direction such that;

$$T = R_{T(SP)} - SFC \tag{6.5}$$

where $R_{T(SP)}$ is the resistance with a rotating propeller.

Figure 6-5 presents the differences in Thrust coefficient (K_T) and Torque coefficient ($10K_Q$) between calculated results and experimental data. As can be seen from the figure, 3-D propeller method agrees well with experimental data and average values from Tokyo 2015 CFD workshop participants while the virtual disk method underpredicts K_T and K_Q values.

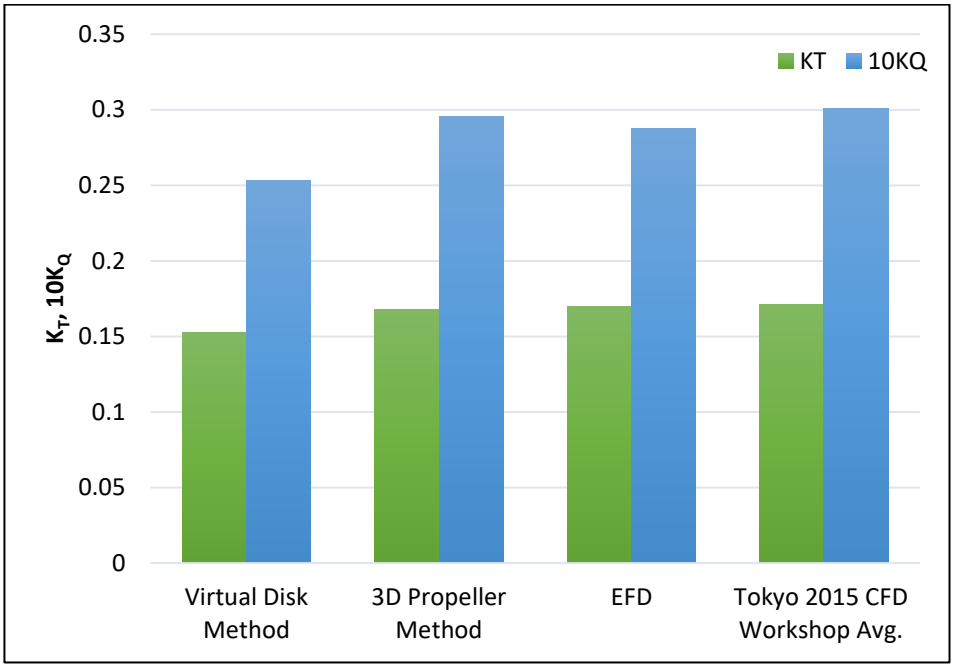

Figure 6-5 Thrust coefficient (K_T) and Torque coefficient ($10K_Q$) values obtained from both methods compared against EFD (Hino, 2005) and Tokyo 2015 CFD workshop average values

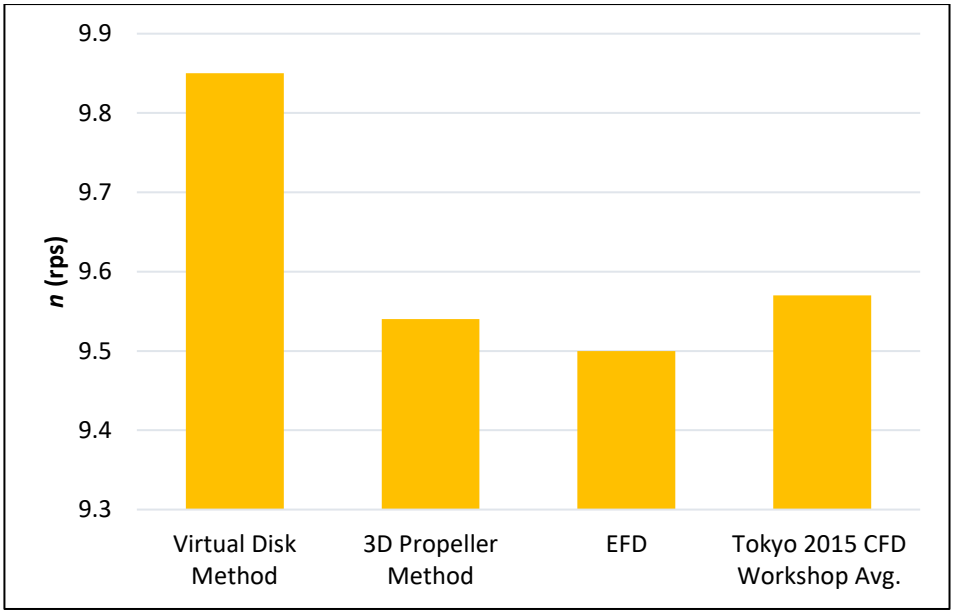

Figure 6-6 Rotational speed of the propeller (n) values obtained from both methods compared against EFD (Hino, 2005) and Tokyo 2015 CFD workshop average values

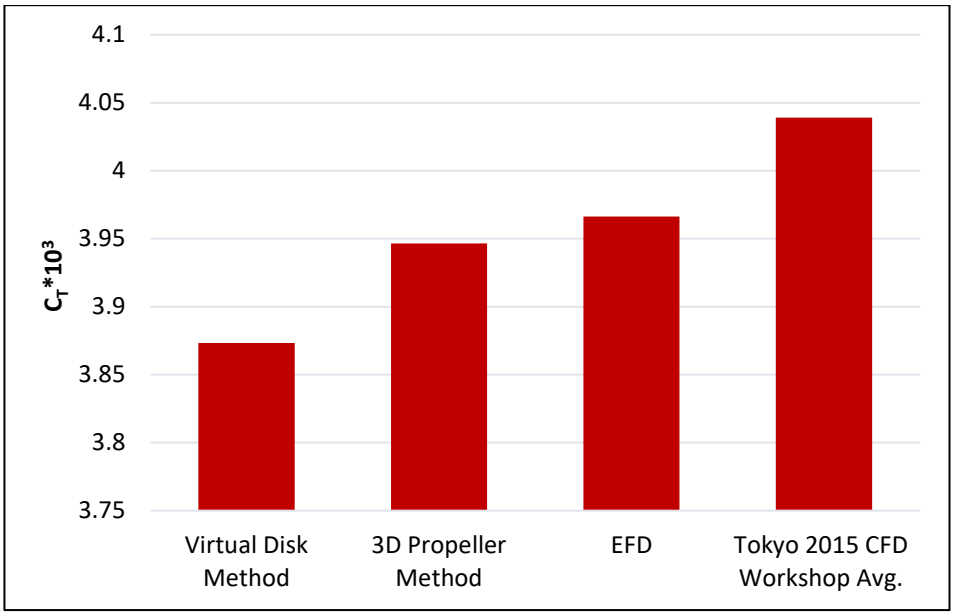

Figure 6-7 Total resistance coefficient (C_T) values obtained from both methods compared against EFD (Hino, 2005) and Tokyo 2015 CFD workshop average values

Figure 6-6 and Figure 6-7 compare the results for rotational speed of the propeller (n) and total resistance coefficient (C_T), respectively. Percentage errors are shown in Table 6-4.

Table 6-4 Self propulsion parameters comparison

	EFD	*Virtual Disk Method*	*E%D*	*3D Propeller Method*	*E%D*	*Tokyo 2015 CFD Workshop Avg.*
C_T*10^3	3.966	3.873	-2.35	3.935	-0.8	4.039
n (rps)	9.5	9.85	3.68	9.55	0.55	9.57
K_T	0.170	0.152	-10.25	0.167	-1.4	0.171
$10K_Q$	0.288	0.253	-11.90	0.295	2.73	0.301

Table 6-4 summarises results for obtained self-propulsion parameters from virtual disk and 3-D propeller methods and percentage differences against experimental data. It can be seen that 3-D propeller method results agree well with the experiments with relative differences for C_T, n, K_T, and $10K_Q$ are -0.8%, 0.55%, -1.4% and 2.73% respectively. Results from virtual disk results can be considered as within fair agreement with the experiments with differences of -2.35% and 3.68% for C_T and rotational speed of the propeller (*n*) while prediction errors are larger for K_T and $10K_Q$ with differences around -10%. It should be noted that self-propulsion simulations with 3-D propeller method took 5600 CPU hours to complete while the virtual disk method took 1225 CPU hours.

6.2.7 Results

6.2.7.1 Trim effect on resistance components

Changes in pressure resistance, frictional resistance components and total resistance are analysed for each trim angle for both nominal resistance and self-propulsion simulations. The difference of resistance components at trimmed conditions with respect to even keel operation is defined by $(R_\theta-R_0)/R_0*100$ where R_θ is resistance value at the trimmed condition and R_0 is resistance value at even keel condition.

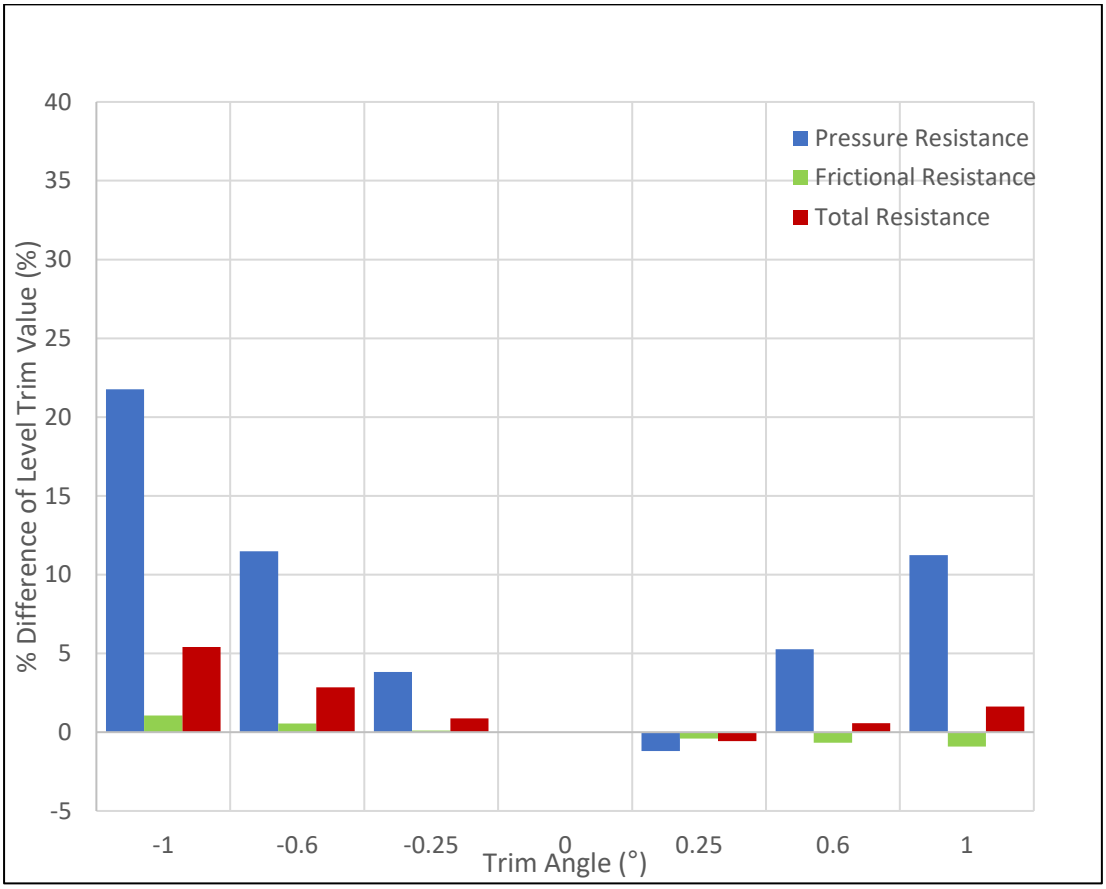

Figure 6-8 Changes in resistance components for nominal resistance simulations

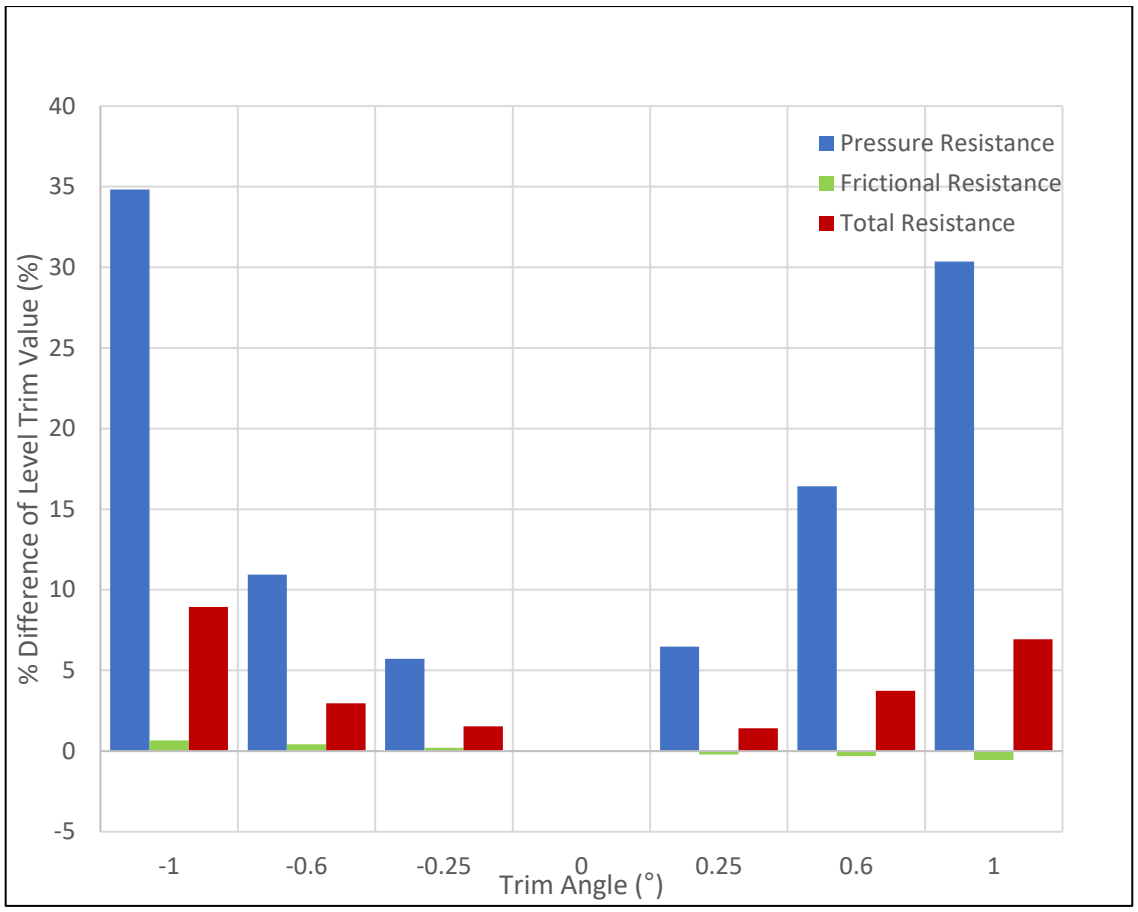

Figure 6-9 Changes in resistance components for self-propulsion simulations

Figure 6-8 and Figure 6-9 presents results for changes in resistance components at different trim angles for nominal resistance and self-propulsion simulations, respectively. Nominal resistance variations were discussed in detail in Chapter 4 for the 1/75 scale of KCS. According to nominal resistance simulations, 0.25 degree trim by bow operation resulted in the lowest total resistance value however in self-propulsion simulations level trim operation resulted in the lowest total resistance. Total resistance obtained from towed simulations was found to be 1% lower at 0.25 degree trim by bow when compared against level trim operation. However, total resistance obtained from self-propulsion simulations showed an increase of 1.4% at the same trim angle. Considering all other trim angles, increases in total resistance values are significantly higher for self-propulsion simulation cases when compared against towed simulation cases. In order to better understand the underlying reasons for these differences, changes in resistance components are investigated.

As seen in Figure 6-8 and Figure 6-9, pressure resistance increases significantly for trimmed conditions at self-propulsion simulations especially for trim by bow conditions. This may be

due to the effects of propeller-hull interaction and its effect on the stern wave formation. Propeller submergence also decreases with trim by bow which increases resistance due to reduction in the stern pressure. Frictional resistance variation shows a similar trend between nominal resistance and self-propulsion simulations. Resistance components for self-propulsion simulations are obtained from 3-D propeller method for this comparison.

Table 6-5 Resistance components comparison between resistance and self-propulsion simulations

	Frictional Resistance	*Pressure Resistance*
Resistance	81.43%	18.57%
Virtual Disk	75.20%	24.80%
3-D propeller (Self-Propulsion)	71.72%	28.28%

Table 6-5 presents the results for resistance components proportions obtained from resistance and self-propulsion simulations. As can be seen from the Table, the pressure resistance ratio increases in self-propulsion simulations. This may be due to the suction effect of the propeller which can increase the total force on surface of the hull and propeller influence on the wave formation around the hull. This effect is better captured using 3-D propeller method. Differences in stern wave formation between resistance and self-propulsion simulations are shown in Figure 6-10 below. Stern wave formation is significantly different in self-propulsion simulations due to the propeller effect. This also contributes to the differences in resistance components between towed and propelled cases.

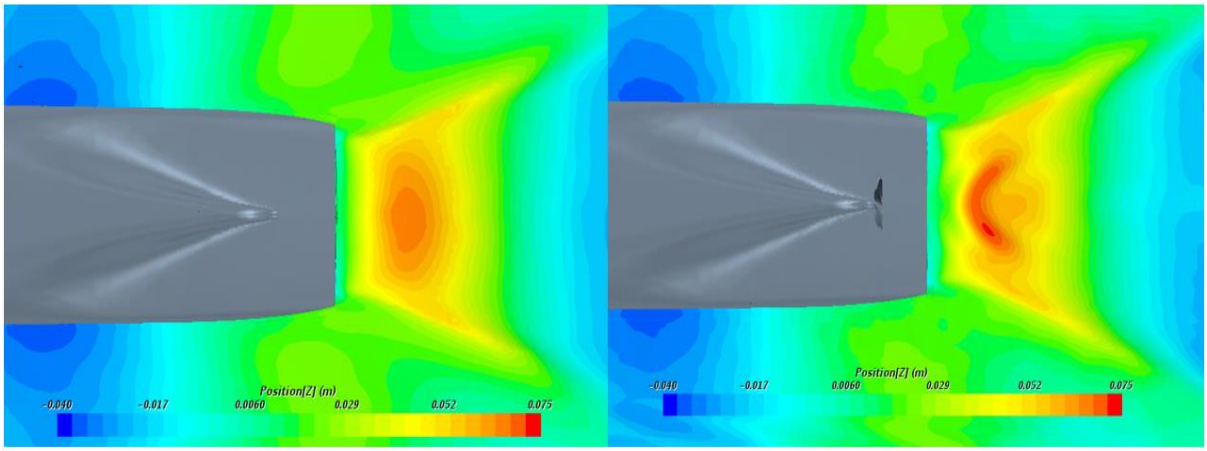

Resistance Simulations Self Propulsion Simulations

Figure 6-10 Wave formation at the stern comparison for resistance and self-propulsion simulations

6.2.7.2 Trim effect on thrust deduction factor and wake coefficient

Total hull efficiency is a function of thrust deduction (t) and wake fraction (w).

Thrust deduction is defined as;

$$t = \frac{T + SFC - R_T}{T} \tag{6.6}$$

In which R_T is the total resistance in towed condition and SFC is Skin Friction Correction which is the towing force actually applied in the propulsion test as mentioned earlier. (ITTC, 2017)

Wake fraction is calculated as follows;

$$w = 1 - \frac{JnD}{v} \tag{6.7}$$

Where J is advance ratio, n is the propeller revolution, D is the propeller diameter and v is the vessel speed. Thrust deduction and wake fraction values are calculated for each trim angle using both methods.

Figure 6-11 show obtained thrust deduction (t) values at different trim angles using both virtual disk and 3-D Propeller methods. In large bow down trim condition, propeller

submergence reaches a critical level and hence thrust deduction increases. Considering the results from 3-D propeller simulations, the increases in thrust deduction coefficient were found to be 6.5%, 18% and 23% in 0.25 degree, 0.6 degree and 1 degree bow trim operation, respectively. In aft trim conditions, there is not a significant effect of trim on thrust deduction coefficient with differences less than 1 per cent. In virtual disk simulations, a similar trend can be observed while predicted values are 10 per cent lower than 3-D propeller method.

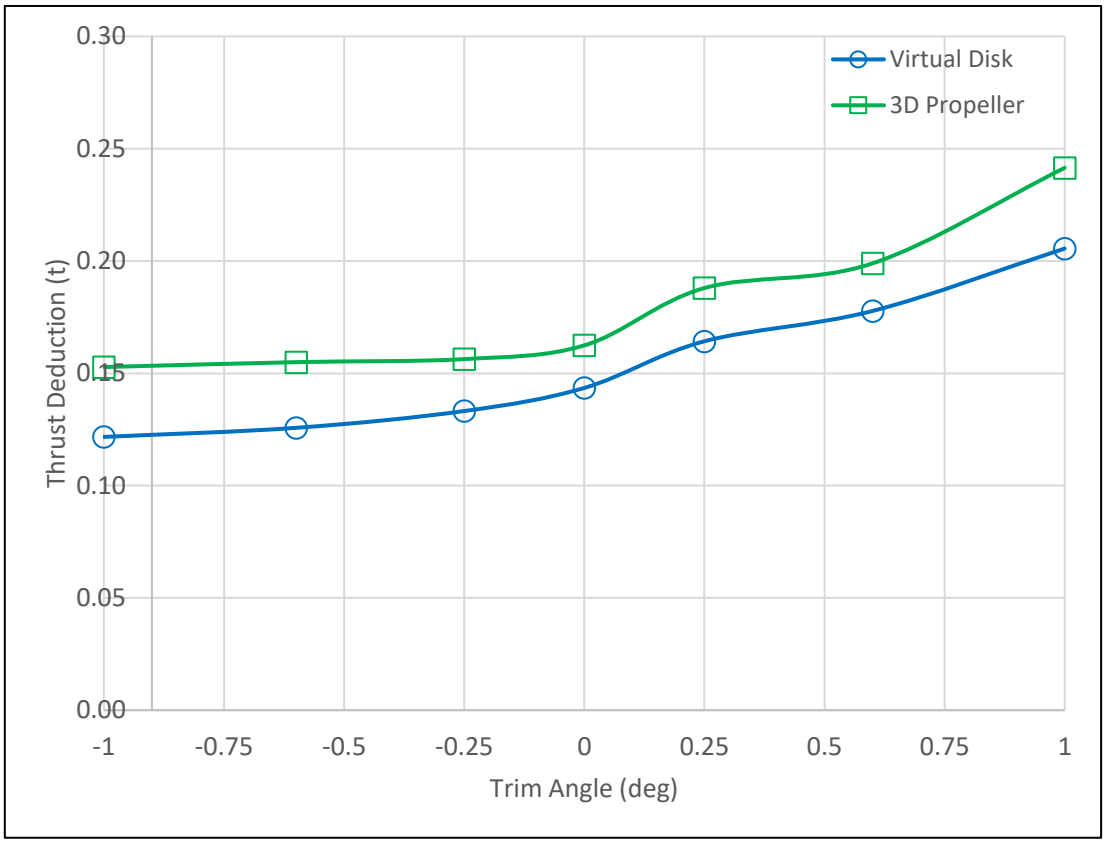

Figure 6-11 Thrust deduction variation at different trim angles

Figure 6-12 presents wake fraction values at different trim angles. As seen in the figure, trim by bow operation increases the wake fraction value which is desired in order to improve overall hull efficiency. Increasing the trim by bow causes shallower draft at the propeller operating area and hence higher wake fraction is observed due to changes in flow velocity at the propeller plane. This also imply that wake fraction depends on the aft draft which change with varying trim. Increase values were found to be 2.8%, 7% and 11% for 0.25, 0.6 and 1 degree trim by bow operation. Trim by stern causes −5.5%, −17.7%, and −20%, reduction in

wake fraction when operating at 0.25 degree, 0.6 degree and 1 degree trim by stern, respectively.

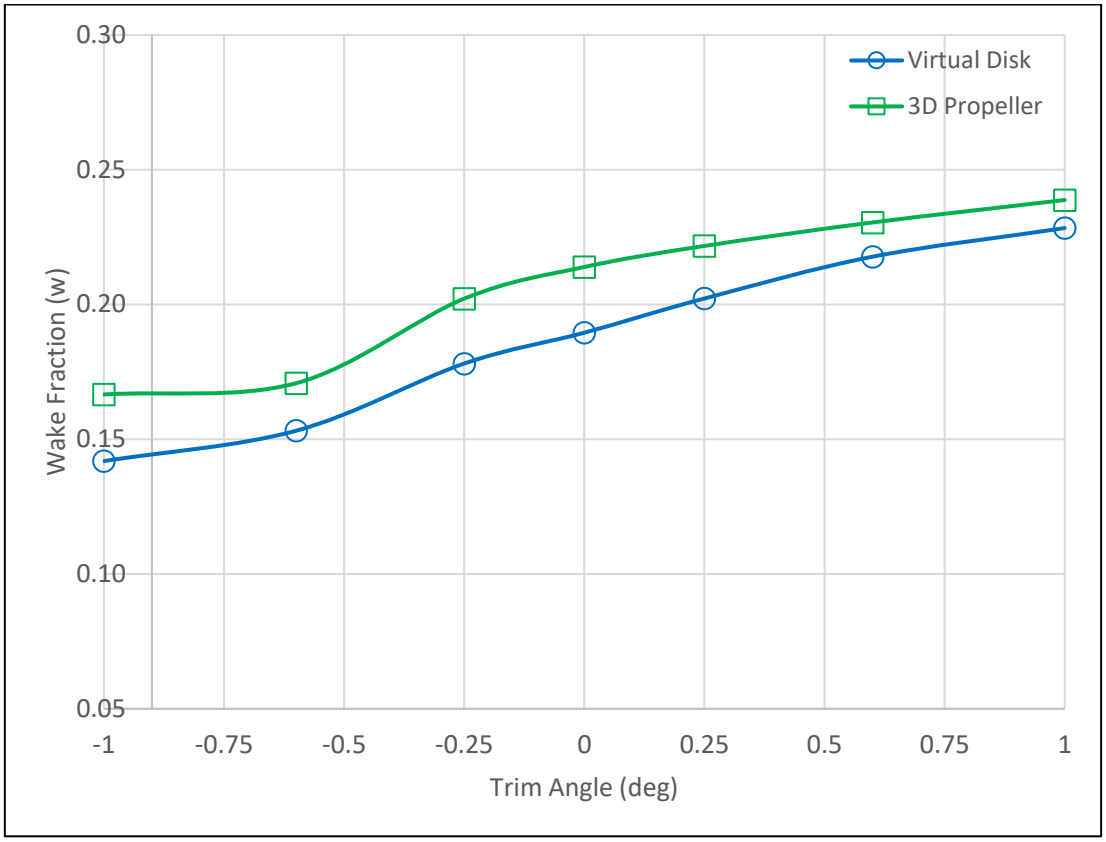

Figure 6-12 Wake fraction variation at different trim angles

Figure 6-13 shows the velocity contour of V_x/V_{Ship} at the centreline (y/LPP = 0) for different trim angles. It was already discussed that flow velocities are affected by trim angle. It can be seen from the figures that velocities behind the ship going into the propeller are larger for trim by aft conditions. Also, velocities behind the propeller are increasing with increasing trim by aft which can be related to the higher rotational rates of the propeller. In trim by bow conditions, propeller inflow velocity is slightly lower than level trim condition.

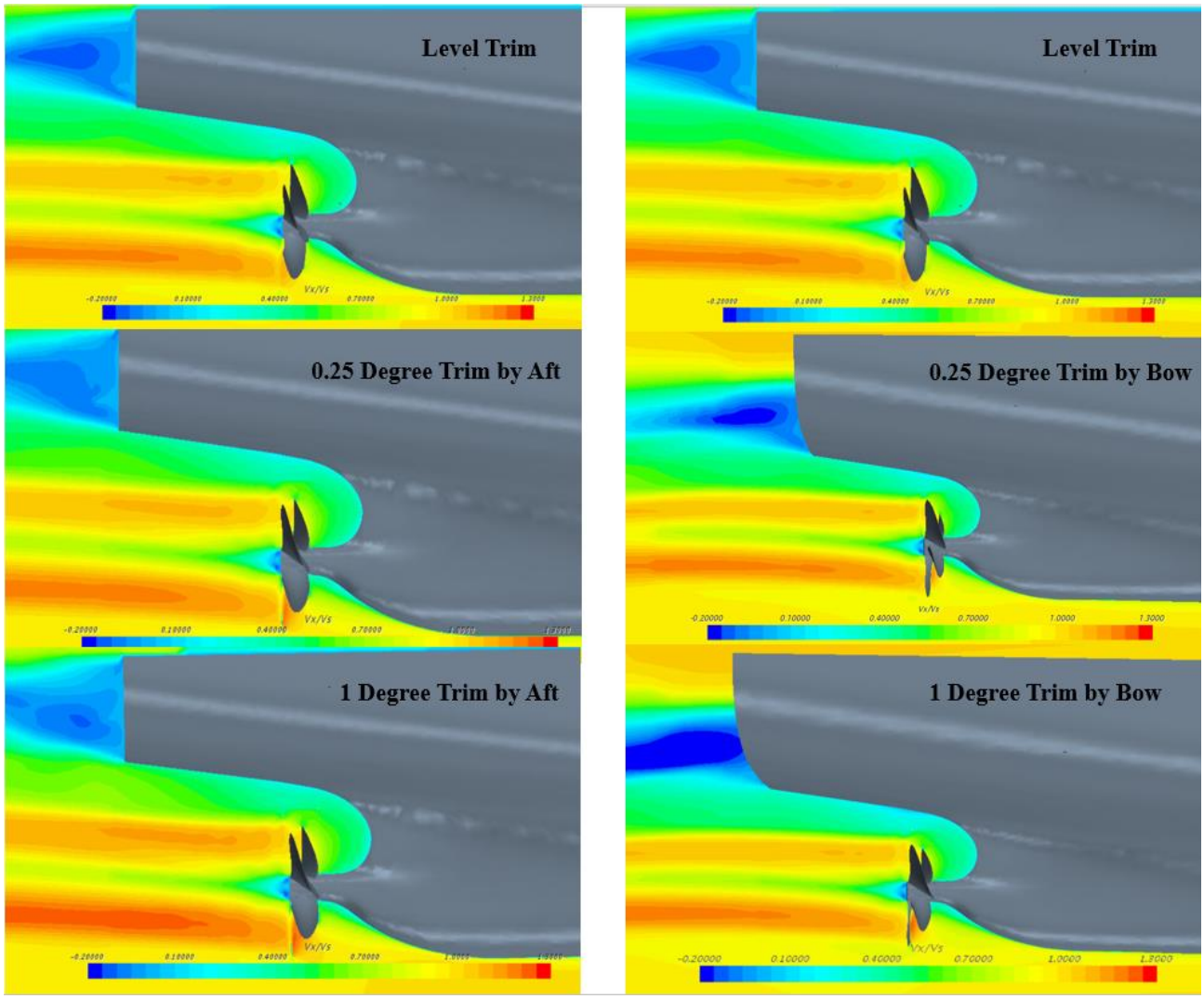

Figure 6-13 Contours of axial velocity for different trim angles

6.2.7.3 Changes in Delivered Power due to Trim

The changes in delivered power due to trim were investigated using the simulation results. Delivered power at the propeller can be computed using propeller torque (Q) and propeller rotational speed (n):

$$P_D = 2\pi \cdot n \cdot Q \tag{6.8}$$

Figure 6-14 presents the percentage differences in delivered power at self-propulsion points for each trim condition using results from both virtual disk and 3-D propeller methods.

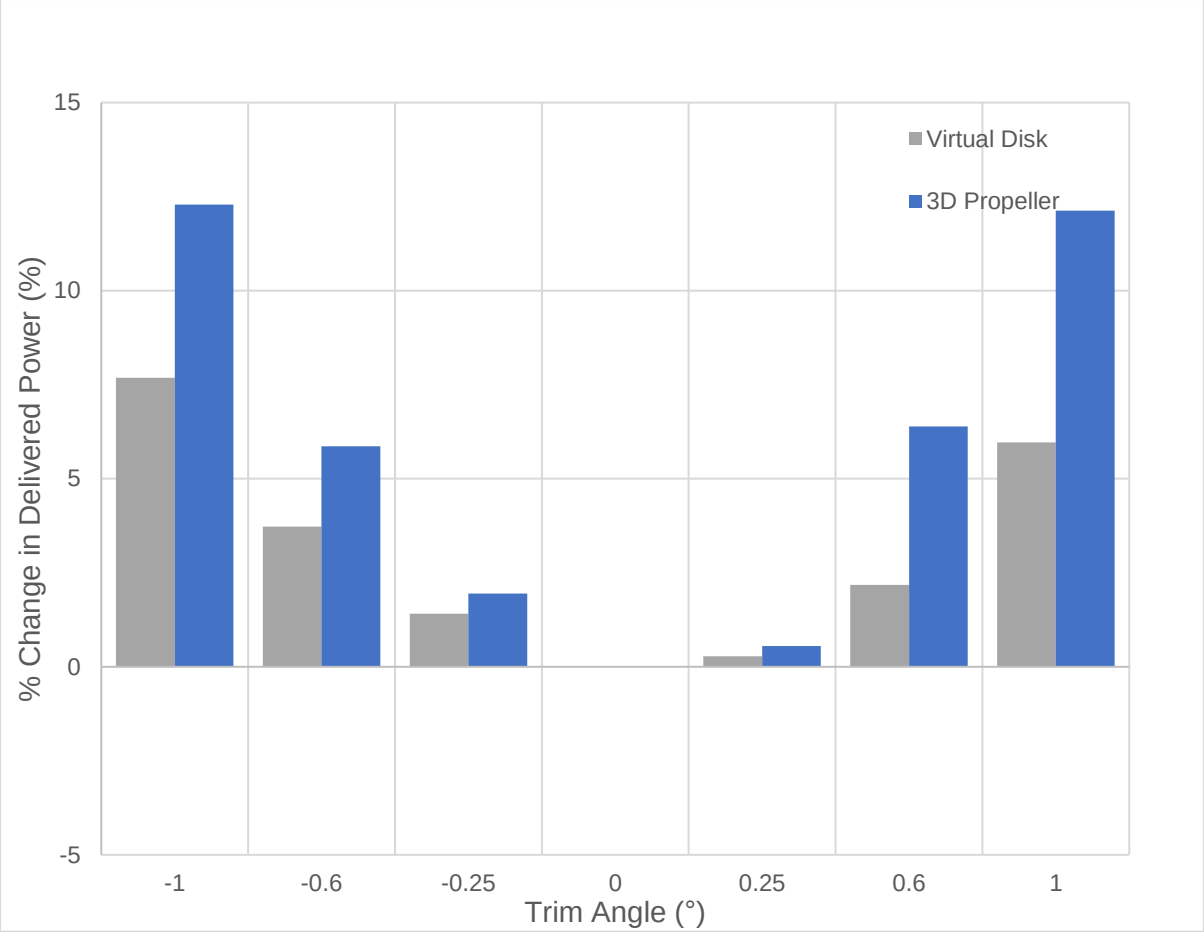

Figure 6-14 Delivered Power (PD) variation at different trim angles

As can be seen in the figure, all trim conditions both bow and stern cause an increase in delivered power. Both methods show a similar trend in estimating delivered power at different trim angles. However, the virtual disk method under-predicted the magnitudes of increases in delivered power when compared against the 3D propeller method. Increases in delivered power from 3D propeller method were found to be 0.6%, 6.4% and 12% while virtual disk method predictions were 0.28%, 1.6% and 5.9% in trim by bow conditions. For trim by stern, the delivered power requirement increases with increasing trim angle. 3-D propeller method predicts increases of 1.9%, 5.9% and 12.2% for 0.25 degree, 0.6 degree and 1 degree trim, respectively.

The differences in effective power and delivered power are also compared in order to investigate the necessity of self-propulsion simulations for trim optimisation studies. Effective power values were obtained from resistance simulations. Delivered power values obtained from the 3-D propeller method were used for comparison study.

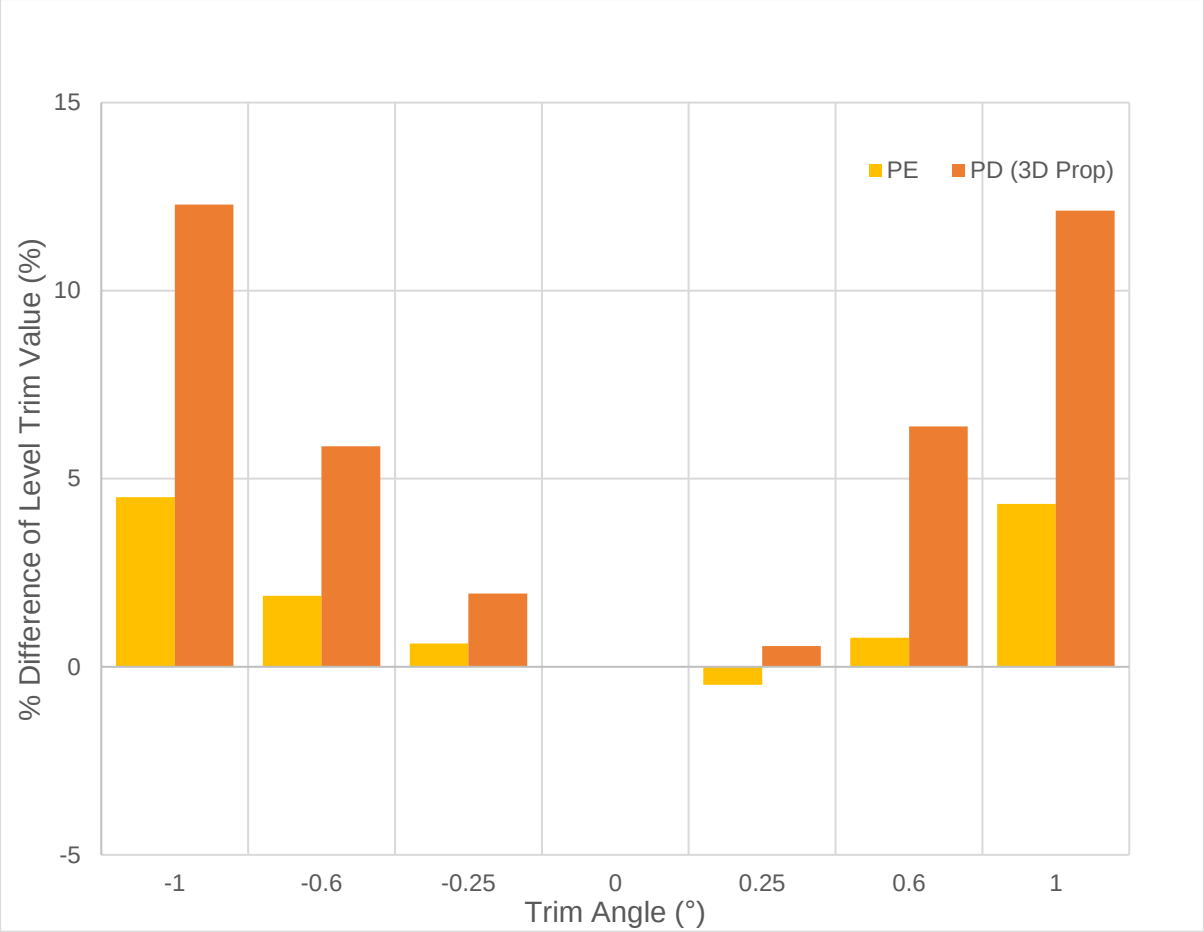

Figure 6-15 Effective Power and Delivered Power differences at each trim angle

It can be seen from Figure 6-15 that optimum trim angle based on delivered power differs when compared against effective power obtained from nominal resistance simulations. While 0.25-degree trim by bow resulted in the lowest effective power, delivered power obtained from self-propulsion simulations at the same trim angle showed an increase of 0.5% when compared against level trim. Magnitudes of potential savings and increases in power requirements can be better estimated using self-propulsion simulations. Thus, the influence of trim on propulsive performance should be investigated for trim optimisation studies in order to understand the real effects of trim on power requirements. In this way, it would be possible to have a more accurate idea of how trim influences the fuel consumption of the vessel.

6.3 Full scale investigation

6.3.1 Numerical Modelling of Self Propulsion at Full Scale

In order to investigate the scale effects on propulsion characteristics and optimum trim, full scale self-propulsion simulations have been carried out. Computational domain, boundary conditions and mesh structure were kept the same with model scale investigation. Details of these can be found in Section 6.2. The stationary domain consisted of hexahedral cells and the rotating domain consisted of polyhedral cells. Local refinements were applied as in model scale investigation. Full scale mesh consisted of around 4.9M cells, with approximately 2.4 million cells in the rotating domain. It should be noted that mesh was updated for each trim condition. Figure 6-16 shows a cross-section of the generated mesh. Surface mesh on propeller and bulb areas are shown in Figure 6-17.

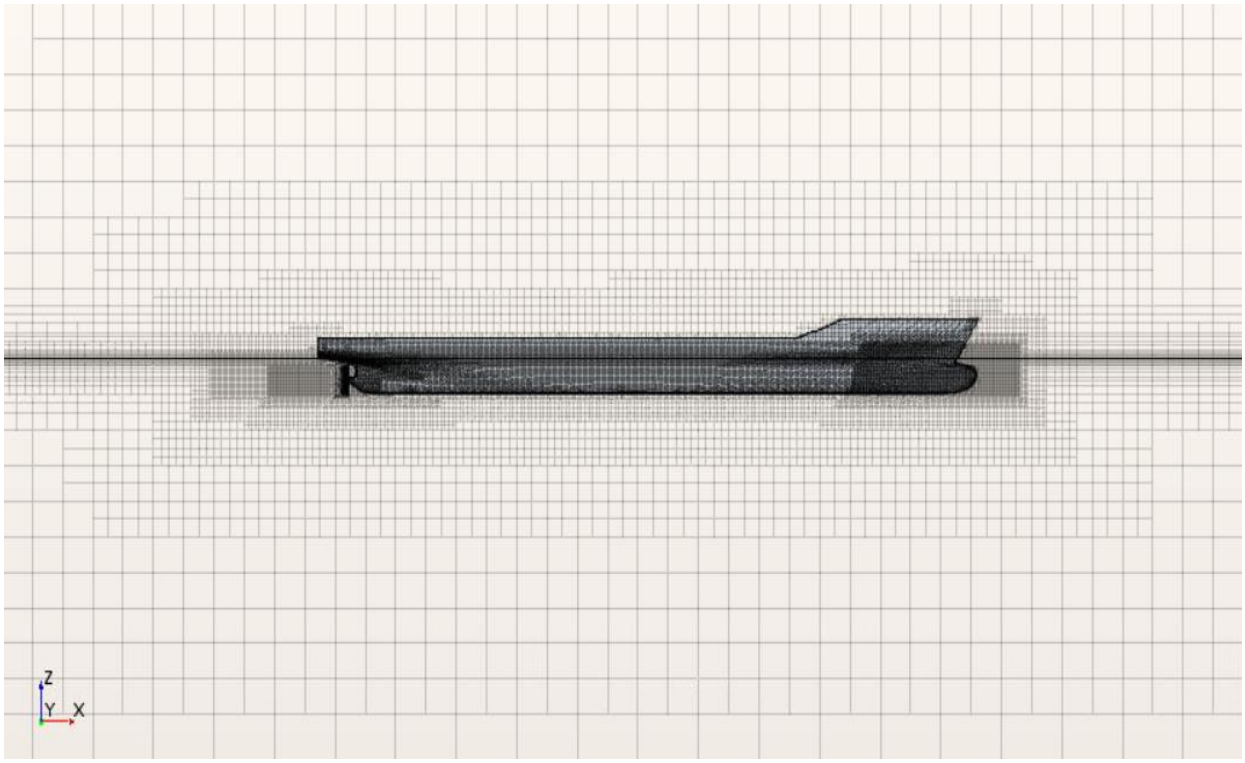

Figure 6-16 Cross section of the generated mesh showing refinement areas around the hull

Figure 6-17 Surface mesh on bow and propeller of the hull

6.3.2 Full-Scale Comparison Study

As full-scale data is not available, obtained values are compared against available data in the literature. Castro et al. (2011) and Song et al. (2020) conducted full scale simulations for the KCS without a rudder at the same speed corresponding Froude number of 0.26 and their results are compared with the findings from this study. Table 6-6 summarizes the comparison of self-propulsion parameters obtained from this study with EFD and other studies found in the literature.

Table 6-6 Comparison of full scale self-propulsion simulation results with EFD and other studies in literature

	C_T*10^3	**K_T**	**10K_Q**	***n*(rps)**	**J**	**1-w_m**	**1-t_m**	**PD (kW)**
CFD	2.54	0.157	0.262	1.73	0.746	0.828	0.86	2.64E+04
EFD (Hino, 2005)	-	0.17	0.288	-	0.728	0.792	0.853	-
Difference (%)	-	*7.6%*	*9%*	-	*2.5%*	*4.5%*	*0.8%*	-
Castro et al (2011)	2.773	0.166	0.261	1.721	0.714	0.793	0.842	-
Difference (%)	*8.3%*	*5.4%*	*0.4%*	*0.5%*	*4.4%*	*4.5%*	*2.1%*	-

Song et al (2020)	2.583	0.1579	0.263	1.736	0.74	0.823	0.81	2.73E+04
Difference (%)	*1.6%*	*0.6%*	*0.4%*	*0.35%*	*0.8%*	*0.6%*	*6.1%*	*3.3%*

Obtained self-propulsion parameters show good agreement with the literature calculations as calculated self-propulsion values are mostly within 3 per cent of other studies. Prediction errors are larger when compared against EFD results as experiments were conducted in model scale. This can be expected as the Reynolds number of full scale ship is two order magnitude larger than the model scale. The differences between model and full scale self-propulsion simulation results will be discussed further in the results and discussion section.

6.3.3 Results and discussion

In order to investigate the trim influence on full scale propulsion performance, full scale self-propulsion simulations were conducted for all seven trim angles. Differences between model scale and full scale simulation results for delivered power and effective power are discussed in this section.

Differences in delivered power at full scale are compared against model scale findings from the previous section and shown in Figure 6-18. As can be seen from the figure, patterns in delivered power variations for full scale and model scale outcomes at trimmed conditions are similar. In trim by aft conditions, increase in delivered power at full scale is higher when compared against the model scale simulation results for all three trim angles. Increases in delivered power from model scale simulations were found to be 1.9%, 5.9% and 12.2% while full scale simulation predictions were 3.3%, 7.6% and 16.5% increase in trim by aft conditions. As total resistance is significantly higher for trim by aft conditions, higher trust is required to achieve self-propulsion point. In order to achieve higher trust with fixed pitch propeller, propeller revolution speed is increased. Hence, higher power demand can be observed for operating at aft trim conditions. A similar trend is observed in trim by bow conditions. Percentage increase in delivered power is higher in full scale simulations for all trim angles. Operating at 0.25-degree trim by bow results in 1% increase in delivered power at full scale while power demand was up around 0.6% according to model scale investigation.

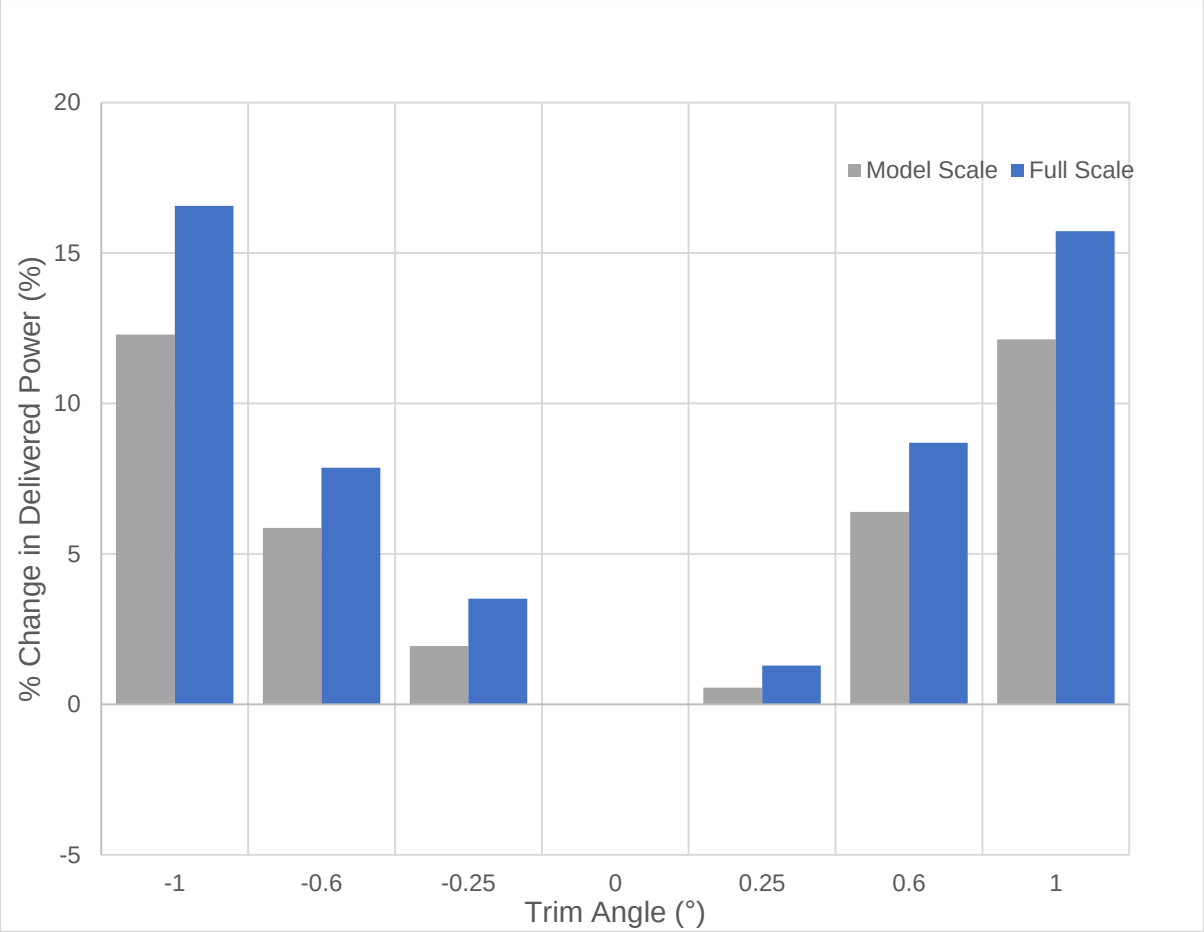

Figure 6-18 Delivered Power differences at Model and Full Scale KCS for different trim angles

Differences in full scale and model scale calculations are discussed further in order to understand the underlying reasons. As the changes in resistance components were discussed in Section 6.2.7.1 for resistance simulations in model and full scale and for self-propulsion simulations in model scale, Table 6-7 lists all results from these simulations along with results from self-propulsion simulations in full scale. As seen in the table, pressure resistance has the highest ratio of the total resistance in full scale self-propulsion simulations. Pressure resistance accounted for 29.88% of total resistance in full scale resistance simulations while this value increased to 42.78% in full scale self-propulsion case. When comparing the differences in self-propulsion simulations, pressure resistance contribution to total resistance increased from 28 per cent in model scale to 42 per cent in full scale.

Table 6-7 Comparison of total resistance components between model scale and full scale resistance and self-propulsion simulations

	Frictional Resistance	*Pressure Resistance*
Model Scale (Resistance)	81.43%	18.57%
Model Scale (Self-Propulsion)	71.72%	28.28%
Full Scale (Resistance)	70.12%	29.88%
Full Scale (Self-Propulsion)	57.22%	42.78%

The effect of the propeller on resistance components can be seen clearly based on these results. The suction effect of the propeller increases forces on the hull surface and resistance components significantly. The pressure resistance component is almost 50 per cent higher in self-propulsion simulations when compared against towed simulation cases. Similar results are also observed in other studies in the literature which compares model scale and full scale simulations. (Sun et al. (2020), Mizzi (2020))

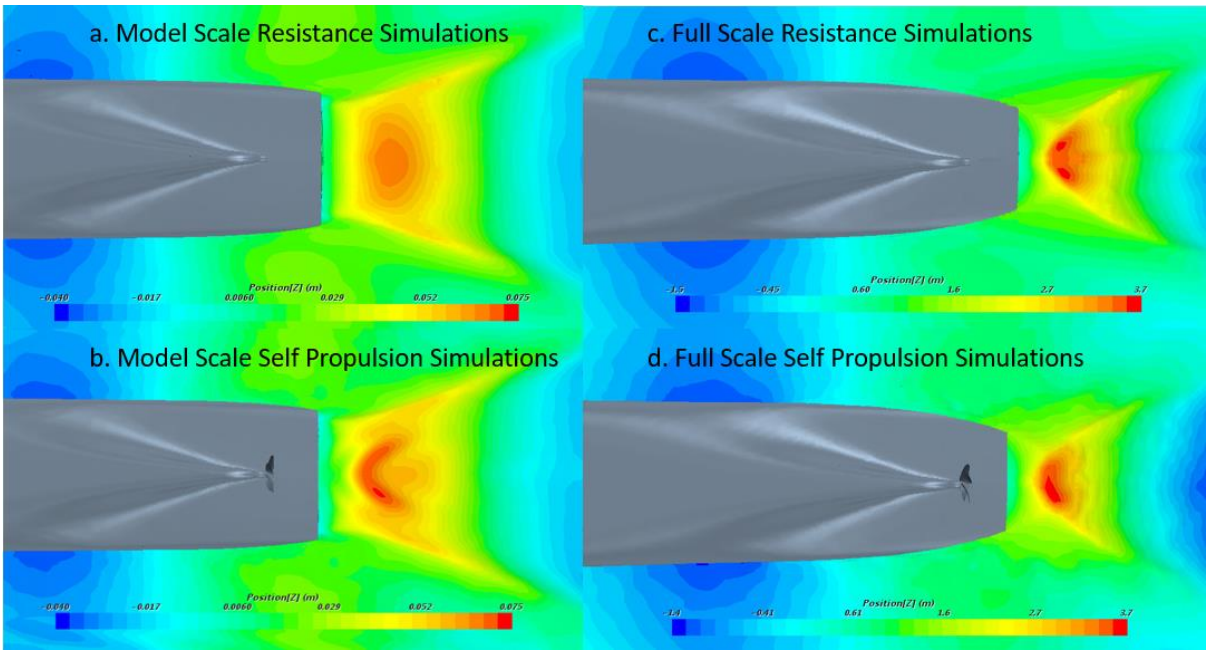

Figure 6-19 Wave formation at the stern comparison between model scale and full scale resistance and self-propulsion simulations

Figure 6-19 compares wave formation at the stern of the ship from resistance and self-propulsion simulations in model scale and full scale. The differences between model scale and full scale resistance simulations were discussed in Section 4. Differences in stern wave

formation between model scale resistance and model scale self-propulsion simulations were also discussed in previous Section 6.2.7.1. When comparing Figure 6-19 c and Figure 6-19 d, the effect of the propeller on stern wave formation can be seen clearly between towed and self-propelled cases. Comparing model scale and full scale self-propulsion simulations in Figure 6-19 b and Figure 6-19 d, differences can be observed in stern wave formation. the formation of the shoulder wave is slightly pushed downstream in full scale self-propulsion simulations due to higher wake velocity.

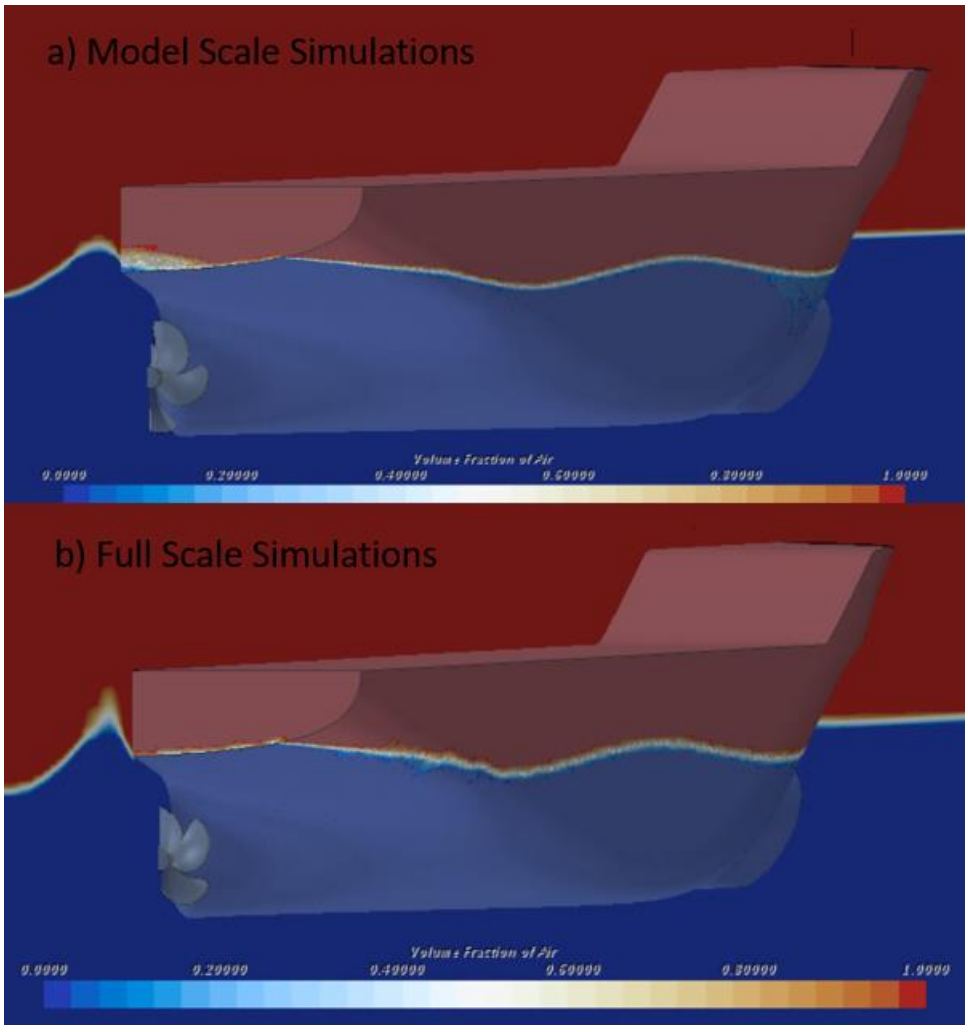

Figure 6-20 Comparison of the free surface wave pattern on the hull for model scale and full scale self-propulsion simulations

Figure 6-20 shows free surface wave pattern comparison between model scale and full scale self-propulsion simulations. It is possible to say that the free surface wave pattern on the hull

does not show a significant difference between model and full scale simulations. As can be seen in the figure, the stern transom plate of the model scale ship is partly wetted while it is dry in full scale due to the thinner boundary layer. Higher rooster tail can be seen in full scale simulations. This also helps to explain the larger pressure resistance that is seen in full scale simulations.

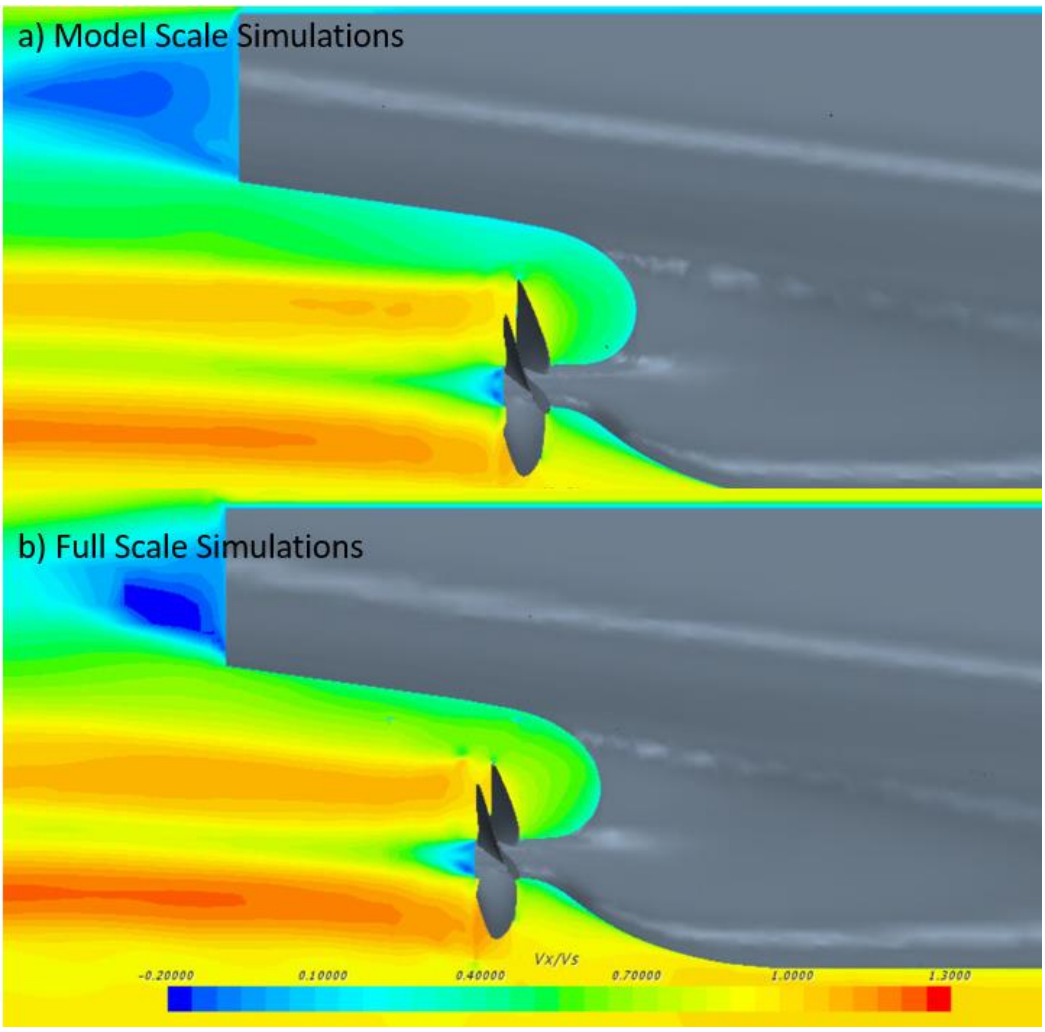

Figure 6-21 Comparison of axial velocity at centreline for model and full scale self-propulsion simulations

Figure 6-21 shows the velocity contour of V_x/V_{Ship} at the centreline (y/LPP = 0) from model scale and full scale simulations. It can be observed that incoming velocity is faster at full scale. Impelled velocity behind the propeller is also faster in full scale simulations. Full scale ship has higher wake velocity hence wake fraction of the full scale ship is smaller as expected. Changes in incoming propeller velocity at different trim angles were discussed in

Section 6.2.7.2. A similar trend is observed in full scale simulations with increasing flow velocity at trim by stern operating conditions.

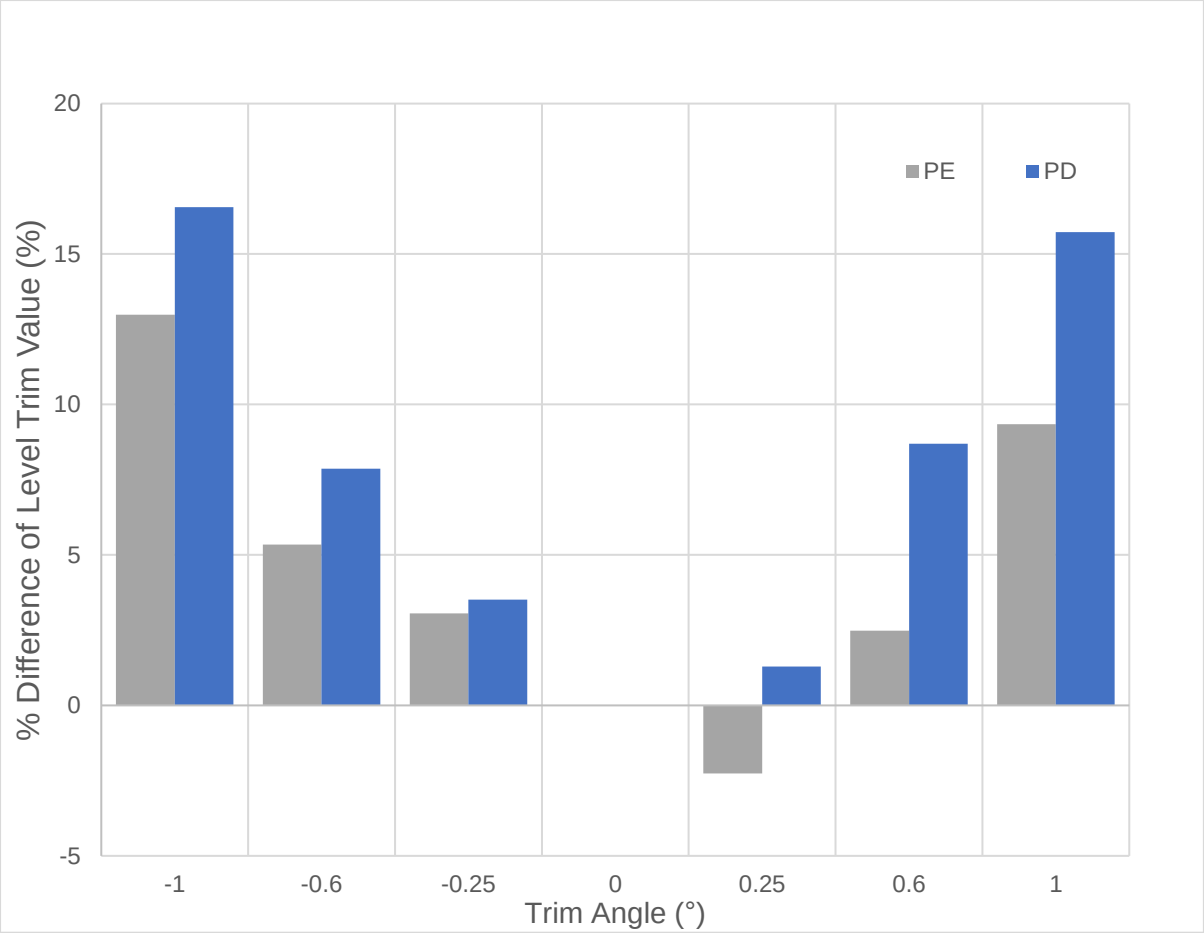

Figure 6-22 Differences between Effective Power (PE) and Delivered Power (PD) of full scale KCS at different trim angles

Figure 6-22 presents the percentage differences in effective power and delivered power for each trim condition using results from full scale resistance and self-propulsion simulations, respectively. As it was discussed earlier in the model scale section, the optimum operating condition differs considering the results from self-propulsion simulations. 0.25 degree trim by bow resulted in 2% reduction in effective power derived from full scale resistance simulations while delivered power obtained from full scale self-propulsion simulations at same trim angle showed an increase of 1% when compared against level trim. In other trim angles, increases in delivered power are higher than increases in effective power when compared against level trim operation. For fully loaded design draft condition at design

speed, it is normal to see level trim operation proves to be the optimum operating condition as ship is designed for this condition. Therefore, it is safe to say that self-propulsion simulations are required to find the real influence of trim on hull performance.

6.4 Conclusions

In this chapter, self-propulsion simulations were conducted to investigate the influence of trim on ship self-propulsion characteristics. Model scale URANS self- propulsion simulations were performed using two different methods, namely, sliding mesh with discretised 3-D propeller geometry and body force method-based virtual disk approach at different trim angles. Full scale self-propulsion simulations were conducted only using 3-D propeller geometry.

A verification study was conducted for self-propulsion simulations with discretised propeller geometry using the Grid Convergence Index method. For the validation of the numerical calculations, results from simulations were compared against experimental data and found to be in good agreement.

Results showed that optimum trim angle differs when comparing the results from self-propulsion simulations and towed ship (nominal resistance) simulations. Pressure resistance component is found to be almost 50 per cent higher in self-propulsion simulations when compared against towed simulation cases. As pressure resistance is the most affected resistance component by changes in trim, self-propulsion simulations may provide more accurate results when investigating the trim influence on hull performance. It was also shown that changes in underwater hull form at trimmed conditions cause significant changes to thrust deduction and wake fraction.

Another interesting finding was the applicability of the simplified body force based virtual disk method at different trim angles. It is important to evaluate the computational cost of self-propulsion and virtual disk methods as trim optimisation study requires the analysis of a large number of different operating conditions. It was found that self-propulsion simulations with 3-D discretized propeller method with fixed ship motions took 5600 CPU hours to complete. The virtual Disk method took 1225 CPU hours and can be considered as a reasonable

alternative as it provides a good balance between computational cost and accuracy of the results.

Following model scale investigation, full scale self-propulsion simulations were conducted and differences with model scale findings are discussed. Similar trends were observed for delivered power variations at trimmed conditions when comparing full scale and model scale results. It can be said that model scale investigation may provide safe information regarding trim effects on propulsion characteristics. When comparing full scale resistance and self-propulsion simulations, effective power and delivered power may show opposite trends at some trim angles. 0.25 degree trim by bow resulted in 2% reduction in effective power derived from full scale resistance simulations while delivered power obtained from full scale self-propulsion simulations at same trim angle showed an increase of 1% when compared against level trim. Thus, it can be concluded that self-propulsion simulations/tests are required in order to understand the real influence of trim on hull performance.

Chapter 7 Conclusions and future research

7.1 Introduction

This chapter presents a summary of the key findings of the studies performed in this thesis, along with a straightforward explanation of how the research aims and objectives proposed in Section 1.4 were accomplished. Following this, a brief discussion on experimental and numerical methods are given. Finally, recommendations for relevant fields of future research related to the current work presented in this thesis are summarised.

7.2 Achievement of research aim and objectives

The main aim of this thesis is to investigate the trim influence on ships resistance, seakeeping and propulsion characteristics.

- To review the literature on trim optimisation of ships and to define the gaps in the literature.

This objective was achieved in Chapter 2 by conducting a critical review on current trim optimisation methods to gain a deeper understanding of existing trim optimization approaches. Initially, fundamentals of trim and different trim optimisation tools were investigated. Then physical components of hull resistance were presented. Following this, experimental and numerical methods that are utilized for the prediction of resistance, added wave resistance and propulsive performance were discussed. Finally, detected gaps were identified and listed at the end of the chapter.

- To develop skills and knowledge in CFD techniques by examining calm-water resistance
- To validate model scale predictions against tank tests
- To examine the impact of trim on calm-water resistance both model scale and full-scale

These objectives were achieved in Chapter 3 and Chapter 4 by conducting towing tank tests and comparing numerical simulation results with tank test results. A series of towing tank tests were conducted to measure the resistance values at different trim angles. Details of towing tank tests were discussed in Chapter 3. Additionally, the work conducted in Chapter 3 has provided the Author with initial knowledge in using commercial CFD software, STAR-CCM+, which was used in numerical RANS simulations. In Chapter 4, model scale and full scale resistance simulations of KCS were performed to examine the impact of trim on the ship resistance components. Before providing the CFD results, experimental results were discussed. The numerical setup of the CFD model was explained in detail. Then, results obtained using CFD were compared to those obtained from experiments. The predicted results agreed well with the model test results.

- To investigate the influence of trim on added resistance of a ship advancing in waves
- To correlate added resistance predictions based on potential flow methods with results obtained from CFD based predictions and model tests
- To indicate ranges of ship speed, trim and wave conditions to which rapid linear potential flow calculations suitable for adoption in preliminary ship design practice may be applicable.

These objectives were achieved in Chapter 5 by performing experiments and numerical simulations for bare hull KCS in regular head waves at different trim angles. Effects of trim

on the added resistance and ship motions (heave and pitch) in regular head waves were investigated.

Firstly, a series of towing tank experiments were performed for six different trim angles at design speed in calm water and regular head waves. The ship motions and added resistance were measured for several wavelength conditions considering short and long wave ranges with wave steepness of 1/60. Next, computations of the towed model in calm water and waves were performed using Unsteady Reynolds-Averaged Navier-Stokes (URANS) CFD and 3-D potential methods. Effects of trim angles on added resistance were analysed and results concerning the performance of the vessel at different trim angles were plotted. Experimental and numerical results for the heave and pitch motions and the added resistance were compared and URANS CFD simulation results showed good agreement with the experimental data for the ship in head waves. Also, the results were compared to those from potential theory and a range of trim and wave conditions were identified for the application of the rapid linear potential flow method.

- To investigate the trim influence on propulsive performance by extending the model to include a detailed model of the rotating propeller, using an approach such as a sliding mesh

- To investigate the applicability of simplified propulsion simulation approaches such as body force method based actuator disk for trim optimisation studies

These objectives were achieved in Chapter 6 by performing self-propulsion simulations at different trim angles. Self-propulsion simulations were performed using two different methods, namely, sliding mesh with 3-D propeller geometry and body force method based actuator disk approach. The commercial CFD software package STAR-CCM+ was used for grid generation and for the numerical simulations of the resistance and self-propulsion tests. Level trim simulations were compared with available experimental data to validate the numerical model. Effects of trim angles on propulsive characteristics were analysed and results concerning the performance of the vessel at different trim angles were plotted. The differences in optimum trim based on pure resistance simulations and self-propulsion simulations were investigated. As trim optimisation studies require the analysis of a large

number of different operating conditions, the applicability and accuracy of the quicker simplified actuator disk approach was tested.

7.3 Main findings

The main findings from this thesis can be listed as below:

- From the investigation of trim influence on calm water resistance in Chapter 4:

1- It was shown that draft, speed and trim all influence the resistance of the vessel. Trim optimisation can help to obtain savings and also to avoid certain operating conditions which can increase the fuel costs significantly. Larger savings are possible for operating at off-design conditions such as operating at slow steaming speed and ballast loading condition.

2- The study showed that using a simpler technique of fixed trim and sinkage, although reducing computational cost, cannot accurately predict the magnitude of the saving at optimum trim. The model test and CFD method agreed well in the prediction of the total resistance trend with respect to trim. It was also confirmed that significant reductions in total resistance are achievable by operating the ship at optimum trim.

3- Model scale investigation can capture the effect of trim on total ship resistance accurately regarding the prediction of increase, decrease in resistance at trim by stern, and bow respectively. However, the magnitude of prediction is different from full scale investigation. Model scale investigation can provide an initial information about trim effects however full scale investigation would be a more appropriate technique to understand the real potential savings.

- From the investigation of trim influence on added resistance in Chapter 5

1- In the experimental results, it was shown that the trends for added resistance at different trim angles are close to the calm water ones in the short wave region. Although the optimum trim trends at calm water and waves are similar for short waves, in long waves optimum trim angle trends are not always the same with calm water results.

2- Potential flow method can be applied in moderate wave range for small trim angles to achieve a quick estimation of the added resistance of ships at different trim angles in regular waves. In larger trim angles by aft and bow, however, the potential flow method provided poor results for the prediction of added resistance. Thus, this method may not be suitable for computing added resistance in various trim angles.

3- After validating added resistance and heave and pitch motions with experimental data, computations and measurements correlated favourably. Motion response comparison for heave and pitch motions showed good agreement with experimental data. Although CFD methods can capture more relevant physics than traditional potential flow methods, improved accuracy may be costly as CFD simulations require powerful computers and are time-consuming

- From the investigation of trim influence on propulsive performance in Chapter 6:

1- Results showed that optimum trim angle differs when comparing the results from self-propulsion simulations and towed ship (nominal resistance) simulations. It was also shown that changes in underwater hull form at trimmed conditions cause significant changes to thrust deduction and wake fraction. Therefore it is possible to say that self-propulsion simulations are required to better understand the effects of trim on hull performance.

2-Results show that the body force based virtual disk method can be utilised in order to achieve a faster estimation of propulsive performance at different trim angles. This method can also be used in cases when 3-D propeller geometry is not readily available.

3- When comparing full scale and model scale self-propulsion simulation results, similar patterns were observed for delivered power variations under trimmed conditions. Hence model scale investigation, it can be said, can provide safe information on trim effects on propulsion characteristics. When comparing full scale resistance and self-propulsion simulations, effective power and delivered power may have contrasting patterns in some cases.

7.4 Discussion

In this study, experimental and numerical methods were used to investigate trim influence on resistance, seakeeping and propulsive performance of KCS. The main findings of these studies were summarised and discussed in detail in the previous sections.

Traditionally hull forms are optimised at a single point i.e. level trim at full load condition. Moving from single point optimisation to multi point optimization involves considering resistance and added resistance at different trim angles at different loading conditions. It was shown that considerably improved fuel efficiency and reduced greenhouse gas emissions can be achieved throughout the vessel's operational life in this way. The effect of operating the ship at different trim angles should be considered during the ship design process. In performance monitoring, not only added resistance but also added power should be considered. Trim as a result, could reduce fuel consumption and GHG emissions without a significant amount of initial capital investment. Trim effects on hull performance are generally investigated by conducting systematic tests in towing tank or by conducting CFD analysis as discussed in this thesis.

Towing tank experiments remain as a fundamental tool to solve marine hydrodynamic problems. Towing tanks provide reliable information about ship performance thanks to the standardisation of experiments. Extensive standards are developed by ITTC for the majority of tests and consistent results can be achieved from different towing tank tests. Regarding the limitations of model tests, one can argue that time and cost are the biggest limitations of traditional model tests. As it is necessary to build the physical model, towing tank tests do not allow much room for different design explorations. Towing tank test availability and costs to hire these facilities are also significant factors that can limit the use of experiments. Flow field visualisations is another limitation of towing tanks as it requires expensive tools and not all the facilities have these tools.

It was shown that full scale CFD simulations may provide the most accurate information regarding the trim effects on hull performance. Full scale CFD can be used as an innovative tool to identify causes of poor performance in existing vessels and to predict the effectiveness of energy saving measures that improve the hydrodynamics and aerodynamics associated with the vessel in question.

As for full scale CFD simulations, it is important to build confidence in CFD methods and the accuracy of predictions within the maritime industry. It is still challenging to compare full scale CFD results with real life measurements from ships. It is hard to obtain full scale data to validate numerical results. It is not only hard to find data but also difficult to measure accurately. Many recent technical publications emphasise both the need for, and the validation of, full scale CFD in ship hydrodynamics. Regarding the limitations of ship scale CFD, high number of cells and smaller time step sizes especially in full scale self-propulsion simulations lead to very long simulation times. Limited computational resources remain a limiting factor for industry-wide adoption of full scale CFD simulations. Cloud computing may provide an affordable choice for solving such complex simulations in a faster way as it does not require the purchase of costly high performance computers. It is likely that continuous improvements in numerical methods and increased use of cloud computing solutions will enable the use of CFD as a standard tool for full scale performance prediction.

7.5 Recommendations for future work:

Recommendations for further studies related to the study discussed in this thesis are briefly outlined below.

- An interesting future study could be the investigation of trim influence on the manoeuvring performance of the ship. Trim of the ship influences the course stability and turning ability of the ships. Vessels are trimmed by stern for improved steerage. Trim by bow is expected to decrease manoeuvring capabilities. This can be investigated especially for cases when trim by bow provides a reduction in total resistance as it was found in Chapter 4 of this study. CFD can be used for virtual manoeuvring tests to investigate the trim influence on manoeuvring characteristics.

- In Chapter 5 trim influence on added resistance and ship motions was investigated only for head waves condition. Further studies can be performed in different heading conditions to better understand the influence of trim on seakeeping performance. In this respect, the future study should be extended to include a rotating propeller to investigate the effect of trim on propulsive performance in a seaway.

- In Chapter 6, trim influence on propulsion performance is only investigated in calm water condition by numerical method. It would be useful to conduct self-propulsion experiments at trimmed conditions to further validate the findings. This work can be extended to investigate trim influence on propulsion performance in waves. Further full-scale self-propulsion simulations in irregular waves can be conducted to understand the issues related to wave-induced unsteady hydrodynamics on the hull-propeller performance. Increasing computational resources would enable conducting such complex simulations using sliding mesh with a fully discretized propeller. This allows modelling the whole ship in real operating conditions such as a self-propelled ship in irregular seas while manoeuvring. These further investigations would help to understand the importance of propeller submergence in waves and the effects of waves on propulsive performance at trimmed conditions.

- In order to extend the work done within Chapter 6, trim influence on propeller cavitation can also be investigated. Cavitation can be captured by creating a more refined numerical mesh around the propeller. Novel methods such as adaptive mesh refinement can be adopted to solve cavitating flow around the propeller for different trim angles.

- This work can be extended to investigate trim influence on ship stability to identify feasible trim conditions. Feasibility of operating at some trim angles will be decided by stability and structural integrity criteria of the ship. This would be especially important for operating at larger trim angles.

References

Abrahamsson, S., 2009. Trim Optimisation – Sustainable Savings. SSPA Highlights 2–3.

Bertram, V., 2016. Added Power in Waves – Time to Stop Lying (to Ourselves), in: 1st Hull Performance & Insight Conference HullPIC 2016. pp. 5–14.

Bertram, V., 2014. Trim Optimisation – Don't blind me with science! Nav. Archit. 14–15.

Bertram, V., 2012. Practical Ship Hydrodynamics.

Bhushan, S., Xing, T., Carrica, P., Stern, F., 2009. Model- and Full-Scale URANS Simulations of Athena Resistance, Powering, Seakeeping, and 5415 Maneuvering. J. Sh. Res. 53, 179–198.

Boese, P., 1970. A Simple Method for the Calculation of Resistance Increase of a Ship in a Seaway. J. Sh. Technol. Res. 17.

Bugalski, T., Hoffmann, P., 2011. Numerical Simulation of the Self-Propulsion Model Tests. Symp. Mar. Propulsors 1–7.

Carlton, J.S., 2012. Marine Propellers and Propulsion. https://doi.org/10.1016/B978-0-7506-8150-6.50032-2

Carrica, P.M., Castro, A.M., Stern, F., 2010. Self-propulsion computations using a speed controller and a discretized propeller with dynamic overset grids 316–330. https://doi.org/10.1007/s00773-010-0098-6

Carrica, P.M., Wilson, R. V., Noack, R.W., Stern, F., 2007. Ship motions using single-phase level set with dynamic overset grids. Comput. Fluids 36, 1415–1433. https://doi.org/10.1016/j.compfluid.2007.01.007

Castiglione, T., Stern, F., Bova, S., Kandasamy, M., 2011. Numerical investigation of the seakeeping behavior of a catamaran advancing in regular head waves. Ocean Eng. 38, 1806–1822. https://doi.org/10.1016/j.oceaneng.2011.09.003

Castro, A.M., Carrica, P.M., Stern, F., 2011. Full scale self-propulsion computations using discretized propeller for the KRISO container ship KCS. Comput. Fluids 51, 35–47. https://doi.org/10.1016/j.compfluid.2011.07.005

Celik, I.B., Ghia, U., Roache, P.J., Freitas, C.J., Coleman, H., Raad, P.E., 2008. Procedure for

estimation and reporting of uncertainty due to discretization in CFD applications. J. Fluids Eng. Trans. ASME 130, 0780011–0780014. https://doi.org/10.1115/1.2960953

Eca, L., Vaz, G., Goncalo, S., Abreu, H., 2015. The Pros and Cons of Wall Functions, in: OMAE2015.

Enger, S., Peric, M., Peric, R., 2010. Simulation of flow around KCS-hull, in: Gothenburg 2010-A Workshop on Numerical Ship Hydrodynamics.

Faltinsen, O.M., Minsaas, K., Liapis, N., Skjørdal, S.O., 1980. Prediction of resistance and propulsion of a ship in a seaway, in: The 13th Symposium on Naval Hydrodynamics. pp. 505–529.

Fenton, J., 1985. A fifth-order Stokes theory for steady waves. J. Waterw. Port, Coastal, Ocean Eng. 111 (2), pp.216-234.

Ferziger, J.H., Peric, M., 2002. Computational Methods for Fluid Dynamics (Third Edit.). Springer, Berlin.

Fu, H., Michael, T., Carrica, P., 2015. A method to perform self-propulsion computations with a simplified body-force propeller model, in: Proceedings of the Twenty-Fifth (2015) International Ocean and Polar Engineering Conference. pp. 968–975.

Gaggero, S., Villa, D., Viviani, M., 2015. The Kriso container ship (KCS) test case: An open source overview, in: Computational Methods in Marine Engineering VI, MARINE 2015. pp. 735–749.

Górski, W., Abramowicz-Gerigk, T., Burciu, Z., 2013. The influence of ship operational parameters on fuel consumption. Zesz. Nauk. / Akad. Morska w Szczecinie nr 36 (108.

Hansen, H., Freund, M., 2010. Assistance tools for operational fuel efficiency, in: 9th International Conference on Computer and IT Applications in the Maritime Industries, COMPIT 2010. Gubbio, Italy, pp. 356–366.

Hino, T., 2005. Proceedings of CFD Workshop Tokyo 2005. NMRI.

Hirt, C.W., Nichols, B.D., 1981. Volume of Fluid (VOF) method for the dynamics of free boundaries. J. Comput. Phys. 39, 201–225.

Hizir, O., Kim, M., Turan, O., Day, A., Incecik, A., Lee, Y., 2019. Numerical studies on non-linearity of added resistance and ship motions of KVLCC2 in short and long waves. Int. J. Nav. Archit. Ocean Eng. 11, 143–153. https://doi.org/10.1016/j.ijnaoe.2018.02.015

Hollenbach, U., Klug, D.H., Mewis, D.F., 2007. Container Vessels – Potential for Improvements in Hydrodynamic Performance.

HSH Nordbank, 2013. Expert Market Survey: Eco-Shipping.

Iakovatos, M.., Liaropakis, D.E., Tzabiras, G.D., 2014. Experimental investigation of the trim influence on the resistance characteristics of five ship models. Dev. Marit. Transp.

Exploit. Sea Resour.

IMO, 2019. Technical and methodological issues related to the Fourth IMO GHG Study.

IMO, 2016. GUIDELINES FOR THE DEVELOPMENT OF A SHIP ENERGY EFFICIENCY MANAGEMENT PLAN (SEEMP). MEPC.282(70) 9, 10. https://doi.org/10.5151/cidi2017-060

IMO, 2011. RESOLUTION MEPC.203(62) 203, 1–17.

ITTC, 2017. 1978 ITTC Performance Prediction Method 7.5 – 02 0.

ITTC, 2014a. Practical Guide for Uncertainty Analysis of Resistance Measurement in Routine Tests, Recommended Procedures and Guidelines.

ITTC, 2014b. Practical Guidelines for Ship CFD Applications ITTC –Recommended Procedures and Guidelines, section 7.5-03-02-03, International Towing Tank Conference.

ITTC, 2002. Ship Models - ITTC Recommended Procedures 7.5-01-01-01.

Joncquez, S.A.G., Bingham, H., Andersen, P., 2008. Validation of added resistance computations by a potential flow boundary element method, in: Proceedings of the 27th Symposium on Naval Hydrodynamics, Seoul Korea.

Kashiwagi, M., Ikeda, T., Sasakawa, T., 2010. Effects of forward speed of a ship on added resistance in waves. Int. J. Offshore Polar Eng. 20, 196–203.

Kim, B., Shin, Y.S., 2007. Steady flow approximations in three-dimensional ship motion calculation. J. Sh. Res. 51 (3), 229–249.

Kim, H., Choi, S., Hong, C., Yoo, S., Seo, J., Hwangbo, S., 2013. Development and Application of Trim Optimization Techniques Using a Evaluation System (SoLuTion) Based on the RANS for Improvement of EEOI 9. https://doi.org/10.1115/OMAE2014-24296

Kim, K.-H., Kim, Y., 2011. Numerical study on added resistance of ships by using a time-domain Rankine panel method. Ocean Eng. 38, 1357–1367.

Kim, M., Hizir, O., Turan, O., Incecik, A., 2017. Numerical studies on added resistance and motions of KVLCC2 in head seas for various ship speeds. Ocean Eng. 140, 466–476. https://doi.org/10.1016/j.oceaneng.2017.06.019

Krasilnikov, V.I., 2013. Self-Propulsion RANS Computations with a Single-Screw Container Ship, in: 3rd International Symposium on Marine Propulsors. pp. 430–438.

Larsen, N.L., 2011. Understanding the physics of trim 1–10. https://doi.org/10.1051/eas/1152023

Larsson, L., Baba, E., 1996. Ship resistance and flow computations.

Larsson, L., Stern, F., Visonneau, M., 2014. An assessment of the Gothenburg 2010 Workshop.

Larsson, L., Stern, F., Visonneau, M., Hino, T., Hirata, N., Kim, J., 2018. Tokyo 2015: A workshop on CFD in ship hydrodynamics, in: Tokyo 2015: A Workshop on CFD in Ship Hydrodynamics. Tokyo.

Lewis, E.V., 1988. Principles of naval architecture second revision, volume III motions in waves and controllability. Soc. Nav. Arch. Mar. Eng.

Lubke, L.O., 2005. Numerical simulation of the flow around the propelled KCS, in: Proceedings of the CFD Workshop Tokyo 2005. pp. 587–592.

Lv, X., Wu, X., Sun, J., Tu, H., 2013. Trim optimization of ship by a potential-based panel method. Adv. Mech. Eng. 2013. https://doi.org/10.1155/2013/378140

Maasch, M., Turan, O., Khorasanchi, M., Fang, I., 2017. Calm Water Resistance and Self-Propulsion Simulations Including Cavitation for an Lng Carrier in Extreme Trim Conditions 1–10.

Mizzi, K., 2020. The Development of Intelligent Hull Forms of Large Ships for Energy Efficient Transportation.

Muzaferija, S., Peric, M., 1999. Computation of Free-surface Flows Using Interface- tracking and Interface-capturing Methods., in: Computational Mechanics Publications.

Orihara, H., Miyata, H., 2003. Evaluation of added resistance in regular incident waves by computational fluid dynamics motion simulation using overlapping grid system. J. Mar. Sci. Technol. 8, 47–60. https://doi.org/10.1007/s00773-003-0163-5

Park, D.M., Kim, Y., Seo, M.G., Lee, J., 2016. Study on added resistance of a tanker in head waves at different drafts. Ocean Eng. 111, 569–581. https://doi.org/10.1016/j.oceaneng.2015.11.026

Park, H.-S., Seo, Dae-WonHan, Han, K.-M., Kim, D.-H., Ha, T.-B., 2015. A STUDY ON RESISTANCE PERFORMANCE FOR VARIOUS TRIM CONDITIONS - Omae- 1–8.

Peric, M., 2016. Prediction of Ship Resistance.

Reichel, M., Minchev, a., Larsen, N.L., 2014. Trim Optimisation - Theory and Practice. TransNav, Int. J. Mar. Navig. Saf. Sea Transp. 8, 387–392. https://doi.org/10.12716/1001.08.03.09

Roache, P.J., 1998. Verification and Validation in Computational Science and Engineering.

Sadat-Hosseini, H., Toxopeus, S., Kim, D.H., Sanada, Y., Stocker, M., Otzen, J.F., Toda, Y., Stern, F., 2015. Experiments and Computations for KCS Added Resistance for Variable Heading. 5th World Marit. Technol. Conf. 1–15.

Sato, Y., Miyata, H., Sato, T., 1999. CFD simulation of 3-dimensional motion of a ship in

waves: application to an advancing ship in regular heading waves. J. Mar. Sci. Technol. 4, 108–116. https://doi.org/10.1007/s007730050013

Seo, J.H., Seol, D.M., Lee, J.H., Rhee, S.H., 2010. Flexible CFD meshing strategy for prediction of ship resistance and propulsion performance. Int. J. Nav. Archit. Ocean Eng. 2, 139–145. https://doi.org/10.3744/JNAOE.2010.2.3.139

Sherbaz, S., Duan, W., 2014. Ship Trim Optimization : Assessment of Influence of Trim on Resistance of MOERI Container Ship 2014.

SIEMENS, 2017. User guide STAR-CCM+ Version 12.06.010-R8.

Sigmund, S., el Moctar, O., 2018. Numerical and experimental investigation of added resistance of different ship types in short and long waves. Ocean Eng. 147, 51–67. https://doi.org/10.1016/j.oceaneng.2017.10.010

Simonsen, C.D., Otzen, J.F., Joncquez, S., Stern, F., 2013. EFD and CFD for KCS heaving and pitching in regular head waves. J. Mar. Sci. Technol. 18, 435–459. https://doi.org/10.1007/s00773-013-0219-0

Simonsen, C.D., Otzen, J.F., Nielsen, C., Stern, F., 2014. CFD prediction of added resistance of the KCS in regular head and oblique waves, in: The 30th Symposium on Naval Hydrodynamics.

Song, S., Demirel, Y.K., Atlar, M., 2020. Penalty of hull and propeller fouling on ship self-propulsion performance. Appl. Ocean Res. 94, 102006. https://doi.org/10.1016/j.apor.2019.102006

Stern, F., Wilson, R., Shao, J., 2006. Quantitative V&V of CFD simulations and certification of CFD codes. Int. J. Numer. Methods Fluids 50, 1335–1355. https://doi.org/10.1002/fld.1090

Sun, J., Tu, H., Chen, Y., Xie, D., Zhou, J., 2016. A Study on Trim Optimization for a Container Ship Based on Effects due to Resistance. J. Sh. Res. 60, 30–47. https://doi.org/10.5957/josr.60.1.150022

Sun, W., Hu, Q., Hu, S., Su, J., Xu, J., Wei, J., Huang, G., 2020. Numerical Analysis of Full-Scale Ship Self-Propulsion Performance with Direct Comparison to Statistical Sea Trail Results. J. Mar. Sci. Eng. 8, 24. https://doi.org/10.20944/preprints201912.0318.v1

Tezdogan, T., Demirel, Y.K., Kellett, P., Khorasanchi, M., Incecik, A., Turan, O., 2015. Full-scale unsteady RANS CFD simulations of ship behaviour and performance in head seas due to slow steaming. Ocean Eng. 97, 186–206. https://doi.org/10.1016/j.oceaneng.2015.01.011

Tezdogan, T., Incecik, A., Turan, O., 2016. Full-scale unsteady RANS simulations of vertical ship motions in shallow water. Ocean Eng. 123, 131–145. https://doi.org/10.1016/j.oceaneng.2016.06.047

UNCTAD, 2017. Review of Maritime Transport 2017. New York.

UNCTAD, 2010. Oil Prices and Maritime Freight Rates: An Empirical Investigation.

Van't Veer, 2009. PRECAL v6.5 Theory Manual.

Visonneau, M., Deng, G.B., Guilmineau, E., Queutey, P., Wackers, J., 2016. Local and Global Assessment of the Flow around the Japan Bulk Carrier with and without Energy Saving Devices at Model and Full Scale, in: 31st Symposium on Naval Hydrodynamics Monterey, California, 11-16 September 2016.

Weymouth, G.D., Wilson, R.V., Stern, F., 2005. RANS computational fluid dynamics predictions of pitch and heave ship motions in head seas. J. Sh. Res. 49, 80–97.

Windén, B., Turnock, S.., Hudson, D.., 2014. Self propulsion modelling of the KCS container ship using an open source framework. Proc. 17th Numer. Towing Tank Symp. Marstrand, Sweden 28-30 Sept.

Research Outputs

The following publications were generated throughout the timespan of the PhD study.

- Journal Papers (SCI/ SCI Expanded):

1. Shivachev, E., Khorasanchi, M., Day, S. & Turan, O. (2020) Impact of trim on added resistance of KRISO container ship (KCS) in head waves: An experimental and numerical study. In: Ocean Engineering. 211, 15 p., 107594

2. **Shivachev, E.**, Day, S. & Turan, O. (2021) Impact of trim on propulsive performance of KRISO Container Ship (KCS) Ships&Offshore Structures. (In preparation)

3. Yilmaz, N., **Shivachev, E.**, Maasch, M., Turan, O., Atlar, M. Numerical Validation of Ship Scale Resistance and Self-Propulsion Performances with Sea Trials. Ships and Offshore Structures. (Submitted)

- Conference papers:

1. **Shivachev, E.**, Khorasanchi, M., Day, S.. (2017) Trim influence on Kriso Container Ship (KCS): an experimental and numerical study. ASME 2017 36th International Conference on Ocean, Offshore and Arctic Engineering. New York, Vol. 7A. 7 p. OMAE2017-61860

2. Maasch, M., **Shivachev, E.**, Day, A. H. & Turan, O. (2018) A numerical trim methodology study for the Kriso container ship with bulbous bow form variation. Marine Design XIII: Proceedings of the 13th International Marine Desing Conference (IMDC 2018), June 10-14, 2018, Helsinki, Finland.